EVALUATION OF THE HYDROLOGIC EFFECTS OF STOCK PONDS ON A PRAIRIE WATERSHED

by

Jennifer Marie Womack

A thesis submitted in partial fulfillment
of the requirements for the degree

of

Master of Science

in

Civil Engineering

MONTANA STATE UNIVERSITY
Bozeman, Montana

April 2012

©COPYRIGHT

by

Jennifer Marie Womack

2012

All Rights Reserved

APPROVAL

of a thesis submitted by

Jennifer Marie Womack

This thesis has been read by each member of the thesis committee and has been found to be satisfactory regarding content, English usage, format, citation, bibliographic style, and consistency and is ready for submission to The Graduate School.

Dr. Otto Stein

Approved for the Department of Civil Engineering

Dr. Brett W. Gunnink

Approved for The Graduate School

Dr. Carl A. Fox

STATEMENT OF PERMISSION TO USE

In presenting this thesis in partial fulfillment of the requirements for a master's degree at Montana State University, I agree that the Library shall make it available to borrowers under rules of the Library.

If I have indicated my intention to copyright this thesis by including a copyright notice page, copying is allowable only for scholarly purposes, consistent with "fair use" as prescribed in the U.S. Copyright Law. Requests for permission for extended quotation from or reproduction of this thesis in whole or in parts may be granted only by the copyright holder.

Jennifer Marie Womack

April 2012

ACKNOWLEDGEMENTS

I would like to offer my thanks to the members of my committee, Dr. Otto Stein, Dr. Joel Cahoon, and Stuart Challender, for their support and help throughout the project. I especially appreciate Dr. Otto Stein for his guidance through many of the project's stages. The research was funded by the World Wildlife Fund. Their passion for wildlife conservation and protecting the Northern Great Plains was the motivation behind the project, and hopefully this research will benefit future water management decisions. I would like to specifically thank Martha Kauffman of the World Wildlife Fund for helping with data acquisition. I also appreciate the help offered by so many people who live and work near the American Prairie Reserve. Finally, I would like to offer gratitude to my fiancé, Matt Johnson. He was unyielding in his enthusiasm and support for the project.

TABLE OF CONTENTS

1. INTRODUCTION 1

Background 1
Goals and Objectives 4

2. LITERATURE REVIEW 6

Dam Impacts on Hydrology 6
HEC-HMS 9
Hydrology Models 13
SCS Curve Number Method 14
Clark Unit Hydrograph 17
Muskingum-Cunge 21
GIS and Hydrologic Modeling 23

3. STUDY SITE 29

Site Description 29
Site Monitoring 32

4. METHODS 34

Stock Ponds 34
GIS Data 36
HEC-GeoHMS 38
Terrain Preprocessing 39
Subbasin Delineation 44
Watershed Characteristics and Parameters 46
Model Setup 47
HEC-HMS 48
Precipitation 49
Measured Data 49
Frequency Storms 53
Loss Model 54
Runoff Transformation 56
Channel Routing 59
Reservoir Routing 61
Culvert Modeling 65

TABLE OF CONTENTS - CONTINUED

Culvert Survey 66
HEC-RAS Model 68

5. MODELING RESULTS 72

Rating Curve 72
Model Configuration 74
Model Calibration 75

6. ANALYSIS 87

Frequency Analysis 87
Parameter Correlations 93
Pond Removal 103

7. SUMMARY AND CONCLUSIONS 110

REFERENCES CITED 113

APPENDICES 122

APPENDIX A: Data Dictionary 123
APPENDIX B: Grid Cell Parameter File 126
APPENDIX C: Curve Number Table 128
APPENDIX D: Time to Concentration Calculation 130
APPENDIX E: One-Pond-In Results 132
APPENDIX F: One-Pond-Out Results 138

LIST OF TABLES

Table Page

4.1 The statistical data used to construct the frequency storms.....53

4.2 Final parameters used for each subbasin within the model.....58

4.3 Pond characteristics used to describe stage-storage relationships 64

5.1 The events modeled for Box Elder Watershed 78

5.2 The storage coefficient sets applied to the model.....84

6.1 The peak flow rates (cfs) and runoff volumes (in) for the watershed without ponds and the watershed with empty ponds.....89

6.2 The peak flow rates (cfs) and runoff volumes (in) for the watershed without ponds and the watershed with half full ponds (by volume). 89

6.3 The peak flow rates (cfs) for the watershed without ponds and the watershed with full ponds.....89

6.4 R^2 correlation values for each pond's parameter value paired against its percent change in runoff volume and peak flow rate for the developed frequency storms. 95

6.5 Ponds most influential on runoff volume 104

6.6 Ponds most influential on peak flow rate 104

6.7 The ponds ordered based on their effects on runoff volume and peak flow rate.....104

6.8 The individual peak flow increase (cfs) for the three most influential ponds on peak discharge for the one-pond-out analysis……..…108

6.9 The peak flow increase (cfs) caused by the removal of the three most influential ponds at the same time for various return intervals…….....108

LIST OF FIGURES

Figure Page

1.1 Box Elder Watershed; (a) a fence dividing grazed land and land unaffected by grazing and (b) a stock pond....2

3.1 Box Elder Watershed; (a) location within Phillips County, MT and (b) the current network of stock ponds....29

3.2 Figure 3.2: Box Elder Creek; (a) an incised section of the channel and (b) a gravel section of channel substrate....30

3.3 The main Box Elder subbasins containing similar topography and land cover....31

3.4 Box Elder Watershed monitoring gages....33

4.1 Headcut at the outlet of pond 2P1....35

4.2 Map of inventoried stock ponds....35

4.3 Aerial photo showing (a) the entire watershed area and (b) the individual stock pond 4P2....37

4.4 Datasets for (a) land cover and (b) soil....38

4.5 The DEM for Box Elder (a) before reconditioning and (b) after reconditioning....40

4.6 The reconditioned DEM with (a) a false hill in the stream network and (b) the hill smoothed out....41

4.7 The excessively flat area at Box ElderCreek's outlet (a) before correction and (b) after a slope is imposed....42

4.8 The flow direction raster for Box Elder Watershed with each color representing one of the 8 possible directions....43

4.9 The stream network derived from HEC-GeoHMS's default....44

4.10 A watershed delineation error that shows a subbasin border crossing a flow path....45

LIST OF FIGURES - CONTINUED

Figure Page

4.11 The delineated subbasins for the model 46

4.12 100 meter grid cells applied to the watershed..... 48

4.13 Quadrant method schematic from the HEC-HMS Technical Reference Manual..... 51

4.14 Measured incremental precipitation data for (a) West Gage – June 2010, (b) East Gage – June 2010, and (c) West Gage May/June 2011..... 52

4.15 Raster dataset of precipitation for June 16th at 07:30..... 52

4.16 A constructed frequency storm from the alternating block method..... 54

4.17 Curve numbers for Box Elder Watershed..... 56

4.18 The distribution of hydraulic flow lengths for the grid cells..... 58

4.19 An 8-point cross section measured to describe the reach BE_Seg2 for the model 61

4.20 Variables measured to determine the depth and stages of each pond 62

4.21 (a) The assumed geometry for a pond with a single stage-area measurement, and (b) a typical area-stage function used for the ponds..... 63

4.22 (a) A headcut as pond 5P9's outlet, and (b) a low spot as pond 5P3's outlet..... 65

4.23 The culverts at Box Elder's outlet..... 66

4.24 (a) Survey points and (b) drawn cross sections for the areas upstream and downstream of the culverts 67

4.25 Damaged culvert 68

4.26 A cross section with levees and ineffective flow boundaries applied appropriately 70

4.27 Cross sections immediately upstream and downstream of the culverts..... 71

LIST OF FIGURES - CONTINUED

Figure Page

5.1 Rating curve for the gage at the inlet of the Box Elder culverts....72

5.2 A comparison of lumped, distributed, and recorded hydrographs for the precipitation events during June, 2010....75

5.3 The modeled response assuming the precipitation data from May and June 2011 is a single event. 77

5.4 The different k values modeled with a maximum possible initial abstraction ratio of 0.2....79

5.5 Hydrographs from varying initial abstraction ratio slopes....80

5.6 Standard deviation for the peaks of each k value....81

5.7 Hydrographs produced by the different storage coefficient sets represented in Table 5.2 83

5.8 The simulations produced by k = .014 and (a) the initial set of storage coefficients and (b) the R2 set of storage coefficients 85

5.9 The best hydrograph replications for (a) 2011 data and (b) 2010 data 86

6.1 Graph of percent reductions compared to Box Elder Watershed with no ponds for (a) peak flow rate and (b) runoff volume....90

6.2 The hydrographs from varying return intervals and scenarios 92

6.3 Correlation of pond volume and peak flow rate change for a 50 RI storm....96

6.4 Dimensionless parameter sets tested for correlations 98

6.5 A graph for the contributing area parameter set and the corresponding reduction in runoff volume 98

6.6 Percent change in runoff volume plotted against the computed volume coefficient 100

6.7 Dimensionless parameters tested for correlations to change in peak flow rate caused by the inclusion of one pond....101

LIST OF FIGURES – CONTINUED

Figure Page

6.8 The comparison of overall pond rankings and the rankings for every return interval 105

6.9 The rankings for volume runoff influence plotted against the rankings for peak flow rate influence 106

ABSTRACT

The impact of stock ponds on the hydrology of the Northern Great Plains has largely been overlooked despite stock ponds' widespread presence. However, recent conservation efforts have placed a focus on restoring prairie stream systems, and water management decisions require more information regarding the effects of these ponds. This thesis addresses the unknown impacts of stock ponds by modeling Box Elder Watershed located just north of Fort Peck Reservoir in north central Montana. The hydrologic model helped quantify the peak flow rate and runoff volume changes caused by 28 stock ponds on what would have been the undisturbed watershed's flow regime. HEC-HMS was employed to model the watershed. Parameters for the model were abstracted from a GIS and measured in the field. The HEC-GeoHMS extension for ArcGIS 9.3.1 was used to construct necessary model files and create the model components. Measured runoff events from spring 2010 and spring 2011 were used to calibrate non-measurable parameters. To determine the ponds' impacts, frequency storms were run in the model for a watershed with all of the ponds included and a watershed with no ponds included. Results showed that the stock ponds are reducing peak flow rates by 12.66% to 24.08% and reducing runoff volumes by 10.1% to 16.84% depending on the return interval of the frequency storm modeled. In order to apply these results to other watersheds, an attempt was made to find a simplified relationship between pond parameters and an individual pond's influence on the system. This was unsuccessful. The results showed complex model interactions dictating runoff, and some degree of modeling may be required to determine a pond's importance to the hydrology, especially regarding peak flow rate. Finally, the ponds on Box Elder Watershed were ranked in a single list according to their influence on peak discharge and runoff volume. The list will help to prioritize the ponds on Box Elder Watershed for removal since cost and animal water requirements will prevent the removal of all ponds.

INTRODUCTION

Background

The World Wildlife Fund (WWF) is interested in restoring prairie streams on the American Prairie Reserve in north central Montana. Prairie streams provide vital habitat and beneficial processes for several plant and animal species in the area and are critical to successful wildlife conservation. Interest in stream restoration has led the WWF to question the hydrologic effect of numerous stock ponds located throughout the reserve. The unknown influence of the stock ponds provides the motivation for this research.

The hydrology and ecology of the semi-arid landscape of north central Montana has been impacted by agricultural operations (Figure 1.1). While some grains and hay are grown in the region, the majority of the area is considered most suitable for cattle production. This has resulted in the visible alteration of the landscape by the construction of stock ponds to expand livestock grazing range. Because the region is prone to drought, many ephemeral channels have been dammed to store and utilize the limited available precipitation. These stock ponds are ubiquitous in the region and can occur at a density of one to two per square mile. Groundwater typically does not contribute to the water balance of the ponds, and most ponds retain water only on a seasonal basis depending on yearly precipitation amounts. However, a few of the larger ponds can consistently hold water throughout the year. These ponds have likely affected the natural hydrologic cycle of the watershed, but the extent of that change has not been previously investigated.

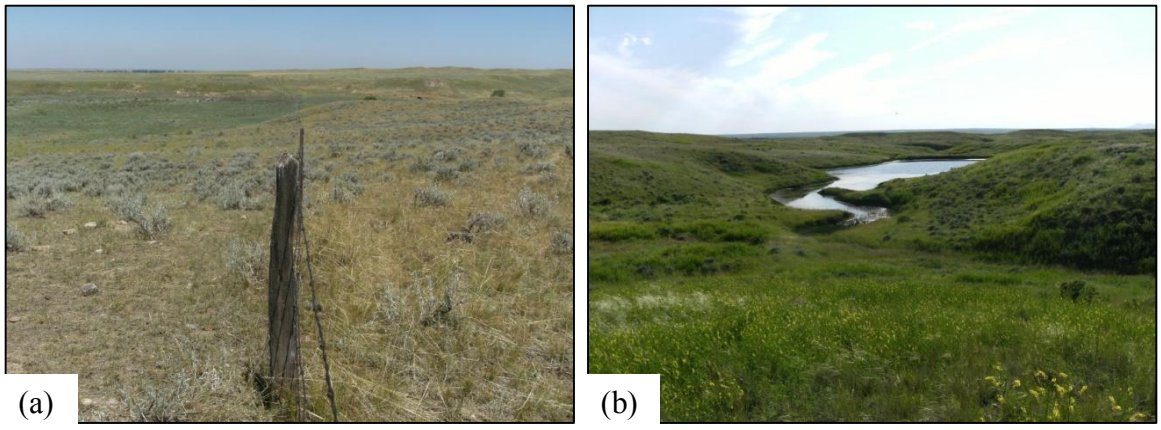

Figure 1.1: Box Elder Watershed; (a) a fence dividing grazed land and land unaffected by grazing and (b) a stock pond.

Few ephemeral watersheds greater than one square mile in the region, including the Box Elder Watershed, have been left in an unaltered condition. Therefore a direct comparison of watersheds with and without ponds is not practical, necessitating the need to model pond removal to determine the ponds' effects. Nevertheless, some general inferences on the influence of the ponds can be made. Stock ponds increase water storage within the watershed and alter the natural hydrologic response of these prairie streams by reducing runoff volume and attenuating peak flows. The magnitude of these changes as well as the impact of these changes on the hydrologic function of these streams remains uncertain, and this study aims to quantify the individual and cumulative effects of stock ponds on the hydrologic regime of the Box Elder Watershed specifically which can serve as a model for other prairie watershed systems.

The Box Elder Watershed was chosen as the study site for an investigation into stock pond effects partly because it has a large percentage of land set aside for wildlife management. Currently 81% of Box Elder is either deeded to the American Prairie

Foundation (APF) or managed by it through blocks leased from the Bureau of Land Management (BLM) or controlled by the CMR National Wildlife Refuge. This better allows for changes in water management to be readily implemented and for the establishment of an experimental watershed.

The WWF and APF, in particular, are motivated to restore this watershed to a more naturally functioning hydrologic state. Concerns over the current state of Box Elder's hydrology include the stock ponds' negative effect on riparian habitat. Stock pond inclusion could be impeding natural processes necessary for seed dispersal. Geomorphic stream changes due to lower flow rates and less sediment in the system may have resulted in new stream and floodplain interactions. Less scouring in the floodplain reduces the size and variability of the riparian zone. A more detailed discussion on the impacts of dams is included in the literature review.

A few projects in the region aim to restore in-stream flows and riparian areas. In-stream dams on two creeks neighboring the Box Elder Watershed have been removed, and native grasses have been re-planted in selected areas. There are plans to observe resultant changes over time, but to date little hydrologic monitoring or modeling has been completed for the area.

While hydrologic restoration is a main priority on the American Prairie Reserve (APR), it is imperative that the watershed still maintain its suitability for a bison herd and other wildlife. Currently, a herd of about 200 bison reside on the reserve and use the ponds as water sources. The herd does not have its historic grazing range to search for water and must have access to water sources year round. The ponds preferred by wildlife

and the ponds having the greatest effect on hydrologic function may or may not be the same, and a compromise between competing objectives may be required regarding which ponds to remove. A developed hydrologic model will provide an immediate tool for ranking the significance of each pond based on its effects on flow rate and runoff volume.

Goals and Objectives

The primary goal of this research was to quantify the cumulative effect of Box Elder Watershed's stock ponds on peak flow rates and runoff volumes through a mathematical model created within the United States Army Corps of Engineers' (USACE) Hydraulic Engineering Center's Hydrologic Modeling System (HEC-HMS). Additionally, determining the effects of individual ponds was a desired outcome of the project so that recommendations could be made regarding their potential removal. These goals were obtained through the following objectives:

1. Field work. Physical characteristics of the ponds and streams were measured for input into the model. Pond measurements were used to develop storage functions and describe the outflow of the ponds. The site was monitored for rain and runoff events for model calibration.

2. Model setup. A geographic information system (GIS) was used to quickly abstract parameters and delineate the watershed. The appropriate files were also created in a GIS for the HEC-HMS model.

3. Model calibration. A rating curve was developed to transform measured stage data into flow rates for calibration. Parameters not related to physical characteristics were then manually adjusted to match observed responses of the watershed.

4. Pond analysis. The HEC-HMS model was run for several scenarios using developed frequency storms. The model was run with all of the ponds in and all of the ponds out to determine the cumulative effects of the ponds. The watershed

was also simulated with only one pond in at a time to determine what, if any, parameters related to the pond could predict their subsequent influence.

5. Pond removal. The model was run with all ponds in except one to determine which individual ponds had the greatest effect on the flow regimes. A list ranking the impact of the ponds was compiled for each of the frequency storms.

LITERATURE REVIEW

In alignment with the purpose and methods of this thesis, the following literature review will examine efforts to describe dam impacts on watersheds, give an overview of the Army Corps of Engineer's Hydrologic Modeling System (HEC-HMS), and discuss methods in hydrologic modeling. Ultimately this review will help to clarify where the Box Elder modeling project stands in the realm of current research and modeling practices.

Dam Impacts on Hydrology

Human development has led to the widespread utilization of river systems through the construction of thousands of dams in the United States. The large prevalence of dams has made them an influential factor regarding streamflow, and it has long been observed that dams can have a significant impact on the dynamics of a catchment [e.g. Graf, 2006; Kingsford, 2000; Williams and Wolman, 1984; Yang et al, 2005]. Investigations into the influence of dams on hydrology have been well documented. While large dams are usually the focus of such efforts, there is a small body of work on the impact of small dams as well [e.g. Callow and Smetten, 2009; Schreider et al 2002; Verstraeten and Prosser, 2008].

The National Inventory of Dams (NID) is maintained by the United States Army Corps of Engineers (USACE) and as of 2009 shows 82,642 dams in the US that are 25 feet or higher and exceeding 15 acre-feet of water, or 6 feet or higher and exceeding 50 acre-feet of water, or dams posing a significant hazard if failure occurs. Dams can be

found on most significant river systems and have had several observable effects. Besides fragmenting watershed areas, these dams often affect the magnitude and frequency of minimum and maximum flows downstream of the dam and alter seasonal baseflows [e.g. Kondolf, 1997; Poff and Hart, 2002; Ouyang et al, 2011]. These flow regime changes have implications for several important environmental processes and stream corridor conditions [Graf, 2006].

The presence of a dam alters other fluvial processes within watersheds as well [Poff and Hart, 2002]. It has been repeatedly shown that large dams reduce the amount of sediment traveling in river systems either through reduced flow or increased storage, and this affects nutrient loads and channel geomorphology [e.g. Anselmetti et al, 2007; Ibanez et al, 1996; Ramesh and Subramanian, 1988; Xu et al, 2006]. Changes in sediment load can alter the channel cross-section morphology in ways hard to predict. A lack of sediment flushing by high flows can force the channel to become wider and shallower, or main channels can become incised because there is less overall sediment in the system. An incised channel can potentially lead to an isolated floodplain even during large precipitation events, and plants dependent on scouring events from high flows will be negatively affected [Sprenger et al, 2002]. Any deviation from the natural channel form leads to new interactions between the stream and floodplain and affects habitat diversity.

While the effects of large dams are well documented, the effects of smaller dams are less studied. The construction of small dams has often been the result of agricultural requirements, and analysis of aerial photographs reveals that they are prolific throughout

many areas in the American west. The high density of small dams indicates that they should be the focus of mitigation methods to reduce fragmentation effects [Chin et al, 2008]. These fragmentation effects include sediment transport and flow fluctuations, and these factors are imperative to how a river's ecosystem functions. Despite small dams' relatively modest capabilities for water and sediment storage, their cumulative effect may culminate in a significant impact on stream hydrology [Nathan et al, 2005].

As previously noted, changing land use and other anthropogenic alterations can result in changes to the amount of sediment transported through a watershed [e.g. Middelkoop et al, 2010; Yang et al, 2011]. However, investigations into changes in sediment loading have often overlooked small reservoirs despite their abundance in certain landscapes [Verstraeten and Prosser, 2008]. Verstraeten and Prosser's [2008] model of small farm dams in Australia indicates that the small reservoirs have a negligible individual effect, but together they may be responsible for a 47% reduction in sediment transport for their modeled subbasins. While this is in part due to the trapping of sediment, it may also be caused by changing flow rates.

While not widely documented, there are a few examples of how constructed small dams affect the subsequent flow rates. Callow and Smetten [2009] showed through several hydrologic indicators that basins unaffected by small dams or diversion banks tend to produce more complex and dramatic hydrographs. Schreider et al [2002] modeled a few catchments containing several small farm dams in the Murray-Darling basin with a lumped model and available stream records. Two of the twelve study catchments showed a notable decrease (up to 10.2%) in mean annual flow due to dam

storage. The results from Schreider et al are consistent with earlier findings from Neal et al [2001] who found that stream flow reductions were directly and significantly related to increases in small dam storage. It is likely that the degree to which flows are affected by small dams is directly related to current climatic conditions [Srikanthan and Neil, 1989]. Flow rates may be negligibly affected during wet years, but they can be dramatically reduced during times of drought.

The studies done on small reservoirs have produced results that point to the need for more thorough investigations. Small dams are so widespread that it is almost certain that they are causing hydrologic altercations to the landscape and affecting the ecosystems they reside in. It will be a multi-discipline effort to discern the effects they have created on the landscape. In general, understanding the magnitude of impacts from different sized dams will lead to better water management strategies.

HEC-HMS

The Army Corps of Engineers' Hydrologic Engineering Center (HEC) created the Hydrologic Modeling System (HEC-HMS) as a versatile runoff modeling software package [USACE, 2000]. It replaces the popular HEC-1 program and is capable of modeling a wide range of watersheds by offering several different mathematical models, all of which are deterministic in nature [USACE, 2000]. Improvements over HEC-1 include a graphical user interface that allows for convenient editing and result viewing [Viessman and Lewis, 2003]. The software is public domain and is often coupled with other models to make forecasts regarding runoff response [e.g. Anderson et al, 2002;

Kang and Ramirez, 2007; McLin et al, 2001]. This section will offer a general overview of HEC-HMS. The specific mathematical models used within HEC-HMS for modeling Box Elder will be covered individually and in greater detail in another section.

HEC-HMS is a valuable tool for forecasting and quantifying the effects of different inputs for a watershed. When compared to field experiments, hydrological models, like HEC-HMS, are more flexible and economical [Li et al, 2007]. Models in general broaden the range of hydrologic investigations through predictive capabilities and can show the sensitivity of a watershed's response when subjected to situations like changing land use, varying climate conditions, or the addition of reservoirs [e.g., Bhaduri et al, 2000; Li et al, 2007; Schulze, 2000]. Beighley et al [2007] used HEC-HMS to study the impacts of urban development and climate changes on California's Atascadero Creek. The study determined urbanization substantially raises peak flow rates and flood risk, and future urbanization will have to take into account careful water planning to mitigate such issues.

HEC-HMS offers model configurations that range from lumped to distributed. Lumped models use composite parameters for large, grouped areas of land while distributed models keep parameters spatially variable. The configuration chosen depends on the end goals of the study and the available data. Generally, lumped models avoid problems with over-parameterization and data limitations, but they may fail to sufficiently explain changing landscapes [Refsgaard, 1987]. Conversely distributed models can deterministically account for varying parameters in the watershed, but describing all of the required parameters accurately can be challenging and

computationally expensive [Legesse et al, 2003]. Specific knowledge of each modeling case must be taken into account when determining how best to represent specific watersheds.

The set up of HEC-HMS enables modelers to select parameters and different mathematical models for each component of the runoff process [Cunderlik and Simonovic, 2007]. It is conceptually set up to represent runoff generation through precipitation loss, direct runoff, baseflow, and channel flow with options for varying degrees of complexity and parameter requirements [USACE, 2000]. The model also gives users options on how to input precipitation.

Precipitation is a necessary input to any hydrologic model, and HEC-HMS recognizes that recent advances in weather monitoring have led to more spatially detailed rain data. Radar data in particular has led to increased resolution for precipitation measurements of many watersheds [Borga, 2002]. HEC-HMS allows for the input of precipitation data in the form of grid based sets [USACE, 2000]. Gridded precipitation data has been used in HEC-HMS with the intention of improving flood forecasting and other hydrologic predictions [e.g. Anderson et al, 2002; Knebl et al, 2004]. In the absence of distributed precipitation data, HEC-HMS has several other options for precipitation input. These include synthetic design storms, gages, or frequency storms [USACE, 2000].

Accounting for precipitation loss is the first interior process that HEC-HMS computes. This is the amount of precipitation that is unavailable for runoff because it is intercepted by the canopy, stored in the soil, or captured in some other manner. The

software is capable of modeling precipitation losses using the Green-Ampt infiltration model, the SCS Curve Number Method, the deficit and constant method, the initial and constant method, as well as the Smith Parlange and Soil Moisture and Accounting methods [USACE, 2000]. The only method listed that is intended for continuous simulation is the Soil Moisture and Accounting (SMA) model [USACE, 2000]. The other models are intended as event-based models only and are not recommended for simulations longer than two weeks [USACE, 2000]. Evaporation is often not modeled during event-based simulations since the amount of precipitation lost in this matter is often negligible for the shorter time period [Cunderlik and Simonovic, 2007].

After calculating precipitation losses, HEC-HMS moves the excess rain (precipitation minus losses) to the subwatershed's outlet using a prescribed translation method. Again, only one distributed method is offered by HEC-HMS, the Modified Clark Method. The other available methods use a lumped approach and include the SCS and Snyder synthetic unit hydrographs, a user specified unit hydrograph, the Clark unit hydrograph, and the kinematic wave model [USACE, 2000]. The kinematic wave model differs from the other methods in that it is based on the physical equations of continuity and momentum while the other models rely on existing gaged data and empirical studies [USACE, 2000].

The resulting flow at the outlet for each subbasin, represented by the direct runoff hydrograph, is routed to the outlet of the watershed by using one of six routing models: kinematic wave, the lag method, Modified Puls, Muskingum, Muskingum-Cunge, and straddle stagger [USACE, 2000]. The models vary in data requirements, but

the simplest routing technique is the lag method as it only translates the hydrograph and does not account for any temporary storage effects [Yawson et al, 2005]. All models are appropriate for use with distributed or lumped setups.

HEC-HMS currently lacks built-in methods to measure uncertainty and perform stochastic modeling [Harris and Hossain, 2008]. The model makes the simplifying assumption that parameters are known and constant. This deterministic setup results in Monte Carlo and other sensitivity analyses being performed manually and on a limited basis. However, there are plans to develop a Monte Carlo tool for HEC-HMS [USACE, 2000]. The inclusion of stochastic methods in HEC-HMS will help to broaden the assessment of results and model structure.

HEC-HMS is a graphic-oriented, hydrologic software program that offers a range of model components. Its user-friendly and flexible setup has led to its widespread use, but its capabilities are still not fully developed. HEC-HMS could benefit from stochastic approaches that look at parameter uncertainty. Despite this weakness, it still provides a valuable deterministic tool for investigating watersheds and predicting the implications of changing landscapes.

Hydrology Models

Several models exist for describing watershed processes. They range from highly complicated physical models to sparse mathematical models, and every type requires varying degrees of computational power. The hydrology models covered in this section are those employed within HEC-HMS for the Box Elder Watershed and are the SCS

Curve Number Method, the Clark Unit Hydrograph, and the Muskingum-Cunge method for routing. The described models simulate excess rain generation, transformation of the excess rain to a direct runoff hydrograph, and the movement of water through the stream network.

SCS Curve Number Method

The SCS Curve Number Method has become a ubiquitous method in science and engineering due to its straight forward conceptual basis of precipitation storage and its computational simplicity. It is a deterministic method based on the catchment properties of antecedent moisture, land use, soils, and surface condition [Ponce and Hawkins, 1996]. The method calculates the amount of rainfall available for runoff and is used by the US Department of Agriculture as a cornerstone model for hydrology and water quality simulations [Garen and Moore, 2005].

The SCS Curve Number method first appeared in 1956 in the National Engineering Handbook (NEH) published by the Natural Resources Conservation Service (NRCS), formally known as the SCS. Its development by a government agency led to a lack of peer review and little documentation on its conceptual origins [Ponce and Hawkins, 1996]. However it filled a void in hydrologic modeling and has come to be used throughout the United States and several other countries.

The SCS curve number method is a lumped, event-based model and comes from empirical studies done on small agricultural watersheds [SCS, 1985]. The method employs the following assumed relationship between precipitation and storage:

$$\frac{F}{S} = \frac{Q}{P - I_a} \tag{21}$$

F = actual retention
S = potential retention
Q = actual runoff
P = precipitation
I_a = initial abstraction

This relationship results in the basic equations used by the model:

$$S = \frac{1000}{CN} - 10 \tag{2.2}$$

$$Q = \frac{(P - I_a)^2}{P - I_a + S} \tag{23}$$

CN = curve number

The model describes the amount precipitation the watershed can store before runoff will commence by the initial abstraction parameter, and this value is taken to be a proportion of the potential retention (Equation 2.4). Usually the initial abstraction ratio is taken as 0.2, but the ratio has been shown to deviate significantly from this value [Ponce and Hawkins, 1996].

$$I_a = \lambda S \tag{24}$$

λ = initial abstraction ratio

These equations lead to a single parameter model that describes how a watershed responds to rainfall. There has been some disagreement on what type of storage is represented by the equations. Ponce and Hawkins [1996] state that the curve number method gives "… a measure of available sub-surface storage…" and has similarities to saturation overland flow. However, Garen and Moore [2005] maintain that it is a mistake

to relate runoff calculated by the curve number method to overland flow, and it has been noted that the curve number method does not compare well to other infiltration theories [Hjelmfelt, 1980]. It may be more appropriate to think of the curve number method as a general quantification of a watershed's ability to abstract rainfall.

There has also been discussion on the curve number parameter. Specifically, the constant nature of the parameter has been called into question [Hjelmfelt, 1991]. Variable watershed conditions like antecedent soil moisture can affect the value of the curve number, and it may be better expressed as a random variable [Hjelmfelt, 1991]. There has also been criticism of the model's extreme sensitivity to curve number. Boughton [1989] noted that runoff can double by a mere 15-20% change in the parameter.

Many of the issues associated with the curve number may be reduced by using the method appropriately. As with most models, the SCS curve number method works best in particular situations. It tends to better predict available runoff when the runoff is a significant portion of the total precipitation [Hjelmfelt, 1991]. It has been advised that if a watershed's curve number is less than 40 another model should be employed [Bosznay, 1989]. Additionally, adjusting the curve number based on antecedent moisture conditions will result in an improved simulation. It should be noted that the method was originally developed for smaller watersheds and should not be applied to large-sized catchments [Ponce and Hawkins, 1996]. Transmission losses can play a larger role in runoff generation for larger catchments, and this alters curve numbers [Simanton et al, 1973].

Overall, the SCS curve number method is a simple and valuable model for expressing available runoff, but it is not without caveats. It should only be applied with careful consideration to both the model's strengths and uncertainties.

Clark Unit Hydrograph

The Clark method [Clark, 1945] describes how a watershed moves excess rain to its outlet. More recently, the Modified Clark method has come into use as a quasi-distributed version of the model for performing this function. The Clark method utilizes basin shape, temporary storage, and timing in order to describe a catchment's hydrologic response [Paudel et al, 2009]. It is a widely accepted method for creating unit hydrographs and has been used in multiple studies [e.g. Knebl et al, 2005; Yusop et al, 2007]. A large degree of its popularity as a transformation method may be attributed to its derivation from hydrologic routing equations and the computational ease with which it is executed [Sabol, 1988].

The method was first introduced by Clark in 1945 and considers conservation of mass in its derivation [Sabol, 1988]. Conservation of mass is used in the form shown below.

$$\frac{dS}{dt} = I_t - Q_t \tag{25}$$

S= storage at time t
I_t = average inflow at time t
Q_t = average outflow at time t

The Clark method also uses the time to concentration and a storage coefficient to calculate the hydrograph resulting from a precipitation event [Wilkerson and Merwade, 2010]. Time to concentration denotes the time for a drop of water to travel from the most

hydrologically remote point in the watershed to the outlet. This parameter is used to determine the timing of the outflow hydrograph. The storage coefficient gives the degree of attenuation in the watershed and prevents the outflow hydrograph from being a simple translation of the inflow hydrograph. A watershed with a large storage coefficient will see a smaller peak flow rate and a longer runoff time when compared to a watershed with a small storage coefficient.

A time-area curve dictates the time discharge histogram before flow is routed through a linear reservoir [Paudel et al, 2009]. The Army Corps of Engineers has developed a smooth function through their watershed studies that describes the time-area curve as a function of the time to concentration of the basin [USACE, 2000]. Relating the time area curve to the time to concentration parameter reduces the model's data requirements, and the relationship is as follows:

$$\frac{A_t}{A} = \begin{cases} 1.414\left(\frac{t}{t_c}\right)^{1.5} & for\ t \leq \frac{t_c}{2} \\ 1 - 1.414\left(1 - \frac{t}{t_c}\right)^{1.5} & for\ t \geq \frac{t_c}{2} \end{cases} \quad (2.6)$$

A= total watershed area
A_t = area contributing to runoff at time t
t_c = time to concentration

Routing the time-area histogram through a linear reservoir allows the method to model attenuation (temporary storage) for the outflow hydrograph. The equation used by the method for linear routing is:

$$Q_t = C_A I_t + (1 - C_A) Q_{t-1} \quad (2.7)$$

Where,

$$C_A = \frac{\Delta t}{R + .5\Delta t} \tag{2.8}$$

R= watershed storage coefficient

The Modified Clark method also uses these basic equations but utilizes them in a grid form to account for spatial variations in precipitation and precipitation loss in the watershed [Paudel et al, 2009]. Also the travel time of each grid cell to the outlet is taken into account. In HEC-HMS a single time to concentration and storage coefficient is required for both the Clark and Modified Clark methods, but the Modified Clark method solves for new time to concentration and storage coefficients for each cell [USACE, 2000]. The Modified method uses the following ratios based on distance to determine individual cells' time to concentrations and storage coefficients:

$$T_{cell} = T\frac{d_{cell}}{d_{max}} \tag{29}$$

$$R_{cell} = R\frac{d_{cell}}{d_{max}} \tag{2.10}$$

T_{cell} = time to concentration of cell
T = time to concentration of the watershed
d_{cell} = hydraulic distance of cell to the outlet
R_{cell} = storage coefficient of cell
R = storage coefficient of the watershed
d_{max} = maximum hydraulic distance in the watershed to the outlet

The previous equations require the hydraulic distance between each cell and the subbasin's outlet be known. HEC-GeoHMS calculates cells' hydraulic distance based on a previously created flow direction raster and compiles the results in a grid cell parameter

file, a text representation of the cells' physical properties that the model uses for calculations.

The parameter most difficult to estimate is the storage coefficient, and this difficulty has been one of the main obstacles in preventing widespread use of the Clark method [Ahmad et al, 2009]. The storage coefficient differs from the time to concentration in that it cannot be abstracted from physical properties of the watershed [Kull and Feldman, 1998]. Gaged data can be used to derive the parameter graphically since it is described as the flow at the inflection point on the receding limb of the hydrograph divided by the time derivative of flow at that point [USACE, 2000]. However a major weakness of this method is the possible variations in hydrograph shape for different precipitation events [Ahmad et al, 2009; Sabol, 1988]. The increased computational power of computers has led to optimization schemes being increasingly employed as an alternative to graphical methods to determine the storage coefficient [Ahmad et al, 2009]. Regionalization techniques have been used with a fair amount of success to estimate the parameter [Straub et al, 2000]. The challenges associated with determining the storage coefficient demonstrate the method's dubious suitability for completely ungaged basins.

Despite the difficulties with estimating the storage coefficient, the Clark method has many advantageous qualities. The use of hydrological routing equations makes for a very mathematically efficient method [Sabol, 1988]. This computational efficiency allows for a distributed form of the model, and this setup may be used with spatially varying precipitation and precipitation loss. The Modified Clark Unit Hydrograph also

comes from widely used hydrologic principles, and this increases its acceptability for a wide variety of watersheds. Overall, the method is a useful analytical technique to transform excess rain into a runoff hydrograph.

Muskingum-Cunge

Channel routing is an important component of a hydrologic simulation, and several models have been developed to perform this function. The Muskingum-Cunge method [Cunge, 1969] is one such model that has a wide range of applicability and provides reasonably accurate results when deriving the outflow hydrograph from a given inflow hydrograph and channel properties [Barry and Bajracharya, 1995].

The Muskingum-Cunge method's foundations come from the kinematic wave approximation of the St. Venant equations, but unlike the kinematic wave method it contains modifications to account for attenuation [Akan, 2006]. The Muskingum-Cunge routing method was developed to overcome some of the main issues of the Muskingum technique, namely the difficulty of estimating Muskingum's parameters K and X for ungaged basins [Ponce et al, 1996]. It is acceptable to use for ungaged basins because Muskingum-Cunge requires only readily measurable reach characteristics such as slope, channel shape, and the Manning's n value.

Channel routing using Muskingum-Cunge uses continuity and the diffusion form of the momentum equation in the following form [USACE, 2000]:

$$\frac{\partial Q}{\partial t} + c\frac{\partial Q}{\partial x} = \mu\frac{\partial^2 Q}{\partial x^2} + cq_L \qquad (2.11)$$

Q = flow rate
c = wave celerity

μ= hydraulic diffusivity
q_L= lateral inflow

With the following definitions used for c and μ:

$$c = \frac{dQ}{dA} \tag{2.12}$$

A = area

$$\mu = \frac{Q}{2BS_0} \tag{2.13}$$

B = top width of water surface
S_0 = channel slope

This is then combined with the classic Muskingum equation to produce the equation below.

$$O_t = \left(\frac{\frac{\Delta t}{K} + 2X}{\frac{\Delta t}{K} + 2(1-X)}\right) I_{t-1} + \left(\frac{\frac{\Delta t}{K} - 2X}{\frac{\Delta t}{K} + 2(1-X)}\right) I_t + \left(\frac{2(1-X) - \frac{\Delta t}{K}}{\frac{\Delta t}{K} + 2(1-X)}\right)(O_{t-1}) + \left(\frac{2\frac{\Delta t}{K}}{\frac{\Delta t}{K} + 2(1-X)}\right)(q_L \Delta x) \tag{2.14}$$

Where,

$$K = \frac{\Delta x}{c} \tag{2.15}$$

$$X = \frac{1}{2}\left(1 - \frac{Q}{BS_o c \Delta x}\right) \tag{2.16}$$

The Muskingum-Cunge method has been used in numerous studies to adequately predict flood wave propagation [e.g. Ponce et al, 1996; Takeuchi et al, 1999; Tewolde and Smithers, 2006]. However, the model has limitations in that it cannot account for effects from backwater due to its uniform flow assumptions [Takeuchi et al, 2000]. The Muskingum-Cunge method may also provide an inadequate description for flow in the

floodplain, but this is endemic to most hydrologic routing techniques [USACE, 2000]. These weaknesses should be taken into account when considering application of the Muskingum-Cunge method to specific basins and rain events.

Despite these obstacles, the Muskingum-Cunge method is a valuable routing technique for hydrologic models. It maintains the computational simplicity of the Muskingum method but has a greater range of applicability by relating the K and X parameters to physical characteristics [Tewolde and Smithers, 2006]. In addition, it is a grid independent solution that foregoes many of the problems of numerical diffusion associated with other kinematic wave models [Ponce, 1991]. These strengths allow it to work well for a wide range of hydrologic models.

GIS and Hydrologic Modeling

Hydrologic modeling has undergone large advancements from the incorporation of spatial data software, and the use of geographical information systems (GIS) has become commonplace in the preparation of data intended for use in a hydrologic model. GIS has greatly expedited analysis of watersheds of all sizes and has been shown to be very adaptive to the needs of the hydrologic modeler.

A Digital Elevation Model (DEM) provides the base for most investigations in hydrology [Li and Wong, 2010]. A DEM is in a raster form (a grid setup) or a triangular irregular network (a vector format) and represents ground elevation data. The United States Geological Survey (USGS) has developed several elevation maps at different resolutions, and their data is a part of the National Elevation Dataset (NED). This is a

seamless data set and is available free to the public. Thirty meter resolution is available for the entire United States, and 10 m resolution is available for much of the United States. Finer resolutions are available through Light Detection and Ranging (LiDAR) technology. The resolution refers to the grid size of a raster, and a 10 meter DEM contains a single elevation value for a 10 meter by 10 meter square on the earth. The grid size of a raster data set has obvious implications to the outcomes of hydrological models that include accuracy and evaluation of parameter values.

Several studies have found hydrological models to be result-sensitive to the resolution of the DEM used for parameter abstraction [Wu et al, 2008; Liu et al, 2005; Zhang and Montgomery, 1994]. Slope, watershed area, flow path, and upslope area have all been shown to have non constant values with varying DEM resolution [Wu et al, 2008]. Consequently, these parameters have been studied in order to better quantify their relationship with a DEM. For example, higher resolution DEMs tend to give steeper slopes [Hill and Neary, 2005], and these steeper slopes will generally produce higher peak runoffs. Slope is used as a primary descriptor of watershed responses in a considerable number of models, such as TOPMODEL, and its value is important for result accuracy [Beven and Kirkby, 1979]. Watershed area, flow path, and upslope usually have smaller values when derived using DEMs of lower resolution, and these parameters can also affect runoff values [Wu et al, 2008]. Smaller values may be due to the fact that coarser DEMs do no pick up subtle ridge lines and show an increased number of flat surfaces on the terrain [Garbrecht and Martz, 1997]. Low relief areas may be more susceptible to errors produced by low resolution DEMs. Wu [2008] studied the

abstraction of important topographic characteristics from different resolution DEMs. Flow accumulation was derived for two watersheds with one of the watersheds having what can be classified as low relief terrain. The low relief watershed experienced a much larger increase in percentage of zero flow accumulation cells as the resolution of the DEM decreased when compared to the watershed with greater topographic variation. Overall, DEM resolution can have a large impact and is necessary to consider when creating a hydrologic model.

Another important aspect of a DEM to examine is its source. Different sources do not share accuracy statistics in horizontal and vertical directions, and these accuracy variations can affect the outcomes of a runoff model [Li and Wong, 2010]. While the NED is the primary source of DEMs for users of GIS systems in the United States, LiDAR data and Shuttle Radar Topography Mission (SRTM) are also prevalent sources. These sources construct DEMs using different interpolation methods which result in varying precision [Wu et al, 2007]. This may be one reason why hydrologic studies do not always agree with one another and may be difficult to replicate [Li and Wong, 2009]. Li and Wong [2009] completed a study in which they found that flood simulation differences were more dependent upon the source of the DEM, and drainage network extraction differences were more closely related to DEM resolutions. They concluded complex relationships dominate DEMs and hydrologic results. Despite inconsistencies and possible errors introduced by DEMs, they continue to be an important source for parameter abstraction.

Several algorithms have been created for a DEM with the intent of deriving watershed parameters. A DEM is commonly used to delineate watershed areas, and many software programs now provide a tool that automates the process. Most spatial analyst tools delineate watersheds using algorithms that use the flow path. The algorithms systematically work to distribute water to lower elevations [Wu et al, 2007], and ultimately show the outlet for the path that a drop of water follows. The nearest-neighbor descent model, also known as the D8 method, is a popular model that moves water from one cell to its neighbor with the largest slope [Wu et al, 2007]. This means that there are eight possible flow directions. The distance from the center of a cell to the center of its neighbor is also taken into account [Wu et al, 2007]. Hec-GeoHMS and NRCS GeoHydro are examples of software programs that utilize parameter extraction algorithms extensively.

The errors that resolution and source introduce into a DEM make it difficult to reflect known hydrology. Several methods have been developed to correct a DEM so that stream networks and other parameters derived from the DEM reflect actual observations. These correction methods are especially utilized when working with low detailed DEMs or low relief terrain.

One problem that commonly presents itself is that of defining a proper watershed boundary using GIS algorithms. Low resolution DEMs often show large areas of flat surface even through truly flat surfaces are rare in nature [Garbrecht and Martz, 1997]. This is due to an insufficient resolution DEM not discerning small changes in elevation [Vieux, 2004]. Problematic depressions can also occur. Depressions and flat slopes cause

slope-based algorithms to report false watershed areas since water stagnates during the execution of the algorithms and the flow direction is indeterminate [Garbrecht and Martz, 1997].

The problem can be partially resolved by burning in a vector stream data map. This process involves decreasing DEM elevation values of converted vector to raster stream grid cells [Maidment and Djokic, 2000]. While running a flow path algorithm on a DEM that has undergone stream burning, flow paths eventually reach a grid cell that has been trenched, and the flow is forced to stay within the defined stream network. Stream burning ensures that the DEM will provide results that are coincidental with a known channel system [Kenny et al, 2008]. There are more complicated methods of stream burning such as fitting the elevation of the stream grids to an exponential curve with the lowest elevation being that of the pour point [Kenny et al, 2008]. This can result in some improvement in watershed boundary determination. Stream burning is not without caveats. The method can introduce parallel streams and affect slope calculations [Callow et al, 2007]. It is important to realize that modifying a DEM can alter slope averages, stream lengths, and watershed areas, and change subsequent hydrological analysis [Callow et al, 2007]. Stream burning also does not address the issue of depressions in the DEM. Several programs have been created to rid a DEM of these sinks.

Depressions in DEMs are more often due to resolution inaccuracies on flatter terrain than due to the natural landscape [Wang and Liu, 2006]. Surface modification is an important step in DEM preparation so that the DEM correctly shows flow paths.

ArcGIS, GRASS, Hec-GeoHMS all have a fill tool that helps smooth the DEM surface and get rid of problematic depressions. These tools work by scanning the DEM for areas in the terrain that are surrounded on all sides by greater elevations. The sink elevation is then raised to match the next highest elevation, effectively smoothing out the depression. Filling a DEM can inadvertently introduce more flat surfaces onto the terrain, but relief can be forced upon the flat areas [Kenny et al, 2008]. Stream burning and sink filling are two of the most common DEM correcting methods used, but variations of these techniques have also been employed to produce a correct hydrological DEM. Modifying a DEM usually results in a better source for watershed delineation when compared to a raw, unaltered DEM [Callow et al, 2006].

DEMs are a valuable source of information when used with GIS. Several techniques, such as stream burning and sink filling, have been developed to reduce resolution and data source errors and improve the information obtained from DEMs. However, they are not without their limitations and must be used critically. While GIS's computation power has replaced tedious methods for determining watershed parameters, it is often hindered by a lack of refined data. DEMs have become an important part of describing a watershed, but they require a large amount of attention when preparing a hydrologic model.

STUDY SITE

The following chapter provides a description of the Box Elder Watershed and the monitoring of rain and runoff events. In addition to the climate characteristics of the area, the location and general physical attributes of the catchment are described. The discussion of monitoring rain and runoff includes installed gage locations and issues with monitoring.

Site Description

The drainage area of Box Elder Creek resides in the glaciated Northern Great Plains in Phillips County of Montana, USA (47.72º N, 107.78º W). The watershed lies approximately fifty miles south of the town of Malta and is just north of the Fort Peck Reservoir on the Missouri River (Figure 3.1). The total area encompasses about 23 square miles with elevations ranging from 2280 to 2770 feet above sea level.

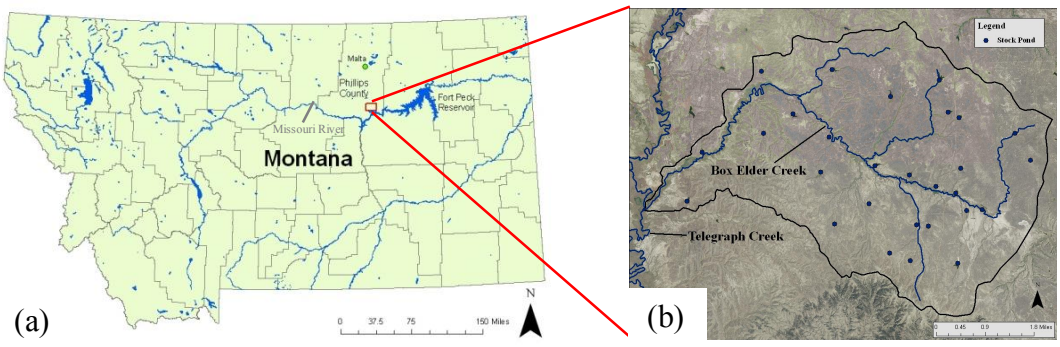

Figure 3.1: Box Elder Watershed; (a) location within Phillips County, MT and (b) the current network of stock ponds.

The ephemeral Box Elder Creek drains into the more significant Telegraph Creek, a tributary that feeds into the Missouri River. Box Elder Creek has historically flowed less than two weeks each year, but the last two years have seen an exception to this trend with the stream experiencing periods of flow of up to a month. The stream is marked by a meandering channel that is incised in some locations and a channel bed consisting of grass, clay, or gravel that alternates with sections of purely vegetative bottom (Figure 3.2). Deep pools and head cuts are also prevalent throughout the stream.

Tributaries of Box Elder Creek typically have vegetated channel beds and flow only after significant storms. The majority of stock ponds located in Box Elder reside on these tributaries, but one pond has been built directly on the eastern end of Box Elder Creek. There are currently 28 stock ponds in the Box Elder catchment. The stock ponds disconnect about 30% of the watershed's area, but much of this is due to the one pond built directly on Box Elder Creek. Without this pond 17% of the watershed would be disconnected by storage structures.

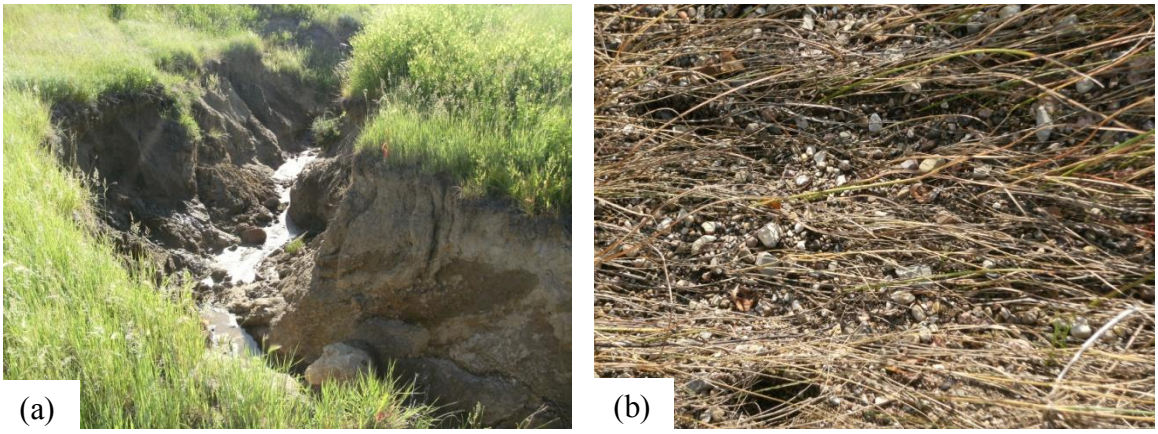

Figure 3.2: Box Elder Creek; (a) an incised section of the channel and (b) a gravel section of channel substrate.

Initial inspection of the watershed led to the identification of six main subbasins containing similar landcover and topography for analysis (Figure 3.3). Vegetation on Box Elder Watershed is characterized by sagebrush, prairie short grass, and other types of brush. Existing soils are the result of continental glaciations and are predominately clays belonging to C and D hydrological soil groups. They tend to drain poorly and produce high runoff yields, resulting in a highly responsive and flashy hydrology. Generally rolling hills and flat expanses account for most of the topography, but there is considerable relief toward the southern border.

The catchment's semi-arid designation means the area often undergoes long periods without rain. The nearby Telegraph Creek receives an average of 11.26 inches of rain annually, and winter snowfall is usually modest at less than 30 inches [DNRC, 1968]. Most runoff volume occurs during the months of May and June when the majority of the yearly precipitation occurs and which, in some years, may be augmented by snowmelt.

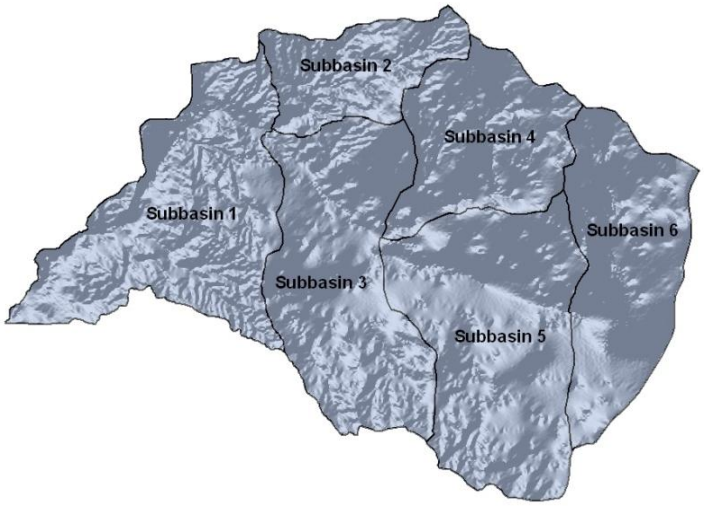

Figure 3.3: The main Box Elder subbasins containing similar topography and land cover.

Site Monitoring

Obtaining precipitation and runoff data for the Box Elder Watershed was an important requirement in developing a hydrologic model for the site. Real-time runoff data provides the basis for parameter calibrations and helps to assess the appropriateness of the model structure. Unfortunately, the area has a limited and intermittent history of being monitored, and this restricted the amount of available precipitation and stream flow data to that acquired over this study's duration.

Since radar data is not available for the area, rain gages were placed in three locations. However, only two gages provided usable data and are shown in Figure 3.4. Budget constraints and equipment malfunctions prevented setting up a more spatially distributed network. The project utilized the popular type of rain gage known as a tipping bucket rain gage. Specifically the RainWise model RGP industrial tipping bucket rain gage was used and provided data at a 0.25 mm resolution. As with any piece of monitoring equipment, tipping bucket rain gages are known to have their disadvantages. Wind-induced undercatch or wetting-evaporation losses have been extensively noted as sources of error for tipping bucket gages [Ciach, 2003]. Despite the possible under-reporting of precipitation events, tipping bucket gages provided a convenient and cost effective tool for monitoring the site.

In addition to rainfall monitoring, a stage gage was installed at the culverts near the outlet of Box Elder Creek and at a single culvert about five miles east. The installed gages were temperature compensating WT-HR TruTraks from Intech Instruments, Ltd. and record water stage at specified time intervals.

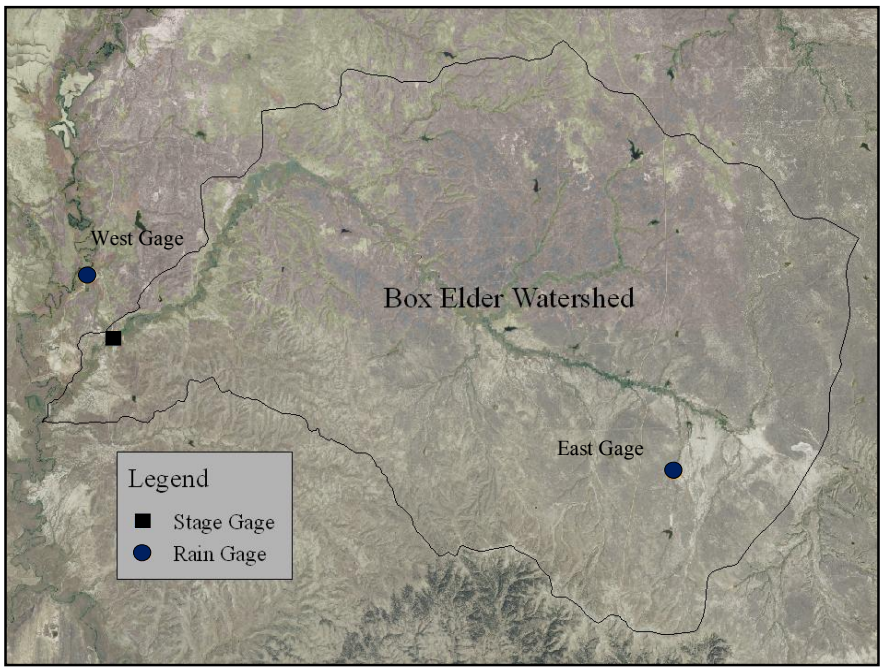

Figure 3.4: Box Elder Watershed monitoring gages.

The Box Elder Watershed provided many challenges in attempting to establish a working network of gages. Throughout the duration of the project regular gage maintenance was difficult to perform because of Box Elder's remote location, and clogged tipping buckets were a common occurrence. Heavy flooding events during spring of 2011 washed away the upstream culvert's gage and only the data from the gage at the outlet could be utilized. These practical limitations negatively affected usable rain data and raised concerns of the spatial distribution of data.

METHODS

This chapter provides descriptions of the methods employed for building the hydrologic model of Box Elder Watershed. Information on fieldwork, data preprocessing, and model construction within HEC-HMS is presented. The development of a rating curve for the stream is also discussed.

Stock Ponds

Modeling the stock ponds effects on flow regimes required a thorough inventory of all stock ponds currently in Box Elder Watershed. Stock ponds for the general area usually occur at one to two per square mile.

The reservoir survey identified 28 stock ponds within Box Elder Watershed on a combination of land owned outright by the American Prairie Foundation, or Bureau of Land Management blocks, or land belonging to the CMR National Wildlife Refuge. The stock ponds were identified mainly from aerial photographs since the water rights records provided by the Department of Natural Resources and Conservation (DNRC) were found to be incomplete. Field work subsequently verified the aerial photo observations. While confirming the location of stock ponds, it was discovered that one pond was “blown out” and a few others had significant damage in the form of headcuts at the outlet (Figure 4.1).

Figure 4.1: Headcut at the outlet of pond 2P1.

The map below displays the results of the stock pond survey and the individual pond names (Figure 4.2). Names correspond to the subbasin number followed by a pond number. For example, 6P2 is the second pond in subbasin 6.

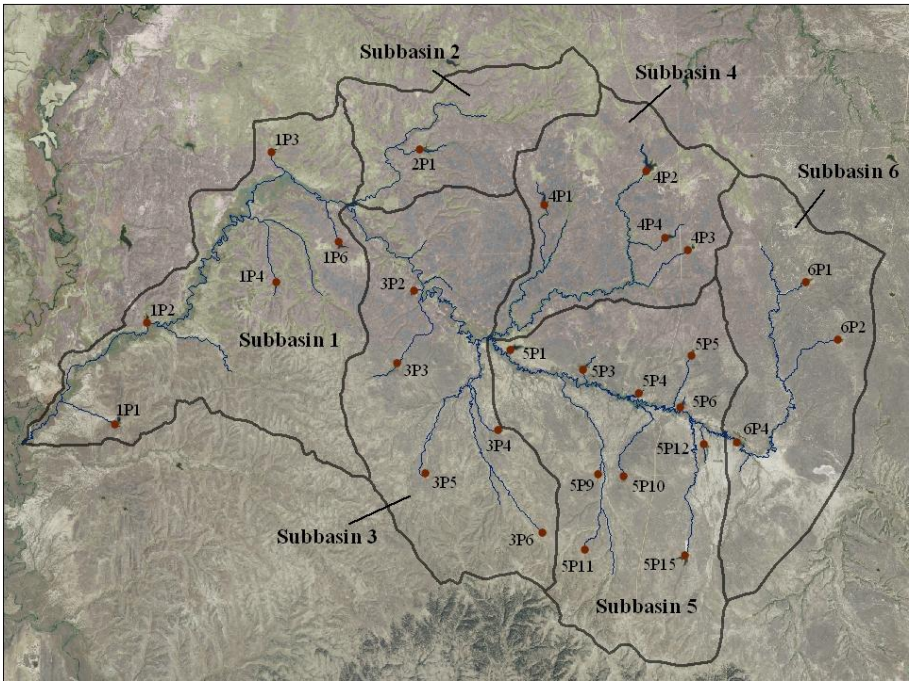

Figure 4.2: Map of inventoried stock ponds and the associated subbasins.

GIS Data

GIS based data played a prominent role in model construction and facilitating parameter abstraction to describe water flows in the watershed. This section will discuss the main datasets used for the Box Elder project. A data dictionary is provided in Appendix A.

One of the most important GIS datasets used for describing the hydrology of Box Elder Watershed was the digital elevation model (DEM). A DEM provides the elevation of individual grid cells covering an area of interest. It serves as the input for several algorithms determining flow directions, watershed boundaries, and hydraulic travel lengths. The 10-meter resolution DEM used for Box Elder Watershed was from the National Elevation Dataset (NED) developed by the United States Geological Survey (USGS).

Aerial photos were used to help identify stock ponds within the watershed and to refine the watershed boundaries determined from the DEM. Aerial photos used for this project came from the USDA-Farm Services Agency aerial photography field office and were accessed through the Montana State Library Natural Resource Information System (NRIS). The photos are orthorectified with a resolution of 1 meter.

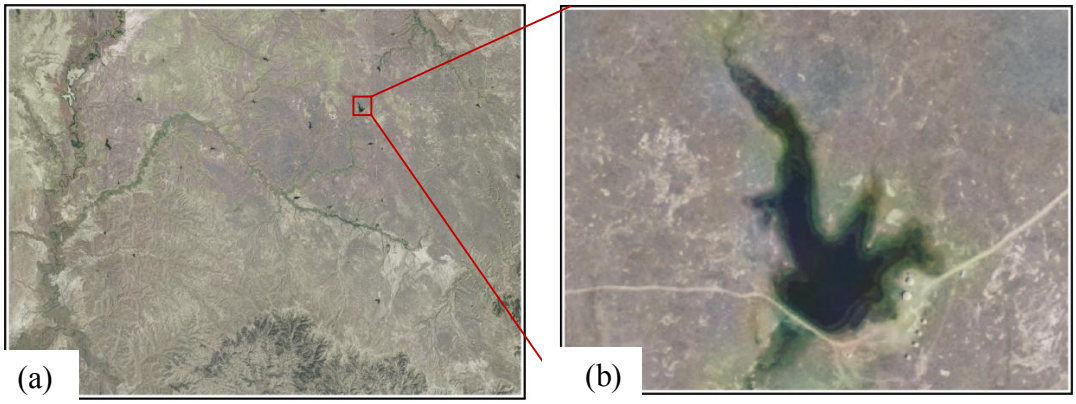

Figure 4.3: Aerial photo showing (a) the entire watershed area and (b) the individual stock pond 4P2.

The representation of the watershed's response to precipitation events required soil and land cover information. Datasets describing these characteristics were accessed through NRIS. The soil map (1:24,000 scale) was developed by the National Cooperative Soil Survey through the U.S. Department of Agriculture and the NRCS and presents one of four possible hydrologic soil groups for every map unit (Figure 4.4b). Hydrologic soil group was the only soil property required for this project. The land cover data set was published by the Wildlife Spatial Analysis Lab of the University of Montana in 1998 and shows land cover at a resolution of 90 meter grid cells (Figure 4.4a).

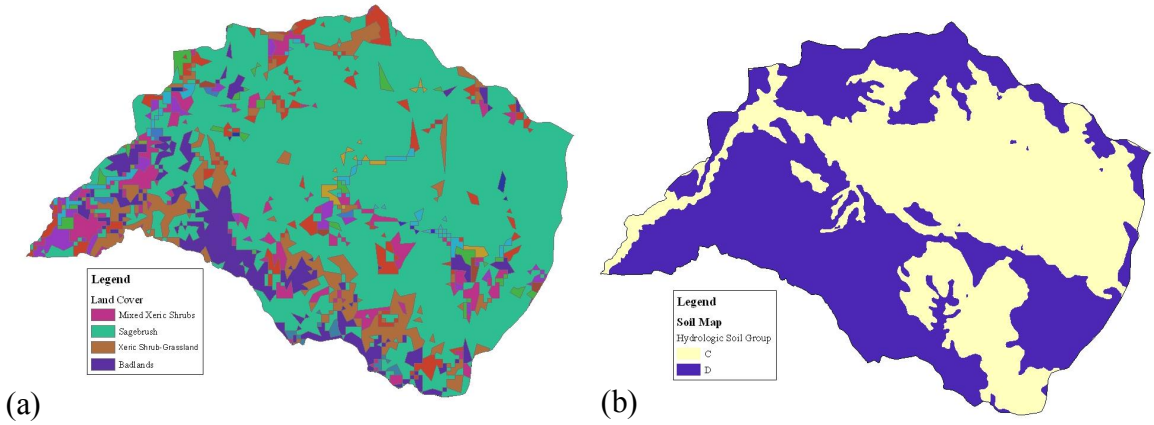

(a) (b)

Figure 4.4: Datasets for (a) land cover and (b) soil. The datasets were used for determining curve numbers for the watershed. Only the four most prevalent land cover types are shown on the legend.

HEC-GeoHMS

The United States Army Corps of Engineers (USACE) developed the Geospatial Hydrologic Modeling Extension (HEC-GeoHMS) with the Environmental Systems Research Institute (ESRI) and the University of Texas in order to use raw data contained in a DEM to form a stream network that can be used in the USACE's hydrologic modeling software (HEC-HMS). Since its inception in 2000, several other versions have been released because of continued development by the USACE and ESRI to update and improve its abilities. The program must be used within ESRI's ArcGIS 9.3.1, a geographical information system (GIS) software commonly used for visualizing and analyzing spatial data.

Running HEC-GeoHMS requires installing the Water Utilities Application Framework, ArcHydro Tools, and the XML Data Exchange Tools. These programs are utilized, in addition to HEC-GeoHMS, to analyze spatial data and create necessary

datasets for a hydrologic model. HEC-GeoHMS also relies on ArcGIS's spatial analyst extension for its raster processing capabilities.

The HEC-GeoHMS algorithms build on the aforementioned software programs to quickly and efficiently abstract watershed characteristics, delineate watershed boundaries, and convert data into a form that is compatible with the HEC-HMS software. It effectively expedites model creation and reduces possibilities for human error. The program is also used to create the necessary files to form a distributed model setup.

Terrain Preprocessing

Terrain preprocessing prepared Box Elder's raw data for parameter abstraction and preceded model construction. Preprocessing is a necessary series of steps that corrects common errors in digital elevation models (DEMs), improves the accuracy of derived model data, and creates datasets necessary to depict how water flows in a basin. All terrain preprocessing steps were completed through the ArcHydro toolbar.

The first algorithms executed in terrain preprocessing worked to hydraulically correct the watershed's DEM. Correcting Box Elder's DEM was especially necessary since its 10m resolution was too course to adequately represent how water travels within the basin's flat terrain. The DEM forms the basis for most datasets created in HEC-GeoHMS, and its accuracy in describing the hydrology is extremely important to overall model effectiveness.

Hydraulically correcting Box Elder's DEM began by hand-drawing water flow paths from aerial photos. The raster cells coinciding with the paths determined which cells would be adjusted by the surface reconditioning tool. Surface reconditioning is an

advanced form of stream burning, a technique that improves watershed delineations and flow path calculations. While stream burning is often necessary for better parameter abstraction, parallel streams and islands can be falsely formed [USACE, 2009]. Surface reconditioning helps to eliminate these possible issues by changing the elevations of the cells bordering the stream to slope down toward the channel. Surface reconditioning for Box Elder Watershed adjusted the elevations for up to two cells (20 meters) on each side of the drawn network. The result of a surface reconditioned DEM for Box Elder is shown in Figure 4.5.

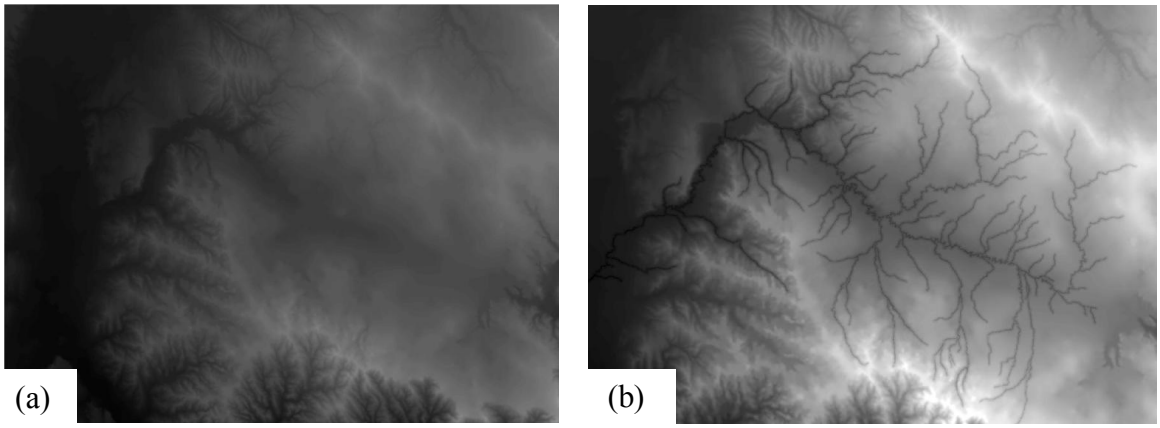

Figure 4.5: The DEM for Box Elder (a) before surface reconditioning and (b) after surface reconditioning. The darkened raster cells of the surface reconditioned DEM indicate that their elevation values have been reduced and show increased differentiation.

The next step in developing a usable DEM was to fill in existing depressions, also known as sinks, to prevent water from stagnating during flow calculations. ArcHydro's "Fill Sinks" algorithm was applied to the surface reconditioned DEM to remove the troublesome depressions. While the ArcHydro preprocessing toolbar does offer several

other DEM preparation tools, filling a DEM's sinks is one of the few that is deemed necessary by HEC-GeoHMS for all DEMs.

After making these improvements, an unexpected problem was found in the DEM. Raster cells representing Box Elder Creek just upstream of the outlet indicated a physically impossible "hill" within the channel. Since the hill would have implications for watershed delineations, the raster calculator was utilized to remove the erroneous hill. An if/then statement was written in the raster calculator to isolate the problem area and to change the cells' elevations to match that of the first cell directly upstream (Figure 4.6).

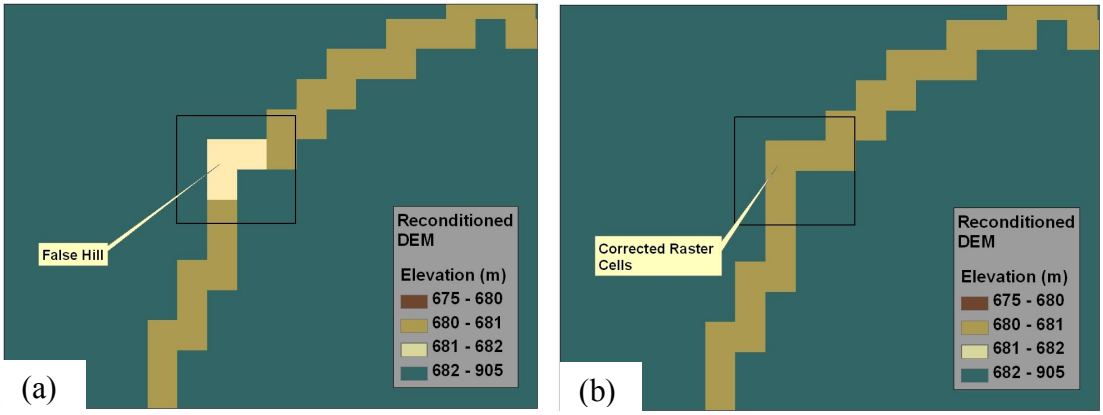

Figure 4.6: The reconditioned DEM with (a) a false hill in the stream network and (b) the hill smoothed out. The hill occurred just upstream of Box Elder's outlet.

The final issue requiring modification was a low relief portion of the stream network being depicted as completely flat by the DEM. The DEM showed no elevation change at the outlet, and flow direction calculations would have trouble moving water through this area. The problem was solved by imposing a slope on the raster cells that contained the excessively flat area (Figure 4.7). A couple of steps were required before this could be accomplished. The ArcHydro toolbar contains a function that adds a linear

slope to a defined line segment in vector form. This function was run on the isolated flat portion of the drawn stream network, and the subsequent sloping line was then converted to a raster. The imposed slope was incorporated into the DEM by combining the newly created stream raster segment and the DEM in ArcView's raster calculator.

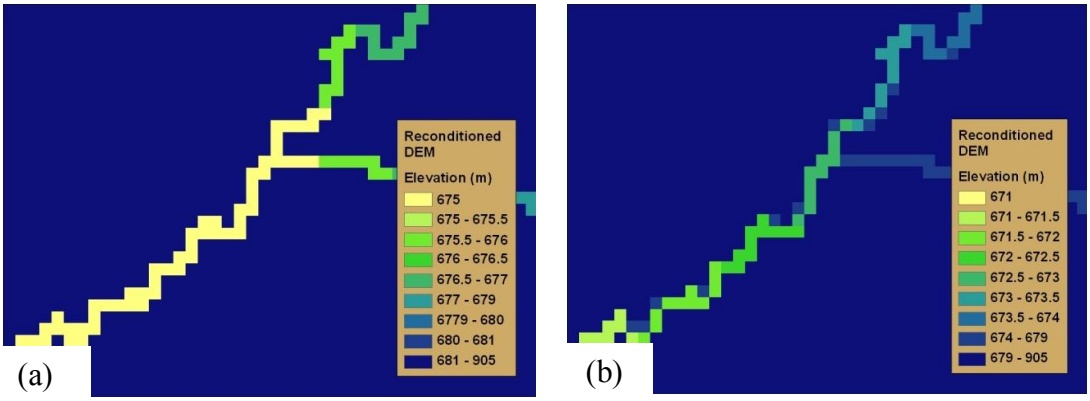

Figure 4.7: The excessively flat area at Box ElderCreek's outlet (a) before correction and (b) after a slope is imposed.

After the DEM was corrected to better represent how water flows, particular datasets had to be created for deriving watershed characteristics. These included the flow direction raster, the flow accumulation raster, and the stream network as abstracted from the preceding layers. The flow direction raster was created first since it is a required input for the flow accumulation layer (Figure 4.8). The flow direction layer is derived from the hydraulically corrected DEM. ArcHydro calculates flow directions by moving water in the direction of steepest descent based on the cells' elevations. A value is assigned to each cell based on which direction water moves from that cell.

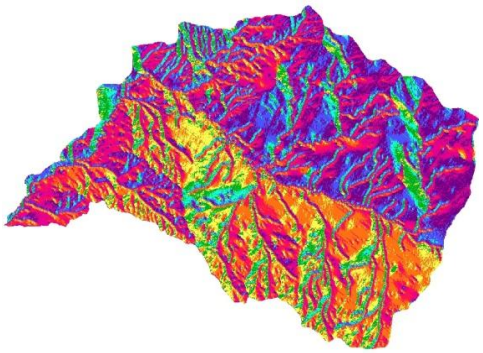

Figure 4.8: The flow direction raster for Box Elder Watershed with each color representing one of the 8 possible directions.

The flow accumulation layer was created next. It determines for every cell in the watershed how many cells are upslope. This was a necessary dataset for abstracting Box Elder's stream network since a user-specified number of upslope cells determines whether or not a cell is included as part of the network.

Specifying the upstream area that initiates a channel was difficult to determine. The literature provided only marginal help in choosing that area for Box Elder Watershed. There are regional techniques [Montgomery and Dietrich, 1989], but few studies have been completed for north central Montana. Tarboton et al [1991] created a method for estimating a stream's required contributing area based solely on a DEM, but the poor quality of Box Elder's DEM made the method impossible to apply. Ultimately, ArcHydro's default was used to abstract the stream network. It dictates that the upstream area necessary to start a stream is 1% of the total watershed area. The resulting stream network was manually edited at a later stage in model development to correspond with field observations and the fact that semi-arid and flat

areas usually require more upstream area to start a channel [Montgomery and Dietrich, 1988]. Figure 4.9 shows the stream network as abstracted using the default method.

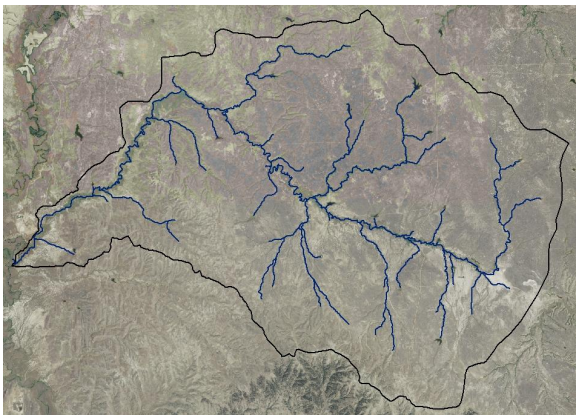

Figure 4.9: The stream network derived from HEC-GeoHMS's default.

Subbasin Delineation

The next step in developing the model was subbasin delineation. Subbasin delineation was completed through ArcHydro and split the watershed into smaller areas for analysis. ArcHydro's delineation function automatically creates a separate subbasin for each stream segment, but this initial delineation may be modified in HEC-GeoHMS to increase or decrease the number of catchments. Editing the subbasins for Box Elder was especially necessary because a subbasin for each stock pond had to be included, errors existed in the automated delineations, and subbasins had to be combined to pare down the total number of catchments to be modeled.

Editing the subbasins was done through the basin processing tools in HEC-GeoHMS. The tools offer the means to merge subbasins, divide subbasins at specific points, and merge river segments. The dividing subbasin tool was especially necessary in

forming each stock pond's contributing area. The tool allows the user to pick a point along the stream network, and the program will delineate a subbasin draining to that point. This was completed for each of the 28 stock ponds with the reservoir location acting as the subbasin's outlet.

Despite reconditioning the Box Elder DEM and filling in its sinks, some errors were discovered in the subbasin delineations (Figure 4.10). A few subbasin borders crossed flow paths identified on aerial photos, and these errors were corrected by manually editing the basin shapefile. Manual edits are not typically required for HEC-GeoHMS projects, but the low relief terrain of the Box Elder watershed mandated extra attention.

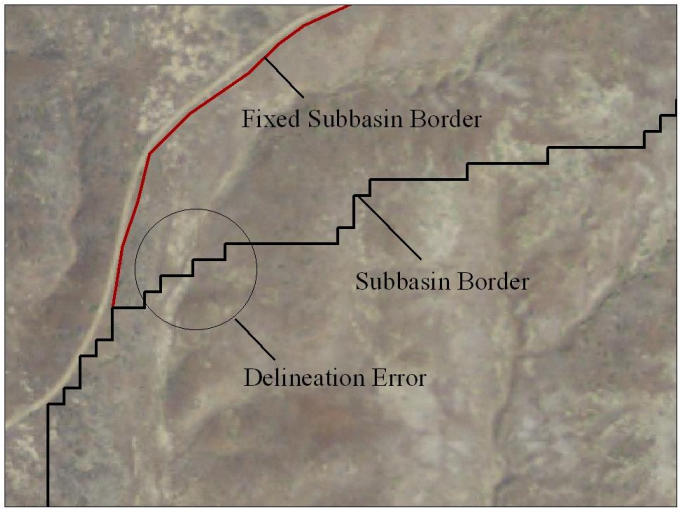

Figure 4.10: A watershed delineation error that shows a subbasin border crossing a flow path. This error was caused by inaccuracies in the course DEM.

Subbasins not belonging to stock ponds or gage sites were typically merged to prevent an unmanageable number of subbasins. However, the existence of 28 stock

ponds still resulted in a fairly divided watershed. Figure 4.11 shows the ultimate configuration of Box Elder's subbasins.

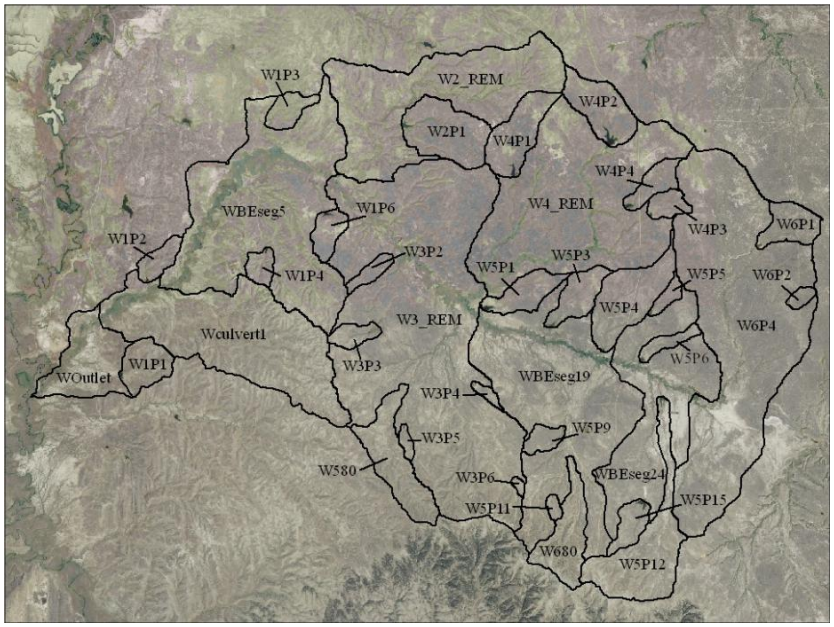

Figure 4.11: The delineated subbasins for the model. A total of 42 subbasins were modeled.

Watershed Characteristics and Parameters

Abstracting Box Elder's parameters was completed after terrain preprocessing and subbasin delineation since these steps provided the necessary input layers to describe watershed characteristics. Parameter abstraction was completed through HEC-HMS since the program contains several tools that quickly determine average basin slopes, stream segment slopes, areas, subbasin centroids, and longest flow paths. Slope values were taken from the unaltered DEM so that answers were not influenced by surface reconditioning. Besides calculating basic physical characteristics for Box Elder, HEC-GeoHMS was also utilized to generate a shape file that showed location points of flow

transitioning from overland flow to channel flow, information required for time to concentration calculations. This file required some modification since the program had trouble picking up water flow paths near the edges of subbasins due to the flat terrain. All parameters derived by HEC-GeoHMS were automatically stored in easy-to-manage attribute tables and were revised as necessary.

Model Setup

The final work performed by HEC-GeoHMS was to convert the abstracted parameters and subbasin delineations into the appropriate formats for the hydrologic model. The program accomplished this through a few important data processing steps that depended on the chosen model setup. This project explored two model setups for the Box Elder watershed: lumped and distributed.

Assigning unique names for each hydrologic component is the first step in data preparation for both model setups. River and subbasin names were automatically generated by the program and then changed for clarity. Components for Box Elder were renamed to correspond with stock ponds and gages. The desired units for the hydrologic model were also specified, and HEC-GeoHMS converted all abstracted characteristics into the appropriate system of units. This greatly eased the transition into the hydrologic model because most calculations done in GIS default to the metric system while it was desired that the hydrologic model use English units. HEC-GeoHMS also checked the parameters for any topological violations. Once all parameters had been reviewed, HEC-GeoHMS created the files to be read by the hydrologic model. This included a

background map file and a basin file that contained Box Elder's components with their parameters.

The distributed model setup required the creation of a grid cell parameter file. This step projects a grid onto the subbasins in order to create smaller units for model calculations (Figure 4.12). 100 meter (328.1 foot) grid cells were used for the Box Elder project. HEC-GeoHMS calculated several parameters for each grid cell including the cell's x-coordinate, y-coordinate, hydraulic travel length to the outlet, and area. Appendix B contains a sample portion of the grid cell parameter file.

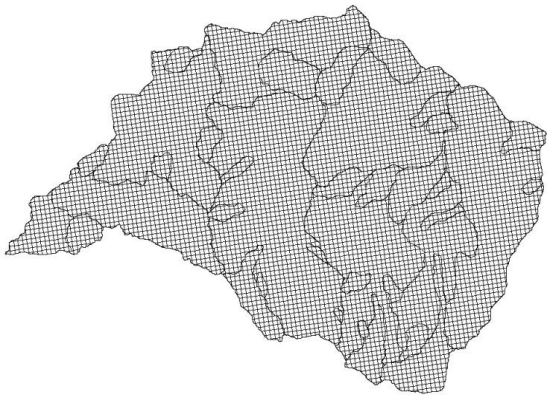

Figure 4.12: 100 meter grid cells applied to Box Elder Watershed.

HEC-HMS

The Army Corps of Engineer's Hydrologic Modeling System (HEC-HMS) was selected to model the Box Elder watershed for this project. Several factors contributed to choosing this model over other available software programs including reservoir routing capabilities, model flexibility, and an easy-to-use graphical user interface. The literature

review provides a more complete overview of the software and the specific mathematical models used.

Precipitation

The following section discusses the precipitation input for the model. Measured and synthetic data were utilized.

Measured Data: HEC-HMS offers several options for representing measured precipitation data for runoff calculations. The configuration chosen depends on the spatial and temporal resolution available and whether or not the model is lumped or distributed. This project utilized the inverse distance interpolation scheme when more than one gage was available for a particular time segment. Otherwise a single precipitation value was used for all subbasins.

Inverse distance is one of the more widely used spatial interpolation methods. It operates under the assumption that the value of an unknown point is somehow related to known neighboring point values, and closer points are more influential than further points. The value of an unknown point at a specific location is calculated by the following formulas:

$$\hat{y}(S_0) = \sum_{i=1}^{n} \lambda_i y(S_i) \tag{4.1}$$

$$\lambda_i = \frac{d_{0i}^{-\alpha}}{\sum_i^n d_{0i}^{\alpha}} \tag{4.2}$$

$\hat{y}(S_0)$= value of unknown point
$y(S_i)$ = value of unknown sample point
λ_i = weighting factor

α = decay rate
d_{oi} = distance of unknown point to known point

There are criticisms of inverse distance weighting. The decay exponent is not based on empirical data and does not consider the distribution of data [Lu and Wong, 2008]. Instead the modeler chooses the exponent arbitrarily, but a value of two is often used as the default. Despite these imperfections, its applicability to limited data sets where more advanced statistical means cannot be applied often makes it the best choice for interpolating values. It is also considered an improvement over courser methods, such as Theisson polygons, that display data as discrete areas.

HEC-HMS executes the inverse distance method automatically for a lumped model configuration once locations and measured precipitation values have been entered for the gages. A single precipitation value is calculated for each subbasin using the distances of the surrounding gages to a subbasin's centroid. HEC-HMS modifies the method slightly to incorporate only four or fewer gages. It does this by dividing the space around an unknown sample point into four equal quadrants with the unknown sample point at the origin (Figure 4.13). Only the closest gage from each quadrant is then used to calculate precipitation. This helps to ensure that the value of the unknown point does not come from a single cluster of data.

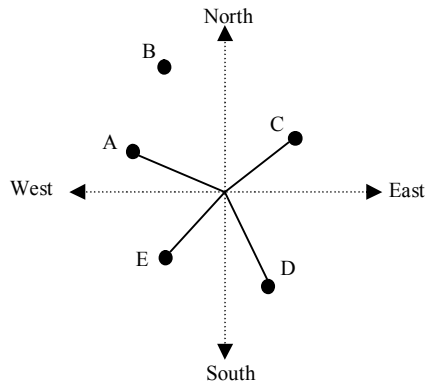

Figure 4.13: Quadrant method schematic from the HEC-HMS Technical Reference Manual.

Utilizing an inverse distance scheme for the distributed model setup was more involved than for the lumped model. Gridded precipitation datasets had to be created through a GIS and then transformed into the proper format for use by HEC-HMS. ArcMap's spatial analyst was used to create the precipitation grids since it contains interpolation algorithms that quickly transform point data into a raster set of precipitation values based on a desired interpolation method. After the spatial analyst tool had been utilized to create the raster for each time step with rain, a conversion of each raster to the American Standard Code for Information Interchange (ASCII) file form was necessary. The ASCII files were then transformed into Data Storage System (DSS) files, a format unique to HEC programs used for reading and storing data. The DSS files could then be read during model simulations to provide an input for precipitation.

The inverse distance technique was applied to the precipitation measured during the periods of June 2010 and May/June 2011 (Figure 4.14). Only one gage was operational during May and June of 2011, and these rain measurements were not subject to inverse distance weighting. Figure 4.15 shows an example of a precipitation raster set

to demonstrate the output of the interpolation scheme for the distributed model.

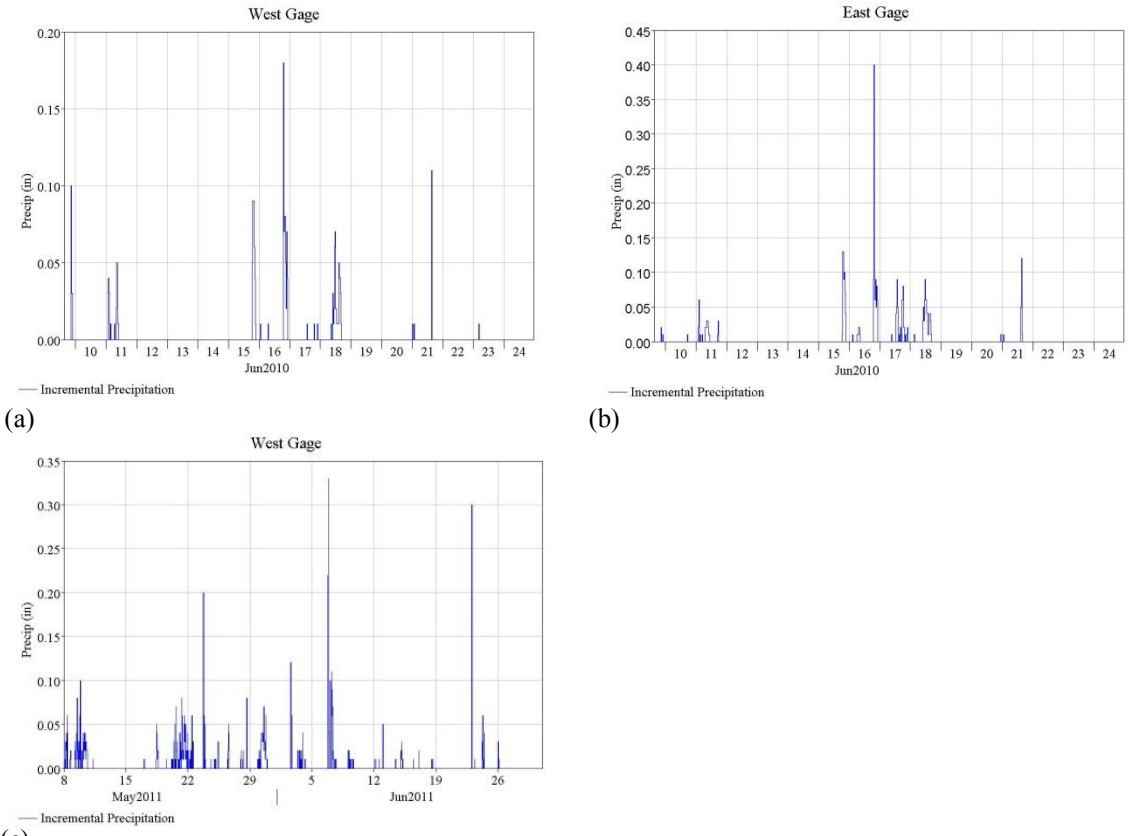

Figure 4.14: Measured incremental precipitation data, (a) West Gage - June 2010, (b) East Gage - June, 2010, and (c) West Gage – May/June 2011.

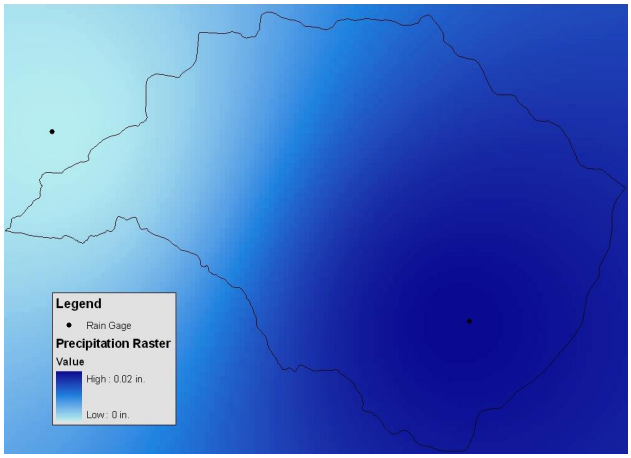

Figure 4.15: Raster dataset of precipitation for June 16th at 07:30.

Frequency Storms: Frequency storms were an integral part of the analysis of Box Elder Watershed. Storms of varying return intervals were created to determine the effect of the stock ponds on flow regimes. HEC-HMS has the capability to generate frequency storms from statistical data, as was done for this analysis.

The frequency storms were constructed from statistical data provided by the National Oceanic and Atmospheric Administration [Miller et al, 1973]. Table 4.1 shows the compiled data for Box Elder Watershed. The data were input into HEC-HMS, and the program used the alternating block method [Chow et al, 1988] to construct the 24 hour frequency storms using 5 minute intervals. Figure 4.16 shows an example of a constructed frequency storm applied to the watershed.

Table 4.1: The statistical data used to construct the frequency storms. The values show the maximum precipitation depth in inches for a storm of a specified return interval (RI).

Duration	2 year RI	5 year RI	10 year RI	25 year RI	50 year RI	100 year RI
5 minutes	0.18	0.29	0.33	0.43	0.52	0.56
15 minutes	0.36	0.56	0.64	0.85	1.03	1.09
1 hour	0.63	0.99	1.13	1.49	1.80	1.92
2 hours	0.72	1.07	1.22	1.58	1.87	2.04
3 hours	0.79	1.13	1.30	1.65	1.93	2.14
6 hours	0.98	1.29	1.49	1.83	2.08	2.39
12 hours	1.20	1.58	1.80	2.23	2.53	2.88
24 hours	1.42	1.86	2.22	2.71	3.10	3.44

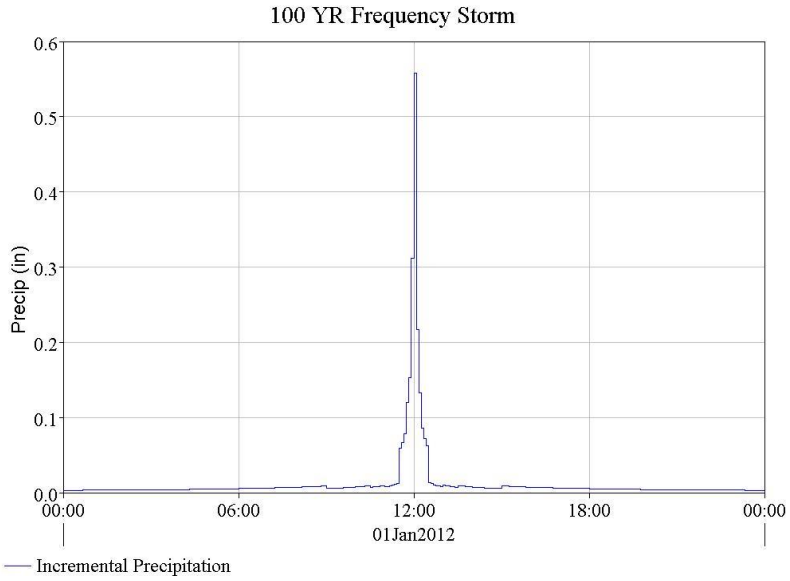

Figure 4.16: A constructed 100 year, 24 hour frequency storm from the alternating block method.

Loss Model

The Soil Conservation Service (SCS) curve number method was chosen to predict and model precipitation available for runoff. In regards to the Box Elder watershed, the method's origins as a predictor for midsized agricultural watersheds make it an acceptable model to use for this project. Also Box Elder's high curve numbers and large percentage of runoff to rainfall reinforce the acceptability of the curve number technique for the catchment. Another desirable feature is that the method does not require large amounts of data and was designed for use in ungaged watersheds, as is the case in Box Elder Watershed.

Selecting curve numbers requires information on land cover, soil type, and coverage condition. As previously discussed, soil and landcover datasets containing this

information were accessed through NRIS. The GIS projected the spatial datasets and was used to perform simple manipulations to determine curve numbers for the watershed.

The first step to determine a curve number within the GIS is to overlay the soil and landcover data sets and create individual polygons containing a single description of soil and landcover. Next, a database table is developed from the SCS curve number table so a lookup function can match curve numbers to each polygon. Applying these steps to Box Elder's datasets resulted in the distribution of curve numbers shown in Figure 4.17. The lookup table developed for the Box Elder watershed has been included in Appendix C. Box Elder's exact landcover types are not included in the standard curve number table produced by the SCS, so equivalent landcover comparisons had to be made in order to create a curve number table applicable to the watershed. Curve numbers ranged from 61 to 89 (a value of 100 was given to open bodies of water), a relatively high distribution of values. High curve numbers aligned with expectations after field observations noted low infiltrations and flashy hydrologic responses. The curve numbers were then distributed according to the modeling scheme used. The distributed model used an average curve number for each 100 meter or smaller cell while the lumped model found a single average curve number for every subbasin (Table 4.2).

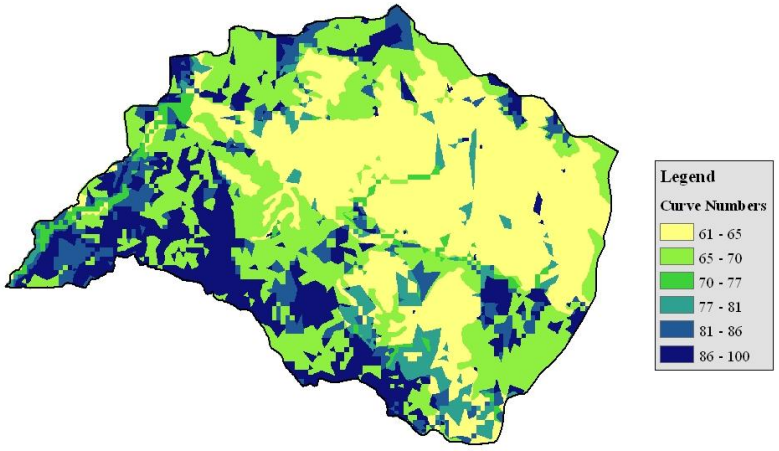

Figure 4.17: Curve numbers for Box Elder Watershed. The values were derived from land cover and soil datasets.

Runoff Transformation

The Clark Unit Hydrograph model described runoff transformation for this project. It was chosen due to the fact that there is a modified, distributed version of the method, and this is the only distributed transformative model offered by HEC-HMS. It is also a well accepted method that offers computational efficiency.

The Clark Method requires two parameters for each subbasin: the time to concentration and the storage coefficient. While obtaining the time to concentration for the subbasins relied heavily on the GIS, the storage coefficient cannot be related back to physical characteristics of the watershed and had to be calibrated through existing runoff data.

Time to concentration was calculated through methods outlined in TR-55 [NRCS, 1986]. The TR-55 method calculates flow velocities during sheet flow, shallow and concentrated flow, and channel flow to arrive at the time it takes for a drop of water at the most hydraulically remote point in the watershed to reach the outlet. This is a much more

physical characterization of time to concentration than empirical methods such as the Kirpich equation. Calculating time to concentration for each of the Box Elder watershed's subbasins required basin slopes, channel slopes, flow lengths, and Manning's n values. Slopes and flow lengths were found through analysis of a DEM in a GIS, and Manning's n values were found by matching field observations to a Manning's n chart [Chow, 1959]. An example of the TR-55 calculation for time to concentration is provided in Appendix D. Some manual calibration was necessary due to uncertainty regarding the hydraulic radius value. Time to concentration values for all of the subbasins are presented in Table 4.2.

As covered in the literature review, the distributed model setup requires the flow distances of each cell to the subbasin outlet in order to determine the time to concentration for each cell. HEC-GeoHMS automatically calculates these values from the flow direction raster during execution of the grid cell processing tool. Figure 4.18 shows the distribution of hydraulic distance to each subbasin outlet within the Box Elder watershed.

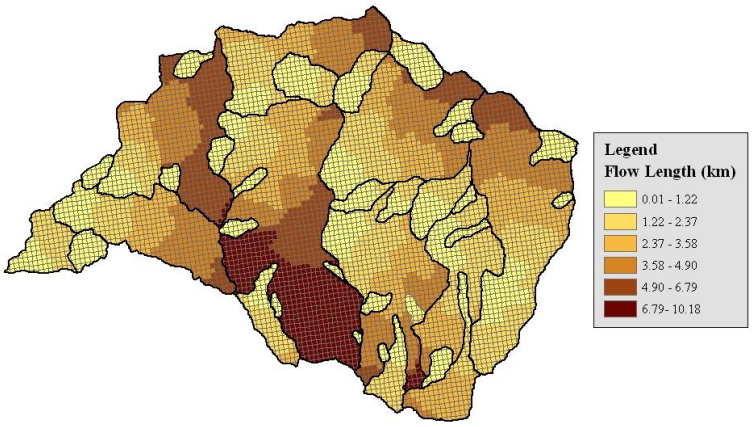

Figure 4.18: The distribution of hydraulic flow lengths for the grid cells. The distances are measured from each subbasin's outlet.

A value for the storage coefficient, R, was determined through manual calibration and the use of several measured storm events (Table 4.2). A more complete account of model calibration, including the value for R, is presented in chapter 5.

Table 4.2: Final parameters used for each subbasin within the model.

Subbasin	T_c (hr)	R (hr)	CN	Area (mi^2)
W6P1	1.7	3.2	66.33	0.18
W6P2	0.8	1.6	63.00	0.04
W6P4	14.3	27.0	67.65	2.88
W5P12	3.0	5.7	74.27	0.60
W5P15	1.0	1.9	69.83	0.12
W5P6	1.9	3.5	63.87	0.07
W5P5	2.3	4.4	63.00	0.05
Wculvert2	5.1	9.6	69.45	1.21
W5P10	1.0	1.9	65.15	0.06
W5P4	5.0	9.4	64.31	0.40
W5P3	2.9	5.5	63.26	0.18
W5P11	0.5	0.9	81.22	0.03
W680	3.6	6.8	79.57	0.31
W5P9	1.4	2.6	66.57	0.08
WBEseg19	10.3	19.4	65.86	0.18
W5P1	4.2	7.9	70.74	1.98
W4P2	1.6	3.0	68.31	0.29
W4P4	2.0	3.8	65.67	0.12

W4P3	1.4	2.6	63.45	0.09
W4P1	4.7	8.8	69.68	0.29
W4_REM	10.3	19.3	65.46	2.20
W3P5	1.0	1.8	82.35	0.03
W580	2.4	4.6	78.79	0.39
W3P6	0.3	0.6	83.53	0.02
W3P4	1.5	2.9	69.25	0.03
W3P3	4.3	8.0	74.84	0.08
W3P2	1.5	2.9	69.51	0.07
W3_REM	26.0	48.9	72.22	3.99
W2P1	4.1	7.7	66.23	0.39
W2_REM	5.2	9.8	75.41	1.50
W1P6	2.4	4.6	72.41	0.11
W1P3	1.3	2.5	72.73	0.11
W1P4	0.8	1.6	75.53	0.08
WBEseg5	5.6	10.6	76.97	2.24
W1P2	1.6	2.9	79.06	0.10
Wculvert1	3.7	7.0	81.92	1.60
W1P1	2.0	3.8	85.71	0.19
WOutlet	2.5	4.8	82.05	0.46

Channel Routing

The outflow from each subbasin must ultimately reach Box Elder's outlet through channel routing calculations. The Muskingum-Cunge method [Cunge, 1969] is one such routing model that has a wide range of applicability and uses deterministic parameters. Modelers of ungaged basins often employ the method since parameters are related to physical properties of channels, reducing the amount of calibration required. The limited amount of runoff data for Box Elder made Muskingum-Cunge a good option for calculating channel travel times.

Parameters required for Muskingum-Cunge routing include length, slope, Manning's n, and cross section for each reach modeled. A combination of analysis in the GIS and field measurements were utilized to obtain all necessary inputs.

HEC-GeoHMS used within ArcGIS determined channel slopes and reach lengths from the original 10m DEM. Care was taken not to use the hydraulically corrected DEM since stream burning and the filling of depressions could incorrectly alter slope values. While the GIS greatly expedited collection of these parameters, channel cross sections had to be taken in the field due to the coarseness of the available DEM.

Only one eight-point cross section can represent an entire reach in the HEC-HMS model, and this led to the rejection of survey-grade channel measurements being taken for each reach. Cross sections were measured by staking measurement tape across the channel and recording depths at eight representative points (Figure 4.19). Up to three cross sections in varied locations were taken for longer reaches or reaches with significant changes in geomorphology. A single cross section was then used that represented the average hydraulic radius, a parameter that governs hydraulic responses.

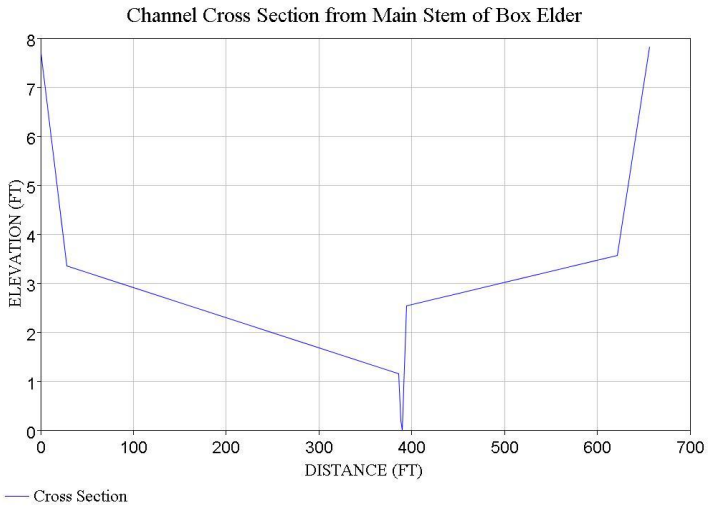

Figure 4.19: An 8-point cross section measured to describe the reach BE_Seg2 for the model.

Reservoir Routing

The outlet structures method for reservoir routing was selected for the ponds of Box Elder. The method computes storage based on a measured elevation-area function and determines the outflow of the spillways from established weir equations.

Establishing stage-area curves for each pond proved difficult because of inconsistent shapes and lack of information on pond construction methods. The DNRC provided the acreage-at-capacity value for a limited number of ponds, but these values did not agree with measurements taken in the field and were not used. In the end, all pond parameters were field-measured.

The first step in describing each pond was to determine the pond's approximate depth. Depth was estimated by measuring the height of the dam and using the slope of the channel. The large size of the dams prevented direct measurement of the height, so the distance and slope from the top of the dam to the base was taken using a tape measure

and an inclinometer. Then a simple trigonometric relationship could be used to solve for the height. The slope of the channel, determined from a GIS, was projected through the width of the dam to arrive at an estimate for the pond depth. It was observed that trapped sediment has likely reduced the depth of the pond, but it was not feasible to determine by how much for each of the 28 ponds.

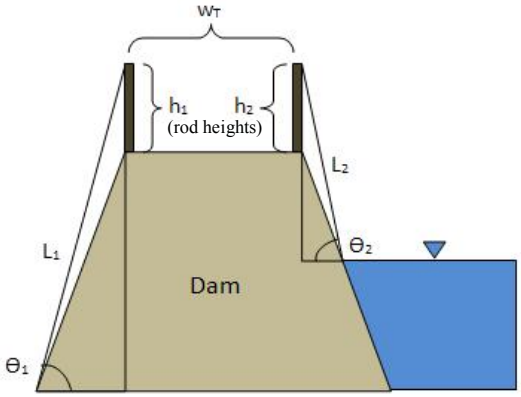

Figure 4.20: Variables measured to determine the depth and stages of each pond.

Since it was not possible to directly measure volume at various stages, area measurements were taken at different stages. In a manner similar to determining the height of the dams, the stage of the pond was measured from the top of the dam. Then a GPS unit recorded the pond area while walking the perimeter of the current water level. Unfortunately, the ponds did not experience significant draw down due to two uncharacteristically wet seasons, and lower stage measurements were not obtained for most of the ponds. A total of one to three area-stage measurements were taken for each pond.

A stage-area function was fitted to the measured data points that could be integrated to arrive at a volume. The function took the following form:

$$A = ah^b \tag{4.3}$$

A = water area
h = water stage
a = fitted constant
b = fitted exponent

A limited number of data points led to the fitted function not exceeding a power of two. For those ponds containing only a single stage-area measurement, the shape of the pond was assumed to be that of an upside down pyramid (Figure 4.21). This meant that the exponent for the stage-area function was taken to be two, the same for a pyramid, and the fitted constant, a, was calibrated to the single data point. This assumed shape will most likely underestimate volumes at low water heights but will provide a suitable estimation of increasing storage with increasing stage. A typical area-stage function is shown in Figure 4.21.

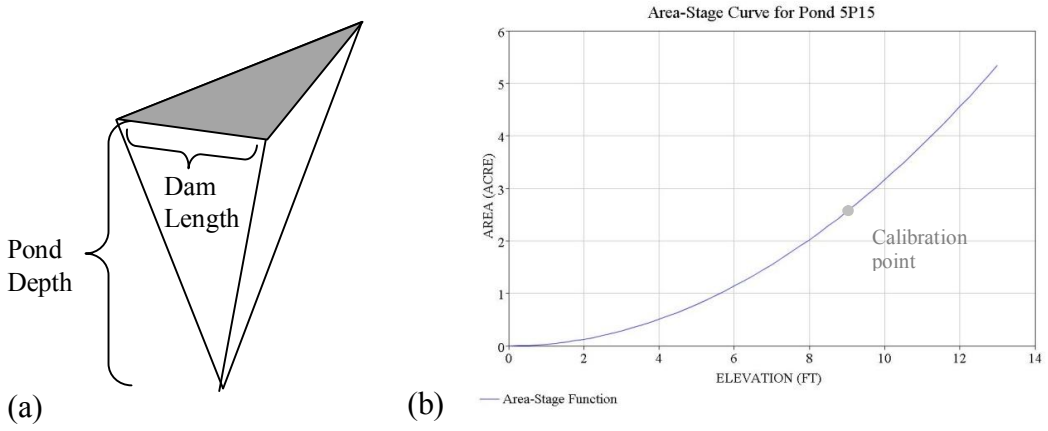

Figure 4.21: (a) The assumed geometry for a pond with a single stage-area measurement, and (b) a typical area-stage function used for the ponds.

In addition to accounting for pond storage, the outlet structures routing method needs to describe the outflows from the spillways. This is done by applying a weir equation to measured outflow structures. Unfortunately, the majority of stock ponds have

water exiting through a low point near the dam, and the exit never behaves as water flowing over a weir. The few exceptions to this statement are a couple of ponds with large headcuts at their outlet (Figure 4.22). Flow over the headcuts does pass through the critical depth at the overfall and can be modeled more reasonably as a weir. Since outflows rarely pass through a critical depth for the rest of the ponds, very little about the hydraulics at their exits could be discerned.

Table 4.3: Pond characteristics used to describe stage-storage relationships. *A value of 2 indicates ponds with only one depth/area data point. The area at full value was determined by the pond's equation.

Pond	a	b*	Area at Full	Dam Height	Spillway Width
1P1	0.17	1.24	1.69	8.8	53.4
1P2	0.01	2.00	0.98	14.6	57.9
1P3	0.06	1.30	1.19	12.1	10.7
1P4	0.01	1.90	1.24	18.0	35.1
1P6	0.02	2.00	2.75	18.8	11.9
2P1	0.02	2.00	1.74	13.8	33.4
3P2	0.01	2.00	0.37	15.0	77.6
3P3	0.02	2.00	4.79	22.0	29.2
3P4	0.04	2.00	0.79	6.0	17.1
3P5	0.00	2.00	0.74	25.5	16.1
3P6	0.11	2.00	4.10	7.1	44.7
4P1	0.11	1.44	3.47	15.0	37.0
4P2	0.03	2.00	6.88	18.8	22.7
4P3	0.01	2.00	1.18	12.8	16.4
4P4	0.07	1.41	1.74	13.1	42.4
5P1	0.09	1.69	2.85	9.6	7.1
5P3	0.05	1.62	2.98	14.0	13.0
5P4	0.04	1.60	0.54	7.6	23.4
5P5	0.03	2.00	1.39	9.9	7.9
5P6	0.03	1.52	1.02	13.8	28.1
5P9	0.03	1.34	0.47	12.4	24.9
5P10	0.09	1.48	1.45	8.4	23.5
5P11	0.01	2.00	0.41	8.7	23.7
5P12	0.53	0.85	2.62	7.5	120.2
5P15	0.03	2.00	3.85	12.9	36.4
6P1	0.02	2.00	1.54	12.4	112.9
6P2	0.03	2.00	0.92	12.7	114.8
6P4	0.22	1.10	2.75	10.8	169.2

The difficulty in describing pond outflows was dealt with by making the simplifying assumption that the spillways could be described as a broad crested weir with a low weir coefficient. Typically the coefficient of a broad crested weir ranges between 2.6 and 4. The 2.6 value was chosen to account for the higher energy losses associated with the nature of flow not passing through the critical point. A GPS unit recorded the approximate length of the low spot through which water exits to be used as the weir's length. The equation for a broad crested weir follows:

$$Q = CLH^{3/2} \tag{4.4}$$

Q = flow rate
L = weir length
C = weir coefficient
H = water height

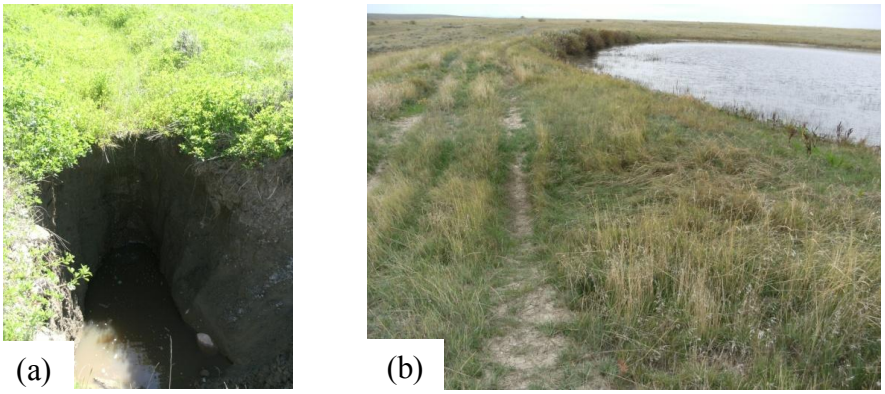

(a) (b)

Figure 4.22: (a) A headcut as pond 5P9's outlet, and (b) a low spot as pond 5P3's outlet.

Culvert Modeling

Preexisting runoff event data in Box Elder Watershed was limited, necessitating setting up a gage at a control point within the watershed to obtain usable runoff data for calibration. A set of culverts near the outlet of Box Elder was selected because of the

predictable hydraulic behavior at culvert structures (Figure 4.23). An installed gage recorded water height, and a rating curve was developed to transform the stage data into a flow rate. The rating curve was developed by modeling the stream reach in the Hydraulic Engineering Center's River Analysis System (HEC-RAS) [USACE, 2008].

Figure 4.23: The culverts near Box Elder's outlet.

Culvert Survey

Transforming the stage data into runoff values required a topographic survey both up and downstream of the culverts. The survey was completed with a total station and a rod and prism. Distance, azimuth angle, and horizontal angle were determined relative to a back sight to form several cross sections upstream, downstream, and at the exit and entrance of the culverts. These raw measurements were transformed into a northing, an easting, and an elevation through basic geometric calculations and then aligned with an aerial (Figure 4.24). Distances between the surveyed points were computed in AutoCAD through the alignment function. The alignment function projects the points onto drawn cross section lines (Figure 4.24) and calculates station distancing between the projected

points. The cross sections were drawn perpendicular to flow paths, resulting in some dog-legged lines.

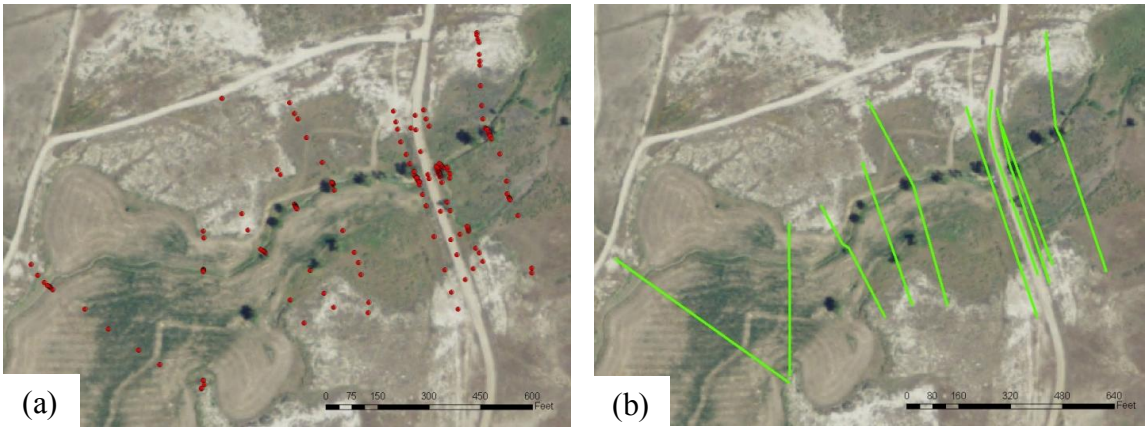

Figure 4.24: (a) Survey points and (b) drawn cross sections for the areas upstream and downstream of the culverts.

After the survey points had been formed into cross sections, a few parameters needed to be extracted from the GIS. The main channel, left overbank, and right overbank distances between cross sections had to be determined. Main channel distances were found by measuring polyline lengths along the channel, and overbank distances were found by measuring straight line distances from the centers of overbank segments.

Additionally, the elevations of the culvert inverts were taken in order to establish the slope of the culverts, and the height and width of the culvert openings were carefully measured by hand. Measurement of the culverts led to the discovery of severe damage to one culvert as a result of the 2011 spring season's severe flooding events (Figure 4.25). Its reduced opening was measured in order to approximate the irregular shape for input into HEC-RAS.

Figure 4.25: Damaged culvert. Both the roof and floor has buckled with sediment deposition on the sides.

HEC-RAS Model

The USACE's HEC-RAS is a one dimensional hydraulic model that is widely used by government agencies and engineering firms for floodplain modeling and other routing tasks. Recent advances in the software have resulted in unsteady flow capabilities that utilize the St. Venant equations [USACE, 2002]. The program supersedes the steady flow program HEC-2 [USACE, 1991] and is comprised of a graphical user interface, data management capabilities, and separate hydraulic analysis components [Brunner, 2002]. HEC-RAS was utilized for establishing a rating curve for the outlet culverts on Box Elder Creek because of its well established suitability for many hydraulic modeling studies in natural channels [e.g. Bockelmann et al, 2004; Horritt and Bates, 2002; Lee et al, 2006; Maingi and Marsh, 2002; Yang et al, 2006] and its availability as a public domain software.

The HEC-RAS model for Box Elder's culverts included building an accurate physical representation of the main channel and floodplain by entering measured cross sections and their parameters. Modeling a culvert in HEC-RAS requires a minimum of four cross sections, two upstream and two downstream, but more were included downstream to minimize influence on the solution from the boundary condition. The cross sections farthest downstream were placed further apart since accuracy was less important in areas not near the culvert. Manning's n varied along the cross sections with higher values designated to the floodplain. Channel values ranged from .04 to .06, and floodplain values ranged from .07 to .16.

Levees and ineffective flow areas were included in the cross sections to better replicate real conditions. HEC-RAS determines water height levels from the bottom up during iterative calculations, and the levees prevent low elevation areas in the floodplain from filling with water before the banks of the main channel have been overtopped. Ineffective flow boundaries for the cross sections were included under the assumption that outer portions of some cross sections were not conveying flow because of contraction or expansion occurrences and were applied to the cross sections approaching and leaving the culvert (Figure 4.26). The extent of ineffective flow on the upstream and downstream sides was determined from the ratio of the floodplain width to the opening of the culvert, the channel slope, and the Manning's n values of the floodplain and main channel. The Hydraulic Reference Manual for HEC-RAS provides a guideline table to estimate ineffective flow boundaries [USACE, 2008]. A straight line representation of

the ineffective flow boundary is deemed adequate to estimate the actual curved division line separating the areas conveying and not conveying flow [USACE, 2008].

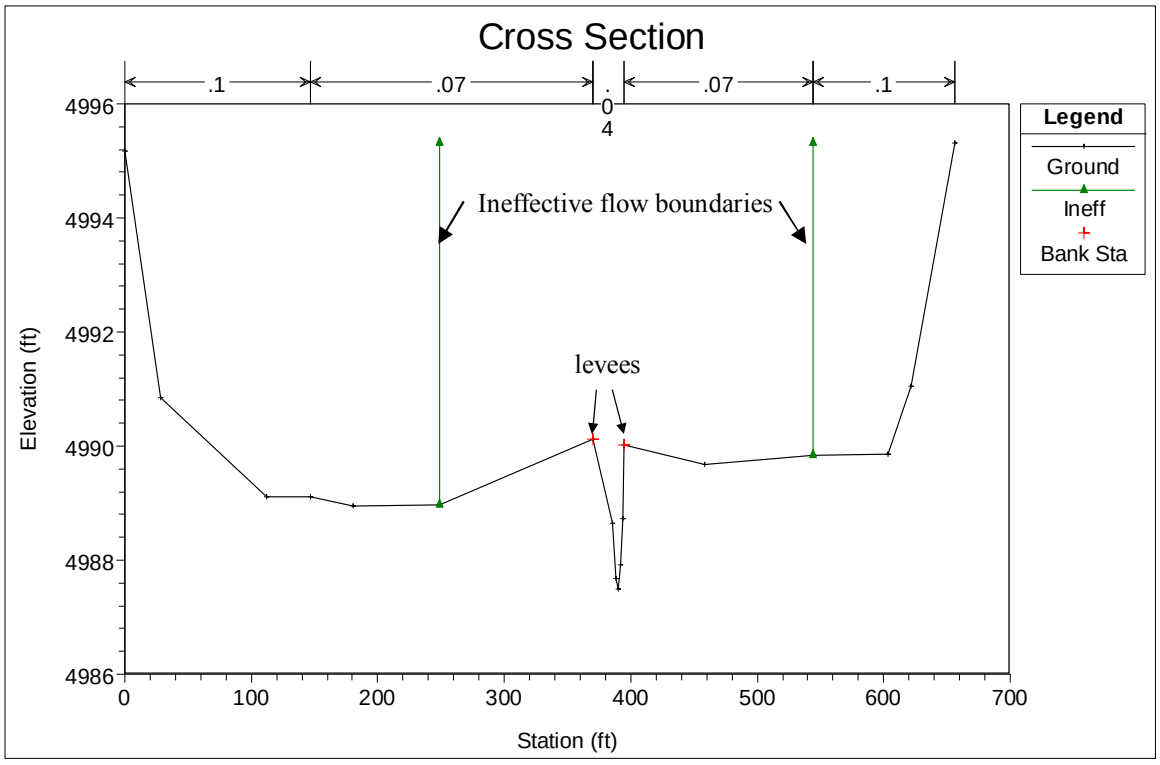

Figure 4.26: A cross section with levees and ineffective flow boundaries applied appropriately. The levees have been applied at the bank station since this is where water must breach before the flood plain is inundated. The varying Manning's n value is shown at the top.

The culverts were entered using pre-established hydraulic structures within HEC-RAS. Both culverts were entered as corrugated metal pipe culverts projecting from fill. The undamaged culvert was designated as circular in shape with a 6.5 foot diameter, and the damaged culvert was estimated as an arch shape with a 5 foot span and 2.5 foot rise (Figure 4.27). The road deck was entered in anticipation of modeling high flows

exceeding the culverts' capacity. These high flow events would result in the road deck behaving as a broad crested weir.

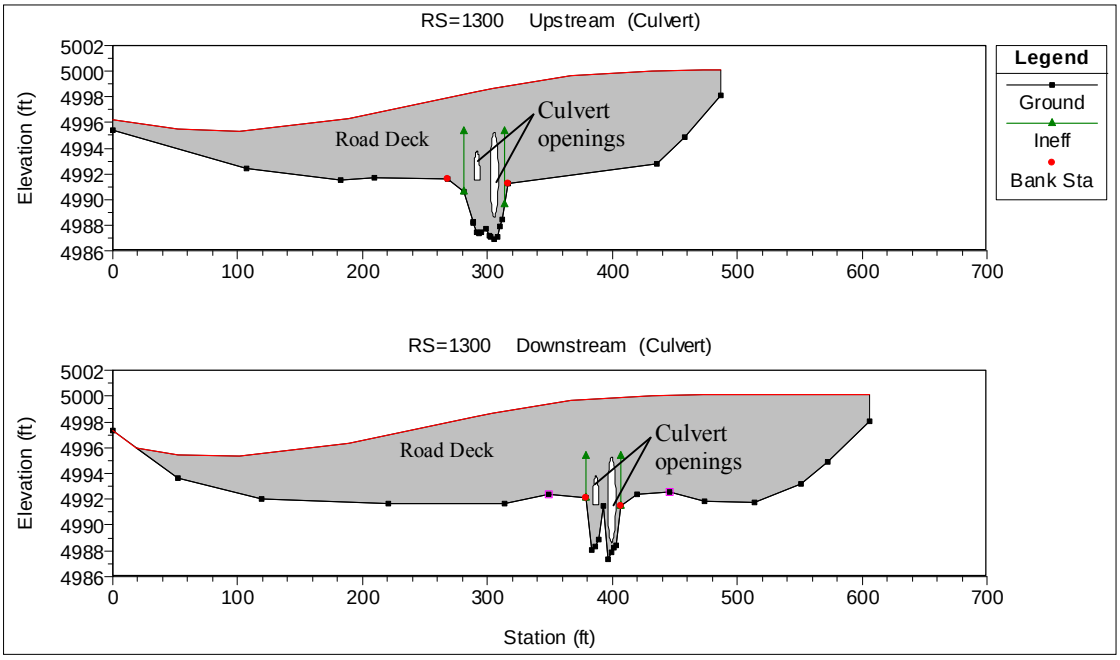

Figure 4.27: Cross sections immediately upstream and downstream of the culverts. Elevations are only measured locally and are not representative of actual elevations above sea level.

After the physical representation of the reach had been determined, HEC-RAS required a boundary condition. The mild slope of Box Elder Creek results in water depths that are subcritical, and a normal flow boundary condition at the cross section furthest downstream was used. The normal flow depth at this cross section was determined from the average slope of the reach. While normal flow is not realistic in a natural channel, the normal flow assumption occurred far enough downstream that it most likely had little effect on calculations at the culvert. The simulations and the rating curve are covered in Chapter 5.

MODELING RESULTS

Rating Curve

A rating curve was necessary so that water heights recorded at the inlet of the culverts on Box Elder Creek could be transformed into flow rates for model calibration. The rating curve was built by running steady state simulations for a range of flow rates in the HEC-RAS model. The model solved for water levels at each cross section, and the water level at the installed gage at the inlet cross section of the culvert was plotted against flow rate to form the rating curve (Figure 5.1).

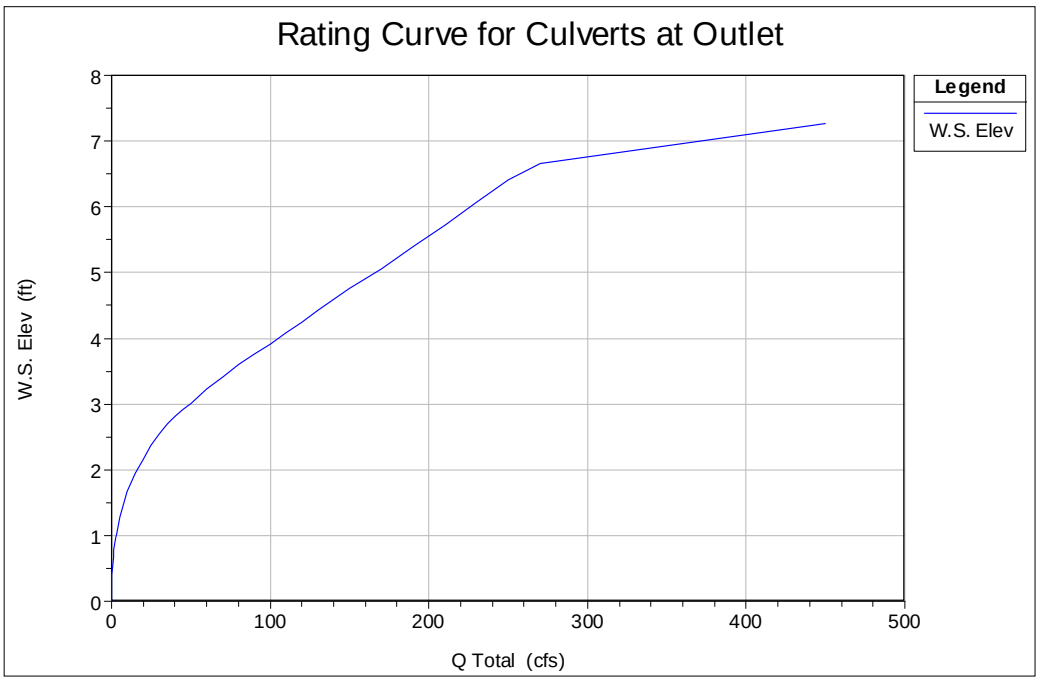

Figure 5.1: Rating curve for the gage at the inlet of the Box Elder culverts. The change in slope just before Q equals 280 cfs indicates water over-topping the road.

The developed rating curve from HEC-RAS did not match field observations of Box Elder Creek made during spring of 2011. The rating curve reported a flow rate of over twenty cubic feet per second (cfs) on a day when the observed water height was slightly more than two feet and flow was not likely over 1 cfs. The already steep slope at the beginning of the rating curve, showing a water level rise from zero to one foot resulting in a flow rate increase of 2.9 cfs, would need to be steeper to match observations. The model was examined for errors, and parameters were adjusted, but no alterations to the model dramatically influenced the rating curve. The area is so wide and flat that the control on flow for the culvert may be beyond the surveyed area.

A second method was attempted to develop a rating curve. The well accepted paper *Measurement of peak discharges at culverts by indirect methods* [Bodhaine, 1968] offers a guide to develop rating curves at culverts for varying types of flow. Methods are based on the energy equation and usually require iteration. Bodhaine defines flow in a culvert that maintains a subcritical depth that never passes through the critical point, the case for the Box Elder culverts, as Type III flow, and the outlined method to solve for these flow depths was applied. Unfortunately, the slightly adverse slope of the culvert prevented convergence of the solution. The uphill slope also prevented the calculation of normal flow within the culvert. A normal flow depth would have provided a general idea of possible depths and flow rates for the culverts. The inapplicability of the method outlined by Bodhaine and the inability to calculate normal flow led to the acceptance of the rating curve from HEC-RAS.

The rating curve's inaccuracies prevented an estimation of runoff volume, and flow rates were used only as a matter of convenience. However, the stage data provides information on relative peak flow rates since the same stages must have the same flow rates. The ability to compare peak size gives valuable information for model calibration. Also, even without accurate runoff volumes, the model still provides insight into relative differences in flow rates and runoff volumes caused by the inclusion of the stock ponds.

Model Configuration

HEC-HMS can model unsteady flow as lumped or distributed, and both model structures were considered for simulating Box Elder watershed. The distributed model uses an average curve number and precipitation value for each grid cell and scales other parameters using each cell's hydraulic flow length to the outlet. The lumped model employs parameters at the subbasin level. Since the lumped model was segmented into 38 subwatersheds to examine the effect of individual stock ponds, it may be more accurate to define it as semi-distributed.

Figure 5.2 shows a comparison between hydrographs produced by the distributed model, the lumped model, and the hydrograph derived from the HEC-RAS rating curve. There are noticeable differences in volume between the models, but there is little difference in shape and number of peaks in the hydrographs. This is most likely due to the coarse precipitation data that had to be interpolated for the distributed setup. Categorizing one estimated hydrograph as a better representative of reality is not possible

because of the uncertainties concerning the rating curve. Therefore, the computationally simpler lumped setup was chosen.

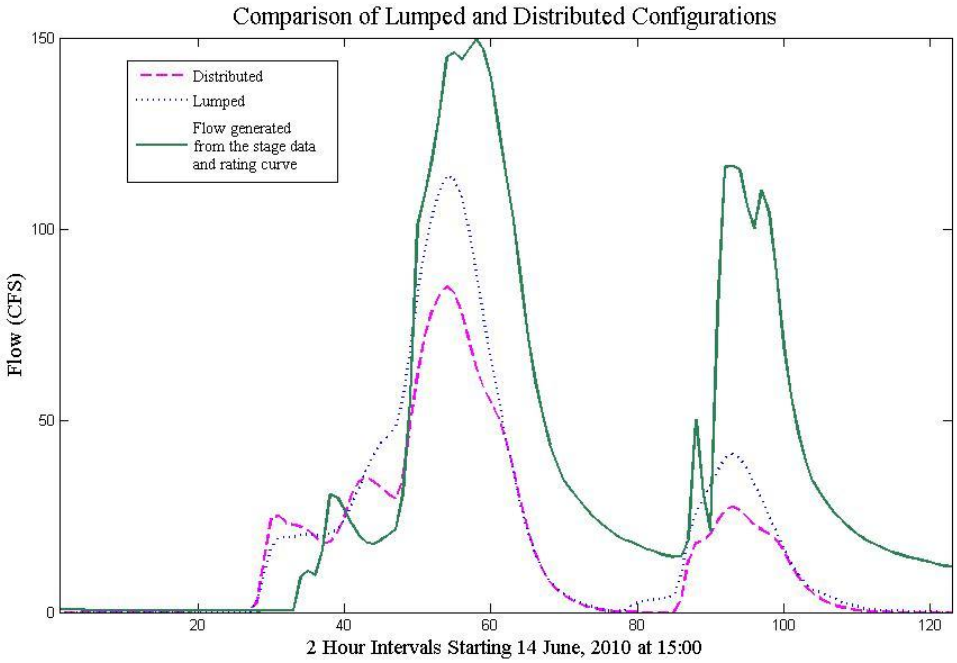

Figure 5.2: A comparison of lumped, distributed, and recorded hydrographs for the precipitation events during June, 2010.

Model Calibration

Calibration is the adjustment of model parameters so that simulations better match observations. This is required when parameters cannot be related to physically recognizable watershed characteristics. Two model parameters required calibration, the initial abstraction parameter of the SCS Curve Number method and the storage coefficient used to determine the Clark Unit Hydrograph. Curve number was specifically not calibrated because of the uncertainties regarding the rating curve and, therefore, runoff volumes.

The initial abstraction determines how much precipitation the watershed will store before excess rain is produced and runoff will initiate. Initial abstraction is expressed as a linear function of the storage by a constant initial abstraction ratio, usually set at 0.2.

A constant initial abstraction ratio of 0.2 proved problematic when applied to runoff events from the 2011 spring season. That season saw a record amount of rain, and Box Elder was observed to have continuous flow for over a month. The SCS Curve Number Method is an event based method that assumes standard conditions at the start of any storm. Therefore, it is ill-equipped to handle variable antecedent moisture conditions. May and June of 2011 rarely had dry periods long enough to allow the watershed to return to standard, dry conditions. The period of near continuous rainfall also led to the need to determine the time between precipitation required to categorize an individual event.

Figure 5.3 shows the results from modeling the months of May and June 2011 as a single event. Measured stage data indicates four events with nearly equal peaks between 0 and 800 hours, but the modeled peak runoff values become increasingly larger for each of these events. Additionally, several minor events are simulated that do not appear in the measured data. Even though the rating curve might not provide the correct magnitude of each peak, it is clear that measured equal peaks are truly equal. Increasing simulated peaks indicate that the model is not accurately predicting the recovery of infiltration capacity and other losses during periods of no rain over the 800 hours recorded.

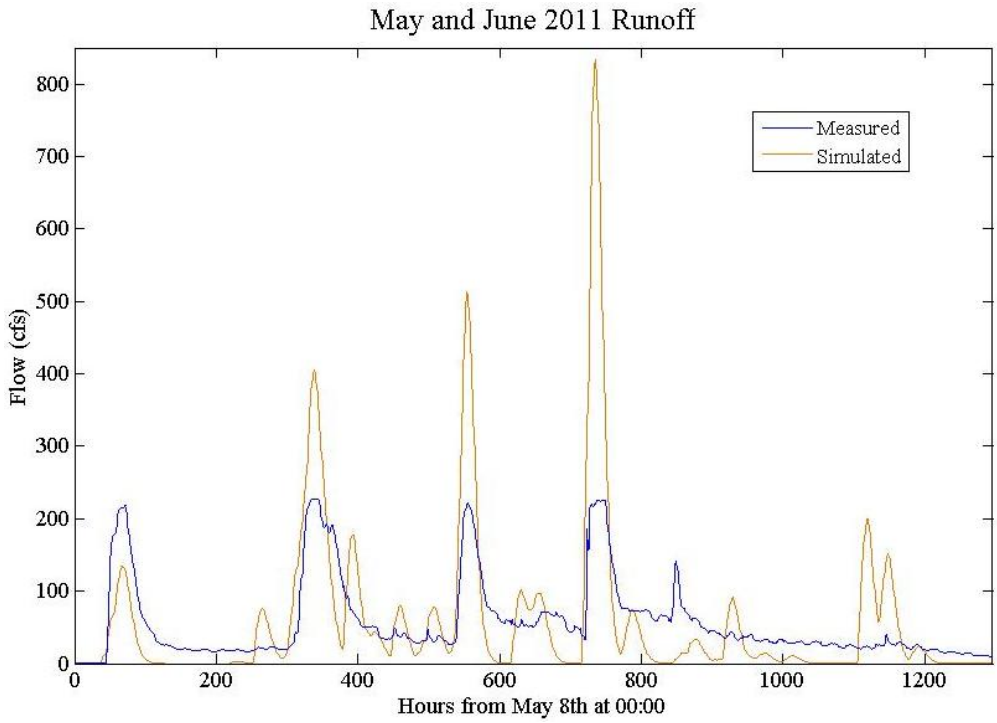

Figure 5.3: The modeled response assuming the precipitation data from May and June 2011 is a single event.

Assuming the entire record is one event underestimates the losses at the beginning of all but the first event, but there is little guidance to determine a length of time with no rain sufficient to separate individual events. Technically, any time gap without rain could be considered as dividing separate precipitation events, but to keep the number of simulations reasonable any rain occurrences within 24 hours were lumped together as a single event. This resulted in 17 events to be modeled individually for the 2010 and 2011 spring seasons (Table 5.1).

Table 5.1: The events modeled for Box Elder Watershed.

EVENT	Start Time	End Time	Time from Previous Precipitation Event
1	5/8/2011 2:59	5/11/2011 6:25	158.5 Hours
2	5/18/2011 9:48	5/22/2011 13:27	171 Hours
3	5/23/2011 17:41	5/25/2011 9:31	28 Hours
4	5/26/2011 10:23	5/26/11 14:17	25 Hour
5	5/27/2011 22:45	5/28/2011 15:13	32.5 Hours
6	5/29/2011 20:07	5/30/2011 23:15	29 Hours
7	6/2/2011 14:08	6/4/2011 4:52	63 Hours
8	6/6/2011 18:30	6/7/2011 15:30	61.5 Hours
9	6/9/2011 1:21	6/9/2011 15:56	34 Hours
10	6/12/2011 1:23	6/15/2011 15:46	57.5 Hours
11	6/16/2011 10:53	6/17/2011 1:27	29 Hours
12	6/18/2011 12:00	6/18/2011 15:31	34.5 Hours
13	6/23/2011 0:38	6/24/2011 10:04	105 Hours
14	6/26/2011 0:03	6/26/2011 2:13	38 Hours
15	6/9/2010 20:46	6/11/2010 17:27	153 Hours
16	6/15/2010 18:41	6/18/2010 16:06	104.5 Hours
17	6/20/2010 23:26	6/21/2010 15:32	55.5 Hours

When these separate rain events were modeled with the initial abstraction ratio set to 0.2, some events with significant observable flow were simulated as having no runoff. This was especially true for events with short time intervals since the previous event. It was likely that the watershed did not have time to return to the dry state described in the model. This led to conceptualizing the initial abstraction as a linearly varying parameter dependent on the time between events (Equation 5.1). While it was noted that the initial abstraction is probably not linear with time, this simplification was necessary because of insufficient data. The method's default value, 0.2, was assumed to be the maximum possible initial abstraction ratio.

$$I_a = \lambda S \tag{2.4}$$

$$\lambda = k * t \tag{5.1}$$

Ia = Initial abstraction
S = Storage
λ = initial abstraction ratio
k = constant
t = time between rain events

Various slopes, representing values of k, were simulated (Figure 5.4). The median slope reached an initial abstraction ratio value of 0.2 after 7.13 days. The initial abstractions for various assumed values of k were simulated for all the events in HEC-HMS, but only the 2011 results are shown for the sake of brevity (Figure 5.5). The observed and modeled data have been normalized to the maximum measured and simulated flows respectively.

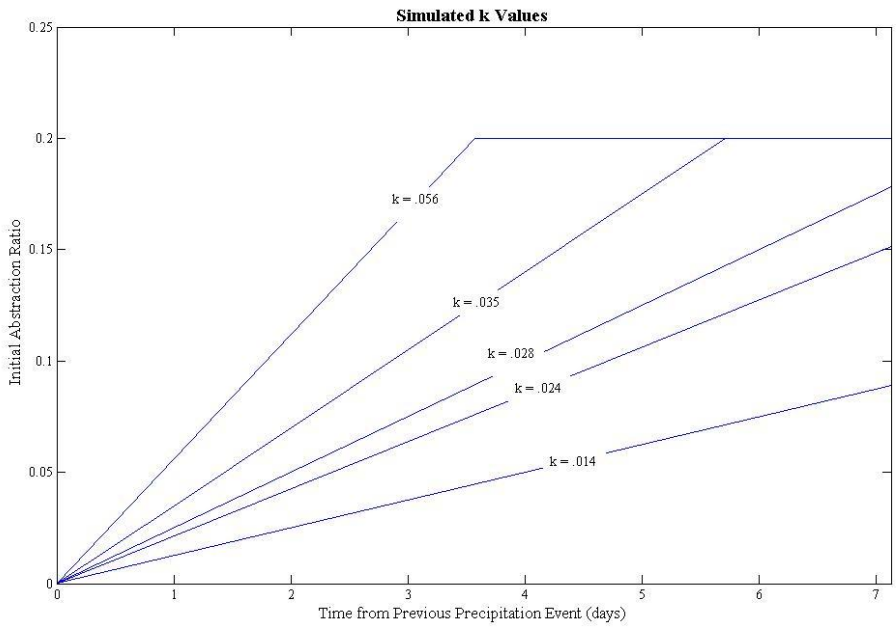

Figure 5.4: The different k values modeled with a maximum possible initial abstraction ratio of 0.2.

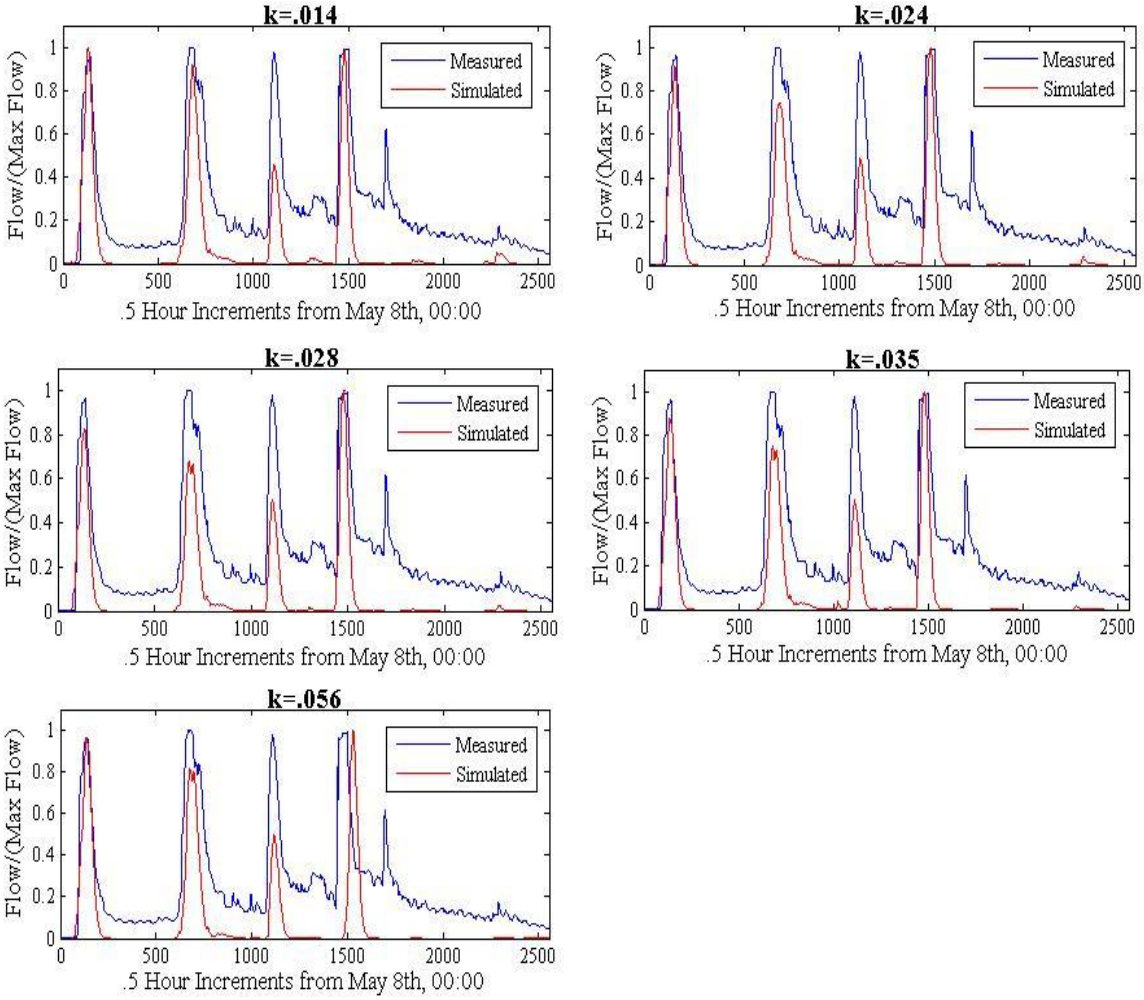

Figure 5.5: Hydrographs from varying initial abstraction ratio slopes.

The results show the sensitivity of the model to initial abstraction and the reset times. Since there was doubt regarding the volume of the measured hydrographs, relative magnitudes were used as the optimizing parameter. This resulted in a focus on peak flows. Taking advantage of the fact that the four main measured peaks were nearly equal, the standard deviation of the four simulated, normalized peaks was used as a goodness of fit. The k value producing peaks with the lowest standard deviation

corresponds to simulated peaks being most nearly the same. A k value of .028 was selected based on this criterion.

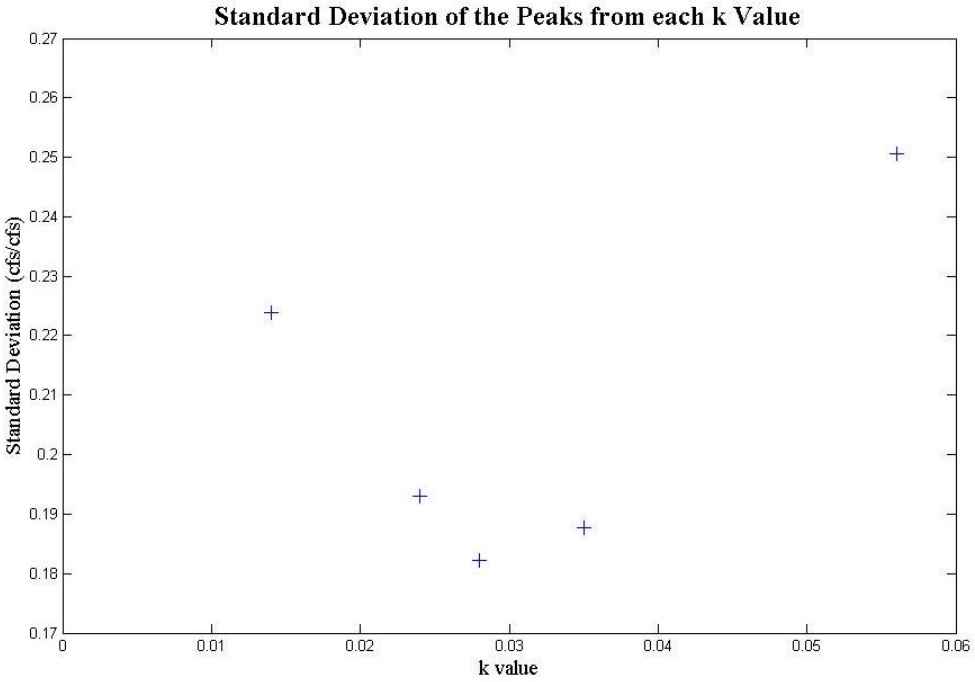

Figure 5.6: Standard deviation for the peaks of each k value. A k value of 0.028 produced the best simulation.

The storage coefficient was the second parameter to calibrate. Each of the 38 subbasins requires a unique storage coefficient, but it was not realistic to calibrate this many storage coefficients from such a limited dataset, so the following relationship from the HEC-HMS Technical Reference Manual [2000] was utilized:

$$\frac{R_1}{T_{c1} + R_1} = \frac{R_2}{T_{c2} + R_2} \tag{5.2}$$

R_1 = Storage coefficient of watershed 1
T_{c1} = Time to concentration of watershed 1
R_2 = Storage coefficient of watershed 2
T_{c2} = Time to concentration of watershed 2

This relationship has been found to be reasonably accurate for watersheds within the same region, and it reduced the number of parameters to calibrate to a single ratio. A ratio for an arbitrary subbasin, subbasin Wculvert1, was selected to serve as the reference ratio for the other subbasins. A range of ratios was applied to this basin, and the corresponding subbasin storage coefficients were generated from Equation 5.2.

Three storage coefficient sets (R1, R2, and R3) calculated from the minimum, best fitting, and maximum ratios, respectively, and their results are presented below (Figure 5.7 and Table 5.2). As with the calibration of k, the data were normalized, and the best storage coefficient set was selected visually. The results show that the smallest values of R (R1) produce hydrographs that recede too quickly, and the highest R values (R3) overly prolong the hydrographs' recession. Because the rating curve's low flow magnitudes are highly suspect, the fact that the model is missing some of the low flow events from the 2011 data is not likely an issue. However, poor precipitation data is probably the cause of the model missing any significant peaks, such as the second peak from the 2010 measured data.

2011 2011

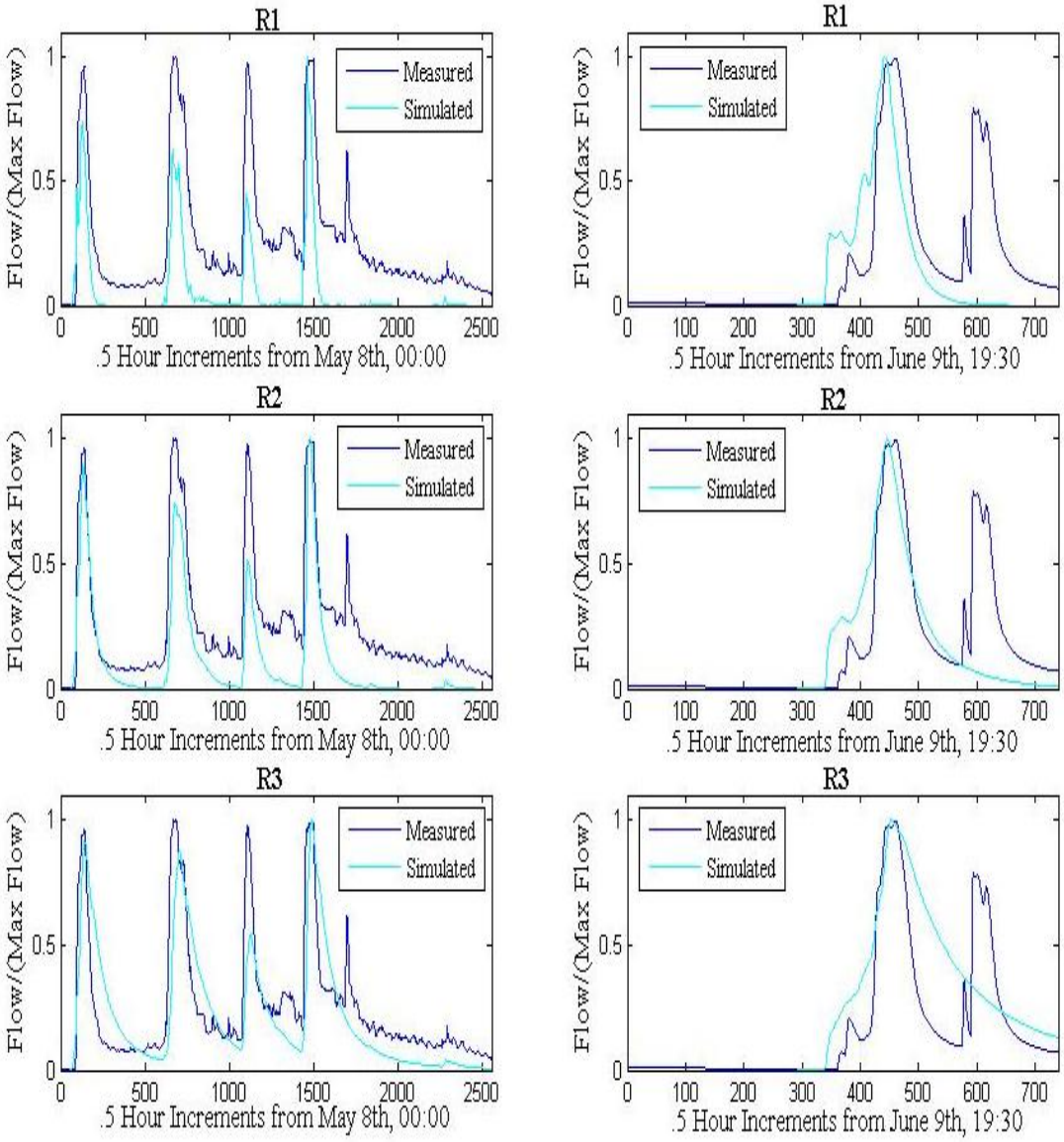

Figure 5.7: Hydrographs produced by the different storage coefficient sets represented in Table 5.2.

Table 5.2: The storage coefficient sets applied to the model.[a]

	SET R1	SET R2	SET R3
Subbasin	R	R	R
W6P1	0.46	3.24	11.57
W6P2	0.22	1.57	5.61
W6P4	3.86	27.00	96.43
W5P12	0.81	5.65	20.19
W5P15	0.28	1.93	6.88
W5P6	0.51	3.55	12.67
W5P5	0.63	4.38	15.65
Wculvert2	1.37	9.59	34.24
W5P10	0.27	1.91	6.82
W5P4	1.34	9.37	33.46
W5P3	0.79	5.50	19.63
W5P11	0.13	0.89	3.16
W680	0.98	6.84	24.42
W5P9	0.38	2.63	9.38
WBEseg19	2.77	19.42	69.37
W5P1	1.12	7.86	28.07
W4P2	0.43	3.01	10.75
W4P4	0.54	3.77	13.47
W4P3	0.38	2.65	9.45
W4P1	1.26	8.84	31.57
W4_REM	2.76	19.31	68.98
W3P5	0.26	1.81	6.46
W580	0.66	4.61	16.46
W3P6	0.08	0.57	2.03
W3P4	0.41	2.90	10.36
W3P3	1.14	8.01	28.62
W3P2	0.41	2.90	10.34
W3_REM	6.99	48.92	174.70
W2P1	1.09	7.66	27.36
W2_REM	1.40	9.83	35.12
W1P6	0.65	4.56	16.28
W1P3	0.36	2.53	9.05
W1P4	0.22	1.56	5.56
WBEseg5	1.52	10.62	37.93
W1P2	0.42	2.94	10.48
Wculvert1	1.00	7.00	25.00
W1P1	0.54	3.77	13.45
WOutlet	0.68	4.78	17.08

[a]The ratio R/(R+Tc) was assumed for the Wculvert1 subbasin and the other R values were calculated from Equation 5.2.

To check the interaction between the calibration of k and R, all of the k values were retested with the best set of storage coefficients, R2, and the best value for k remained the previously chosen .028. Before, the k value had been calibrated based on all R values equaling 5. The results for a k of .014 shows that the modeled peak flow rates are reduced by the new R values, but the peak magnitudes relative to each other stay similar (Figure 5.8). These results were typical for all the k values simulated. Because relative magnitudes were the parameter of interest, the original best k value was retained.

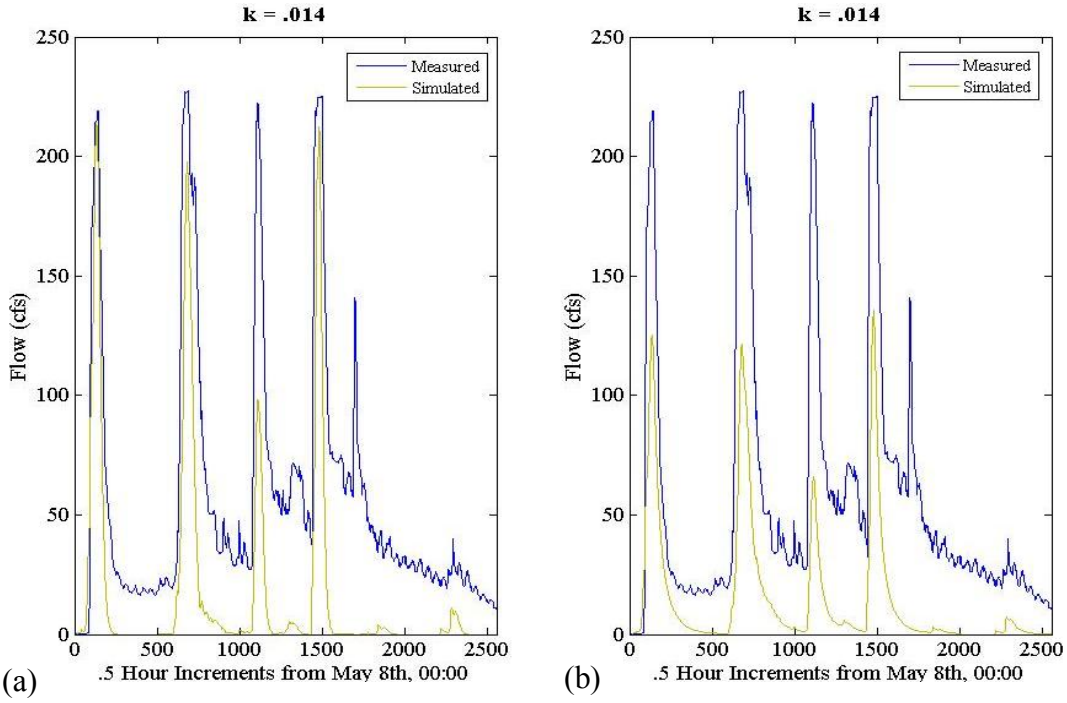

Figure 5.8: The simulations produced by k = .014 and (a) the original set of storage coefficients and (b) the R2 set of storage coefficients.

The best simulations for 2010 and 2011 are shown below and use a k value of .028 and the R2 set of storage coefficients. The data has been normalized to better compare relative peaks and shapes between the measured and simulated hydrographs.

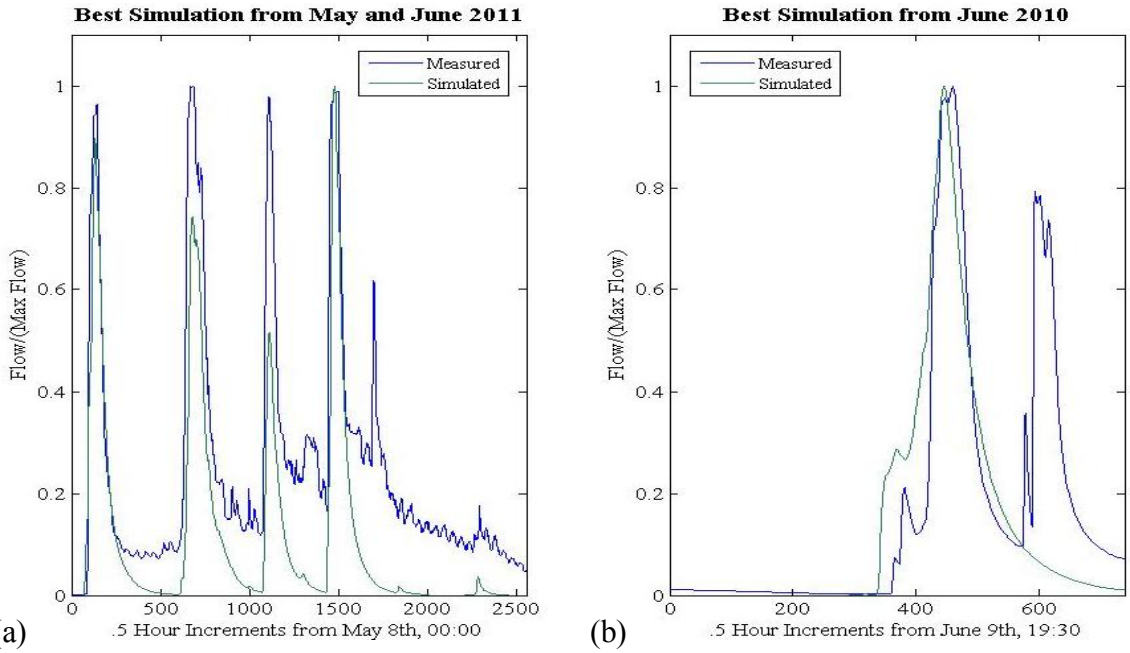

(a) (b)

Figure 5.9: The best hydrograph replications for (a) 2011 data and (b) 2010 data. The simulations are produced by k = .028 and the R2 set of storage coefficients.

ANALYSIS

Frequency Analysis

Determining the cumulative impact of the ponds was accomplished by running a series of frequency-based storms within the model on two watershed scenarios: the watershed as it currently exists with all 28 ponds left in and the watershed in an artificial state with all of the stock ponds taken out. Changes to the flow regime were inferred from peak flow rates and total runoff volumes, factors that influence the ecology of the watershed.

Return intervals of 2, 5, 10, 25, 50, and 100 years were used. A wide range of return intervals was selected to cover a variety of possible dominant channel-forming discharges. Wolman and Miller [1960] define the channel-forming discharge as the discharge that transports the most sediment and, as a result, dictates channel geomorphology. Several studies have shown the channel-forming discharge and the bankfull discharge to be nearly equal [e.g., Leopold, 1994; Powell et al, 2006; Whiting et al, 1999]. Engineers have interpreted this channel-forming discharge to be approximately that of a 1 to 2 year return interval flow [Powell et al, 2006]. While this convenient simplification is often employed, the conclusions of interchangeability for bankfull and channel-forming discharges were not derived from river systems in semi-arid environments.

A few studies have investigated the question of dominant channel-forming flow as it applies to arid and semi-arid watersheds [Friedman and Lee, 2001; Baker, 1977].

Friedman and Lee [2001] noted that the channel-forming flow increases in return interval as watershed size decreases and as the climate becomes more arid. Therefore it may be more appropriate to examine larger events when determining the influence of stock ponds on flow in Box Elder Watershed. Considering the uncertainties surrounding the choice of storm interval to analyze, a range of frequency storms was simulated to insure the most influential storm on geomorphology was modeled.

24 hour storms were selected to coincide with the time to concentration of the watershed. This duration ensures the entire watershed contributes to runoff at once and allows for a maximized peak flow rate to be modeled. Also, an initial abstraction ratio of 0.2 was used as a result of model calibration and the assumption that the watershed began each simulation in its standard condition.

The watershed with all ponds left in was tested for each frequency storm with three different starting pond volumes: empty, half full (by volume), and full. An empty state was selected to replicate drought conditions where the watershed would be most sensitive to the effects of the ponds. The half full start state helped to account for any uncertainty regarding the pond volume measurements, and the full state showed the pure attenuation effects of the ponds. The results are summarized in the tables below.

Table 6.1: The peak flow rates (cfs) and runoff volumes (in) for the watershed without ponds and the watershed with empty ponds.

Watershed without Ponds and Watershed with Empty Ponds							
RI	Precip.	Peak Q w/o ponds	Peak Q w/ ponds	Peak difference	Runoff Volume w/o ponds	Runoff Volume w/ ponds	Runoff Volume difference
	in.	cfs	cfs	%	in.	in.	%
100	3.44	548	437	20.2	1.1029	0.9915	10.1
50	3.10	431	327	24.1	0.8899	0.7936	10.8
25	2.71	314	241	23.0	0.6634	0.5839	12.0
10	2.22	186	143	22.9	0.4013	0.3448	14.1
5	1.86	102	83	18.6	0.2274	0.1891	16.8
2	1.42	29	26	12.7	0.0667	0.056	15.1

Table 6.2: The peak flow rates (cfs) and runoff volumes (in) for the watershed without ponds and the watershed with half full ponds (by volume).

Watershed without Ponds and Watershed with Half Full Ponds							
RI	Precip.	Peak Q w/o ponds	Peak Q w/ ponds 50% full	Peak difference	Runoff Volume w/o ponds	Runoff Volume w/ ponds 50% full	Runoff Volume difference
	in.	cfs	cfs	%	in.	in.	%
100	3.44	548	457	16.5	1.1029	1.0229	7.3
50	3.1	431	356	17.4	0.8899	0.8175	8.1
25	2.71	314	260	17.1	0.6634	0.6011	9.4
10	2.22	186	146	21.3	0.4013	0.3573	11.0
5	1.86	102	84	17.4	0.2274	0.1984	12.8
2	1.42	29	27	7.7	0.0667	0.0573	14.1

Table 6.3: The peak flow rates (cfs) for the watershed without ponds and the watershed with full ponds. There is no difference in runoff volume since the ponds are full and have no storage capabilities.

Watershed without Ponds and Watershed with Full Ponds				
RI	Precip.	Peak Q w/o ponds	Peak Q w/ ponds 100% full	Peak difference
	in.	cfs	cfs	%
100	3.44	548	535	2.4
50	3.1	431	419	2.7
25	2.71	314	303	3.5
10	2.22	186	179	3.7
5	1.86	102	98	4.3
2	1.42	29	29	2.5

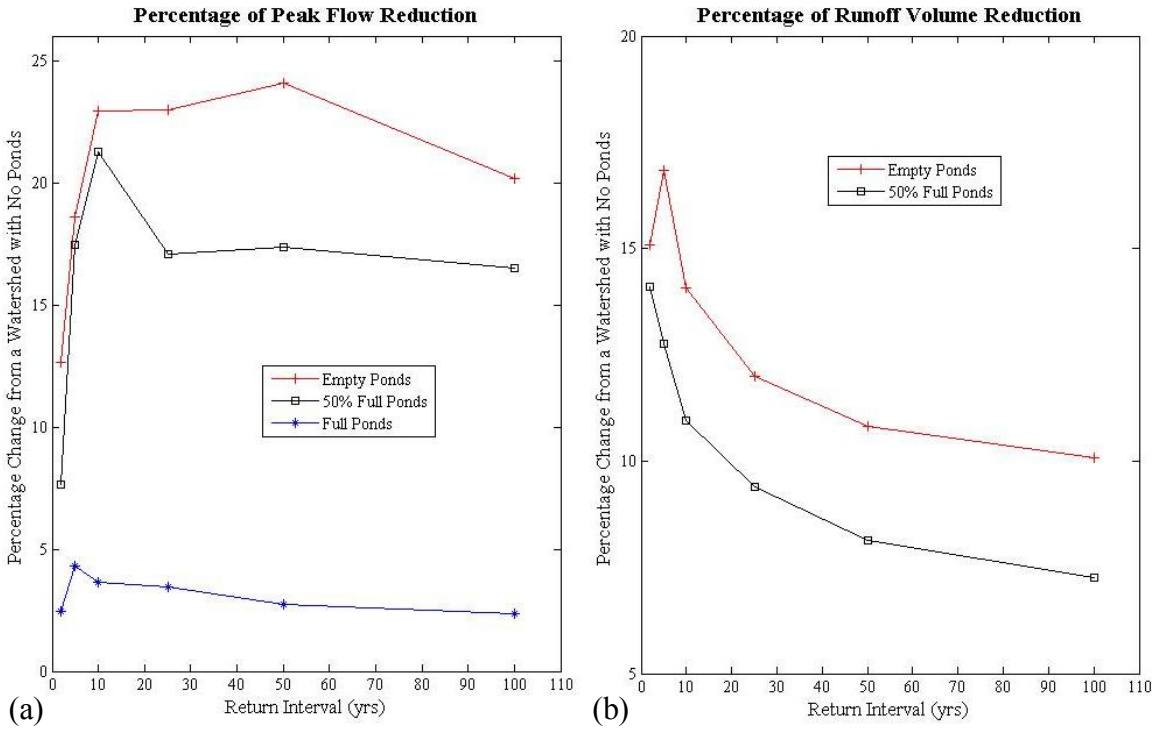

Figure 6.1: Graph of percent reductions compared to Box Elder Watershed with no ponds for (a) peak flow rate and (b) runoff volume.

The results indicate that the ponds have an effect on the flow from Box Elder Watershed. There are differences in the peak flow rates in the various conditions for all modeled return intervals. Peak flow reductions ranged from 12.7% to 24.1% for the watershed with empty ponds, 7.7% to 21.3% for the watershed with ponds half full, and 2.4% to 4.3% for the watershed with ponds at storage capacity. Volume reduction ranges were 10.1% to 16.8% for the watershed with empty ponds and 7.3% to 14.1% for the watershed with ponds half full. The influence of return interval on runoff rate (Figure 6.1a) is not a continuously decreasing function (as is the case for runoff volume, Figure 6.1b) and indicates that there are complex interactions controlling precipitation volume and runoff rate.

Stock ponds slightly alter the timing of peak runoff rates (Figure 6.2). Compared to a watershed without stock ponds, the watershed with empty ponds has delayed peak discharges for large precipitation events. Conversely, the 2-year storm's hydrograph peaks two and a half hours earlier, and the 5-year storm's hydrograph peaks one and a half hours earlier. Earlier peaks occur because most ponds reside on hydraulically distant tributaries and capture most of the excess rain produced by their subbasins. The shorter time to concentrations of areas contributing to runoff leads to earlier peak discharges when ponds are in place. The irregularities of the timing for the 2-year hydrographs can be attributed to bimodal flow. Not all of the subbasins produce excess rain, and the runoffs from subbasins responding to the event arrive at the outlet staggered because of disconnected locations.

The reduction in runoff volume (largest reduction was 16.8% for a watershed with empty ponds and a 5 year event) follows a predictable pattern since the ponds hold a finite volume, and the solution for runoff volume is not dependent on timing of runoff (Figure 6.1b). As the precipitation events become larger the volume held by the ponds becomes a smaller percentage of the total excess rain. The increase in percent reduction for the 5 year event from the 2 year event indicates that some ponds do not reach full capacity for a 2 year event. There was also a noticeable reduction in flow volume for the half-full pond scenario, showing that even a conservative estimation of pond volumes still negatively impacts the watershed.

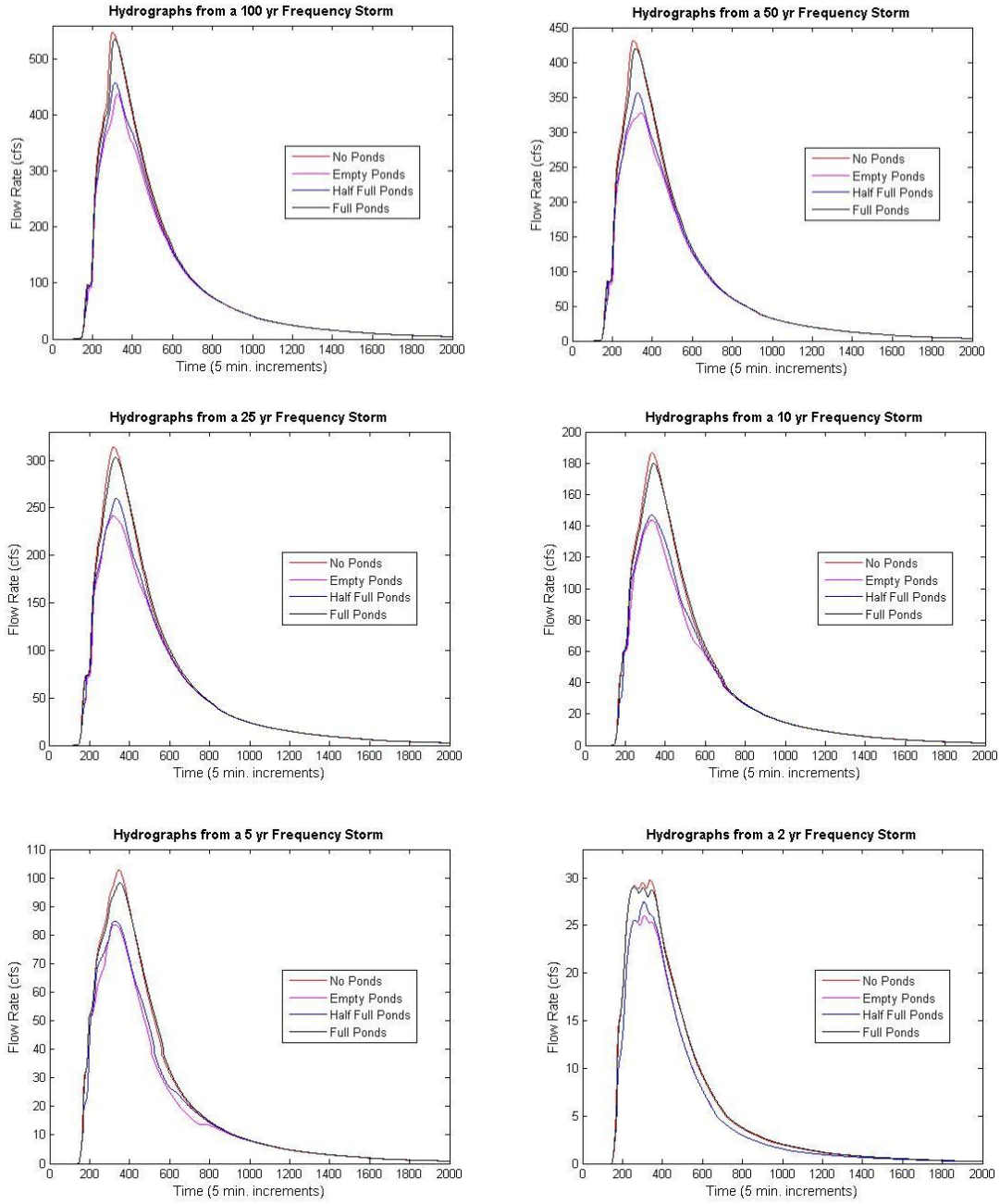

Figure 6.2: The hydrographs from varying return intervals and scenarios.

Parameter Correlations

The next step taken in analysis was to determine whether easily measured parameters could predict the impact of specific ponds. Any relationship found between a particular parameter and pond influence would have obvious benefits for future water management decisions. The analysis was done by simulating a watershed with all ponds but one removed and using the developed frequency storms as the precipitation input. The results were compared to the runoff volume and peak flow rate of an unaltered watershed and the percentage change was used as the dependent variable. A higher percentage of change corresponded to a pond with more influence on the hydrologic regime. Over a hundred simulations were performed. Appendix E contains the results used for the analysis.

An inventory of parameters with a possible influence on flow was compiled including: contributing area (A_c), pond volume (P_v), the pond's subbasin's curve number (CN_{sub}), hydraulic distance of the pond to the outlet (D_h), overall slope of the channel from the pond to the outlet (S), and precipitation depth (P_d). The difficulties in determining hydraulic travel time and time to concentration for ungaged watersheds resulted in not including these parameters in the analysis. Empirical formulas exist, but these equations usually require only slope and hydraulic length, parameters already included in the analysis. Simple linear regression to determine the influence of any individual parameter on peak discharge and runoff volume was generally poor even when separate regressions were performed for each return interval (Table 6.4). Figure 6.3

shows a typical correlation having an R^2 value of only 0.22 for peak flow percent reduction for a 50 year storm vs. pond volume.

Pond volume was the best predictor of peak flow rate, but these values are still statistically weak (R^2 values ranged from 0.13 to 0.38 for the return intervals). Contributing area, curve number, slope, and hydraulic distance are all poorly correlated with peak flow percentage reductions, indicating complex hydrologic interactions. Poor predictions of peak discharge using a single parameter were not surprising considering the complex interactions influencing the exact timing of flows in the watershed.

The correlations for the runoff volume analysis are slightly stronger. The best correlations occur for the pond volume and contributing area parameters. Correlations for the pond volume parameter become better as the return interval increases. Larger events fill the ponds while smaller events do not, making the influence of pond volume on runoff volume more direct for larger events. As the return interval decreases, the likelihood that a pond stores all of the runoff volume increases, and runoff volume becomes more influential. Since contributing area significantly influences the potential runoff volume, the correlations for contributing area go up as return interval decreases. The single best correlation observed was for the contributing area parameter and the 5 year return interval (0.67).

Table 6.4: R^2 correlation values for each pond's parameter value paired against its percent change in runoff volume and peak flow rate for the developed frequency storms. Plotting the parameters by return interval eliminated the need to plot precipitation depth separately.

Pond Volume RI	Correlation to Peak Flow Influence	Correlation to Runoff Volume Influence
2	0.1945	0.0204
5	0.1565	0.0514
10	0.1274	0.128
25	0.1411	0.3142
50	0.2203	0.4793
100	0.3806	0.5826

Contributing Area RI	Correlation to Peak Flow Influence	Correlation to Runoff Volume Influence
2	0.00008	0.4129
5	0.0078	0.6739
10	0.0217	0.6196
25	0.0323	0.4518
50	0.0373	0.2955
100	0.0351	0.1809

CN RI	Correlation to Peak Flow Influence	Correlation to Runoff Volume Influence
2	0.2153	0.2316
5	0.0283	0.0457
10	0.0003	0.0258
25	0.0074	0.0041
50	0.0082	0.00007
100	0.0243	0.0014

Hydraulic Distance RI	Correlation to Peak Flow Influence	Correlation to Runoff Volume Influence
2	0.1684	0.0847
5	0.0053	0.0046
10	0.0138	0.0077
25	0.0536	0.0028
50	0.0326	0.0018
100	0.0547	0.0001

Slope to the Outlet RI	Correlation to Peak Flow Influence	Correlation to Runoff Volume Influence
2	.3263	.1879
5	.0141	.0013
10	.0382	.0005
25	.0616	.0002
50	.0468	.0004
100	.0499	.0004

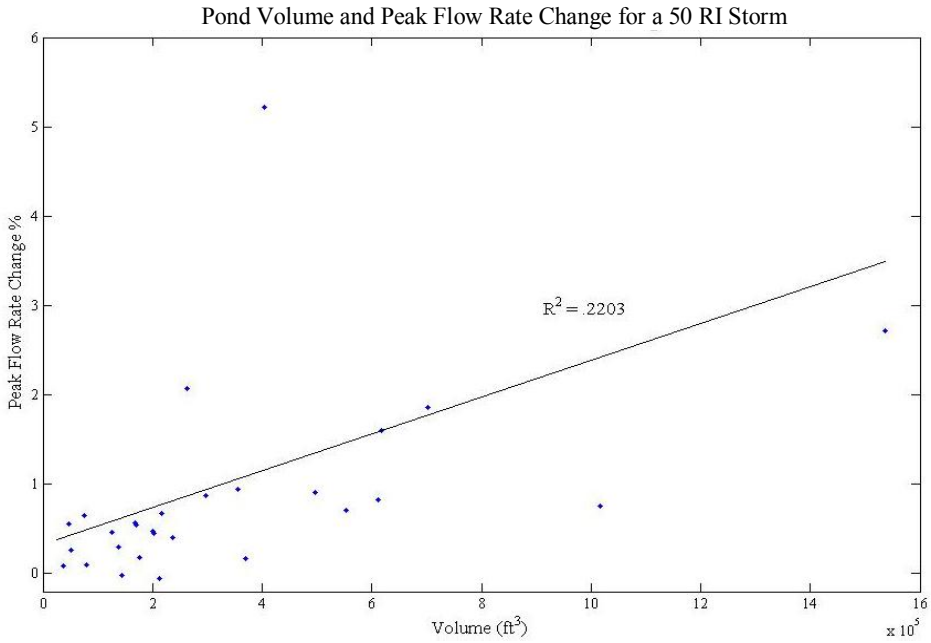

Figure 6.3: Correlation of pond volume and peak flow rate change for a 50 RI storm. The linear regression line fitted to the data shows a low correlation.

The observed correlation trends for runoff volume suggested that combinations of parameters might provide insight into the ponds' influences on runoff volume. The Buckingham Π theorem was used to create dimensionless parameter sets and avoid redundancies. The number of parameter sets generated was dictated by the following equation:

$$p = n - k \tag{6.1}$$

p = number of parameter sets generated
n = number of variables
k = independent fundamental physical quantities represented by the variables

Three predictor parameter sets were generated for the runoff volume influence analysis (Figure 6.4). Hydraulic distance and slope to the outlet were specifically not used in the analysis since runoff volume is independent of a pond's position in the watershed. Generating parameter sets by the Buckingham Π method requires the

selection of repeating variables. The number of repeating variables used should usually match the number of independent fundamental physical quantities represented by the variables. Only length is considered for runoff volume, so only one repeating variable was required. Precipitation depth was chosen as the repeating variable, and the remaining variables were combined with precipitation depth to form dimensionless parameter sets. The following steps demonstrate the generation of a set.

Contributing area, A_c, is a non-repeating variable that represents the fundamental unit length, L.

$$A_c \longrightarrow \{L^2\}$$

A parameter set, Π, is formed by multiplying A_c with the repeating variable raised to the exponent a.

$$\Pi = A_c * (P_d)^a \tag{6.2}$$

P_d = Precipitation depth in the unit of length

The exponent is chosen to create a dimensionless set.

$$\Pi = \frac{A_c}{P_d^2} \longrightarrow \frac{L^2}{L^2} \tag{6.3}$$

The parameter sets were plotted individually against the change in runoff volume from an unaltered watershed caused by the inclusion of one pond ($V_N - V_P$) divided by the runoff volume from a watershed with no ponds (V_N), resulting in three plots. Because the precipitation depth was included as one of the parameters of interest, there was no need to plot the return interval storms separately.

* $\frac{V_N - V_P}{V_N}$

1. $P_d CN_{sub}$

2. $\frac{P_v}{P_d^3}$

3. $\frac{A_c}{P_d^2}$

V_N= Runoff volume for the watershed with no ponds
V_P= Runoff volume for the watershed with one pond
P_V = Pond volume (L^3)
P_d = Precipitation depth (L)
CN_{sub} = Curve number (1/L)
A_c = Contributing area (L^2)

Figure 6.4: Dimensionless parameters tested for correlations to change in runoff volume caused by the inclusion of one pond; * indicates the dependent variable.

Correlations were still weak overall. The highest correlation for runoff volume influence came from the parameter set that included contributing area (A_c) and was .4974. The weak correlations were not completely unexpected since plotting the sets separately does not account for important interactions within the model.

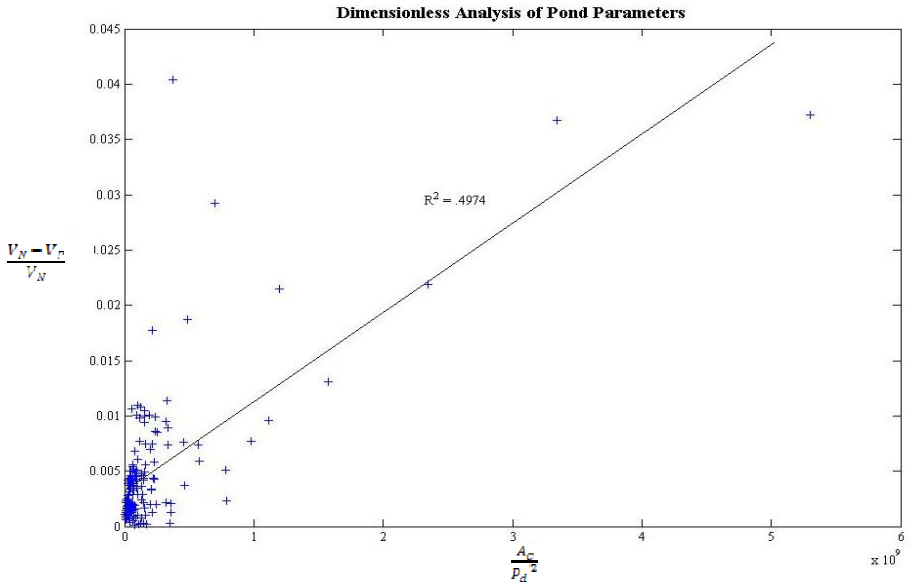

Figure 6.5: A graph for the contributing area parameter set and the corresponding reduction in runoff volume. Significant scatter can be found in the results, and this was typical of all the parameter sets.

The sets were combined to form the following equation in another attempt to find a simple relationship that could be applied to other watersheds:

$$\frac{V_N - V_P}{V_N} = \Pi_1{}^a \Pi_2{}^b \Pi_3{}^c \tag{6.4}$$

Π = A parameter set
a-c = Unknown exponents

The equation was linearized and the exponents were found by least squares regression through MATLAB® [MathWorks, 2010]. The Π values correspond to the labeled parameter sets, and the equation took the following form:

$$\frac{V_N - V_P}{V_N} = \Pi_1{}^{-1.03} \Pi_2{}^{-.20} \Pi_3{}^{.16} \tag{6.5}$$

The equation failed to provide an improved correlation (R^2 = .0354). This led to investigating the equations used by the Curve Number method more closely. It was determined that an inequality relating the volume of the pond (ft^3) and the excess rain volume produced by the pond's subbasin (ft^3) is necessary to describe the level of influence a single pond is having on the system. The relationship is shown by Equation 6.6. The necessary inclusion of the inequality prevented the dimensionless analysis equation from forming any correlations.

$$Volume\ Coefficient = \begin{cases} \dfrac{P_V}{ER_{wtshd}} & for\ P_V < ER_{sub} \\ \dfrac{ER_{sub}}{ER_{wtshd}} & for\ P_V \geq ER_{sub} \end{cases} \tag{6.6}$$

P_v = Pond volume in ft^3
ER_{wtshd} = Excess rain volume produced by the entire watershed in ft^3 (using the curve number equation with a single, composite curve number for the entire watershed)
ER_{sub} = Excess rain volume produced by the subbasin of the stock pond in ft^3 (using the curve number equation with a single, composite curve number for the subbasin)

The working assumption in the use of the equation is that a pond's effect on runoff volume is determined by how much water it can take out of the system through storage. When a subbasin's excess rain volume is less than the volume of its pond, the pond is capable of storing all of that water, and the subbasin's excess rain volume describes the pond's impact on runoff volume. Conversely, when a subbasin's excess rain volume is greater than its pond volume, the pond can only store a volume equal to its own, and the pond's volume becomes the descriptive variable for the pond's impact.

A higher volume coefficient indicates that a pond has a more significant effect on runoff volume. Figure 6.6 below shows the correlation of the volume coefficient to the change in runoff volume from an unaltered watershed caused by a pond. The correlation is high, but not exact, since a composite curve number for the entire watershed was used to estimate total runoff.

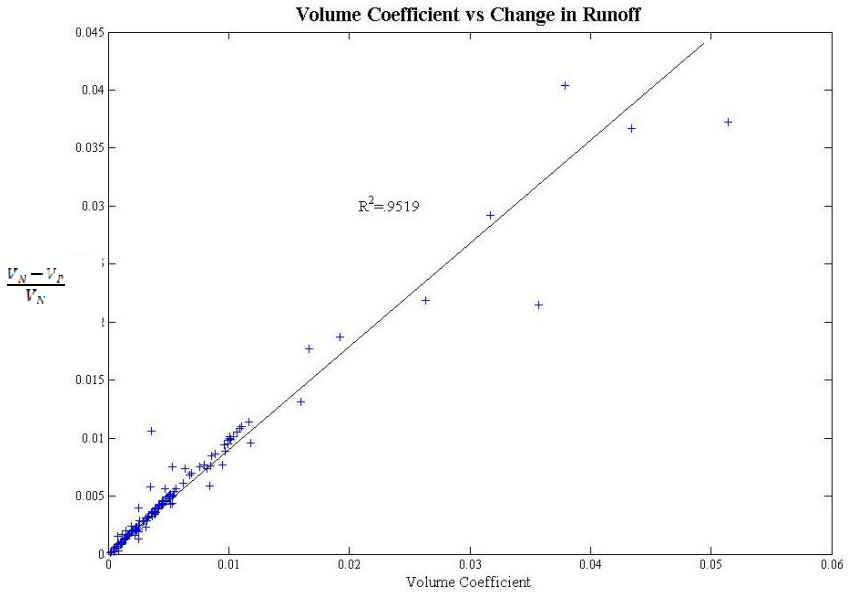

Figure 6.6: Percent change in runoff volume plotted against the computed volume coefficient.

The Buckingham Π method was applied to a pond's effect on peak discharge to complete the parameter investigation. Five predictor parameter sets were generated for the peak discharge analysis (Figure 6.7). Since only length is represented by the non-dependent variables, precipitation depth was chosen as the repeating variable. The remaining variables were combined with precipitation depth to form dimensionless parameter sets.

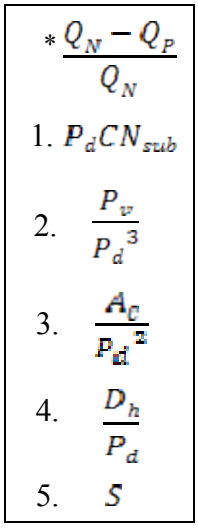

Q_N= Peak discharge for the watershed with no ponds (L^3/T)
Q_P= Peak discharge for the watershed with one pond (L^3/T)
P_V = Pond volume (L^3)
P_d = Precipitation depth (L)
CN_{sub} = Curve number (1/L)
A_c = Contributing area (L^2)
D_h = Hydraulic distance (L)
S = Overall slope from pond to outlet (L/L)

Figure 6.7: Dimensionless parameters tested for correlations to change in peak flow rate caused by the inclusion of one pond; * indicates the dependent variable.

As with the runoff volume analysis, plotting the parameter sets and the dependent variable provided no insight into the relationships determining peak discharge influence. The highest correlation was for the second parameter set containing the pond volume parameter (.047).

The parameters were then combined in an equation in an attempt to account for interactions within the model. The fitted equation follows:

$$\frac{Q_N - Q_P}{Q_N} = \Pi_1^{.0014} \Pi_2^{.0002} \Pi_3^{.0022} \Pi_4^{.0005} \Pi_5^{.0088} \text{ -1*} \quad (6.7)$$

*Some of the dependent values were negative. In order to avoid difficulties during linearization using logarithms, a one was added to the values and then subtracted at the end.

The equation failed to drastically improve results and gave an R^2 value of .0919. The difficulty in finding correlations between simplified, dimensionless parameter sets and their corresponding influence to flow rate may be due to fact that there are no easily measured parameters representing the fundamental unit of time. This is important because the model uses dynamic and time dependent processes to determine peak flow. The watershed's peak flow response is influenced by how a subbasin transforms excess rain and how water is routed to the outlet. Reviewing the Muskingum-Cunge channel routing equation helps to explain the issues related to deriving a simple, predictive relationship for a pond's influence on peak flow. A complete discussion of Muskingum-Cunge is presented in the literature review.

$$O_t = \left(\frac{\frac{\Delta t}{K} + 2X}{\frac{\Delta t}{K} + 2(1-X)}\right) I_{t-1} + \left(\frac{\frac{\Delta t}{K} - 2X}{\frac{\Delta t}{K} + 2(1-X)}\right) I_t + \left(\frac{2(1-X) - \frac{\Delta t}{K}}{\frac{\Delta t}{K} + 2(1-X)}\right) (O_{t-1}) + \left(\frac{2\frac{\Delta t}{K}}{\frac{\Delta t}{K} + 2(1-X)}\right) (q_L \Delta x) \quad (2.14)$$

$$K = \frac{\Delta x}{c} \quad (2.15)$$

$$X = \frac{1}{2}\left(1 - \frac{Q}{BS_o c \Delta x}\right) \quad (2.16)$$

Q = flow rate
c = wave celerity
μ= hydraulic diffusivity

B = top width of water surface
S_0 = channel slope

The time dependent Muskingum-Cunge equation has constantly changing inputs that dictates its solution. For example, the X and K parameters use wave celerity in their definitions. Wave celerity describes the change in flow rate over the change in cross sectional area. It is dependent on the amount of water in the system at a given time step and on across section's geometry. The parameter X requires another temporally changing variable, the top width of a wetted cross section. The continuous transformation of runoff by the routing equation makes predicting the effects of individual ponds without a model exceedingly difficult.

It would have been beneficial to find a simple relationship that predicted which ponds caused the most impact on peak discharge from a water management point of view, but the results do highlight the complex nature of the model. While a pond's impact on runoff volume is easily determined, modeling a watershed may be necessary to determine an individual pond's total influence on the system.

Pond Removal

An important goal of the analysis was to provide a ranking of individual pond influences on runoff volume and peak discharge for pond removal decisions. This was accomplished by running the model with all ponds but one in place for all return intervals. The complete results and pond ownership data for management decisions are shown in Appendix F. Percent changes are measured from the unaltered watershed.

Table 6.5: Ponds most influential on volume runoff.

Rank	RI 2	5	10	25	50	100
1.	1P1	6P4	6P4	6P4	4P1	4P1
2.	6P4	1P1	5P12	5P12	4P2	4P2
3.	1P2	4P1	1P1	4P1	6P4	6P4
4.	4P1	1P2	4P1	4P2	5P12	5P12
5.	1P4	2P1	2P1	2P1	2P1	5P1

Table 6.6: Ponds most influential on peak flow rate

Rank	RI 2	5	10	25	50	100
1.	1P1	5P11	5P12	5P12	5P12	5P12
2.	1P3	2P1	4P2	4P2	4P2	4P2
3.	1P2	3P5	2P1	2P1	6P4	4P1
4.	1P4	4P2	4P1	4P1	4P1	6P4
5.	1P6	1P6	1P6	5P15	5P15	5P15

The exact rankings differ for every return interval, but the most influential ponds for one return interval often reappear near that same ranking for other return intervals. This is especially true for return intervals of 10 years and higher. To reduce variability between return intervals, the cumulative ranking of each pond for both parameters over all return intervals was computed (Table 6.7).

Table 6.7: The ponds ordered based on their effects on runoff volume and peak flow rate. Ponds with a lower rankings sum are having a greater influence on the system.

Pond	Rankings Sum	Pond	Rankings Sum	Pond	Rankings Sum
4P1	47	1P4	148	5P11	222
4P2	53	1P2	157	5P10	226
2P1	80	3P5	158	6P1	231
6P4	89	5P3	158	3P6	233
1P6	90	4P4	164	5P6	236
5P12	106	1P1	168	3P4	251
3P3	110	3P2	203	5P5	256
5P1	117	4P3	213	6P2	295
1P3	119	5P9	217		
5P15	128	5P4	220		

The summed rankings for each pond were then plotted on the x-axis against the sum of the pond's rankings (its ranking for peak flow rate added to its ranking for runoff volume) for the individual return intervals (Figure 6.8). Relatively strong correlations suggest that pond rank does not vary much with return interval, especially for return intervals greater than 5. Poorer correlations for return intervals of 5 and especially 2 suggest that the influence of a pond for a low return interval (low precipitation value) is different than for a higher value. If the channel forming discharge for Box Elder Watershed is from storms of lower return intervals, pond removal decisions might be different than for higher flows.

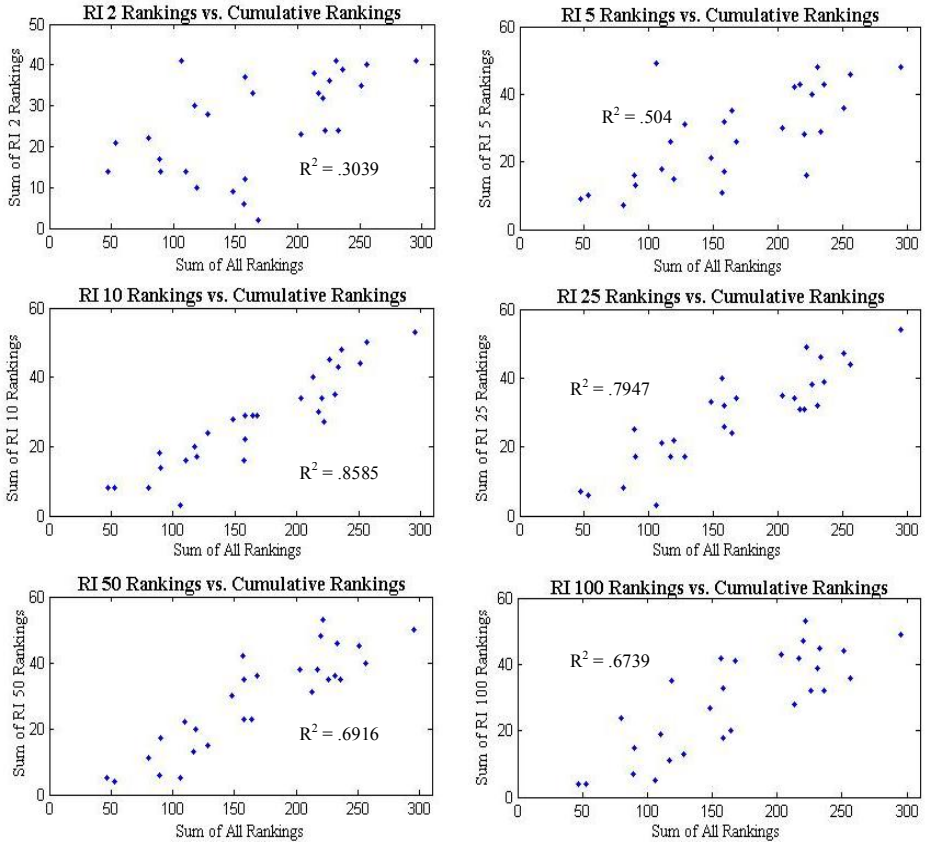

Figure 6.8: The comparison of overall pond rankings and the rankings for every return interval.

Table 6.7 also helps to prioritize pond removal for Box Elder Watershed by combining all of the results into a single list. Lower values indicate a greater influence on the hydrologic response of Box Elder Watershed and show pond 4P1 having the greatest overall effect on the system.

Some similarities in rank between peak flow rate and runoff volume suggest it may be acceptable to design for runoff volume when selecting which ponds to remove from a watershed. The rankings for volume runoff influence were plotted against the rankings for peak flow rate influence to observe any trends between the two ranking sets (Figure 6.9).

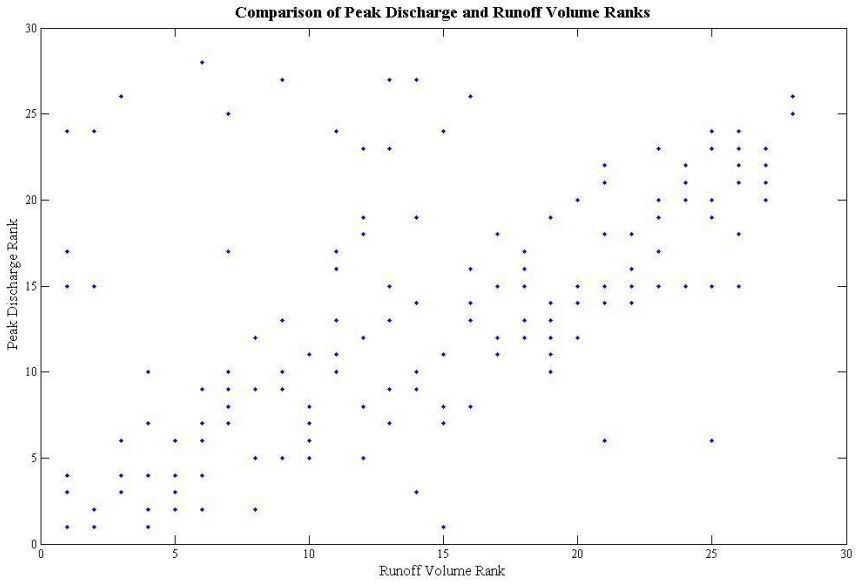

Figure 6.9: The rankings for volume runoff influence plotted against the rankings for peak flow rate influence.

The results show a fair amount scatter, but 46 of the 62 data points that have a ranking of ten or less for peak discharge also have a ranking of ten or less for runoff

volume. Pond removal decisions based on runoff volume influence will most likely include many of the same ponds most influential on peak flow rate.

Determining a pond's effect on runoff volume by calculating its volume coefficient with the Curve Number equations is a much more realistic option for ungaged watersheds when compared to designing for peak flow rate. Since the volume coefficient requires only land cover data, soil data, frequency storms, pond volumes, and watershed areas, the index could be transferred to other watersheds where inexpensive and quick methods are needed for pond removal decisions. While the overlapping results from this project show that reasonable improvements can be made by designing for runoff volume, understanding a pond's full influence on the system still requires an exhaustive modeling effort. Plotting the volume coefficient against a pond's influence on peak discharge gives an R^2 of only 0.113, indicating that the index is inadequate to fully explain a pond's influence on the hydrologic regime.

Wildlife concerns and land ownership may prevent the removal of a specific, influential pond in Box Elder Watershed, but taking out other combinations of ponds could accomplish similar changes in the hydrologic regime since few ponds cascade. The total change in runoff volume for a specific return interval by the removal of many ponds would be the sum of the individual ponds' effects (assuming no cascading effects). The exact peak flow rate reduction from multiple pond removals could not be determined from such a simple summation because of the complex routing equations. Table 6.8 shows the flow rate increase (cfs) caused by the individual removal of the three most influential ponds on peak discharge for the one-pond-out analysis (all other ponds are left

in). Table 6.9 gives the peak flow rate increase (cfs) caused by the removal of the three most influential ponds at the same time for a return interval. The differences between the sum of the individual increases and the increase from all three ponds taken out at once are generally small and indicate that a summation of individual ponds' influences on peak flow rate is an acceptable estimation. The differences between the summed influences and the influence from the ponds removed together will likely increase as the number of ponds removed increases because of the non-linear relationships governing flow rate.

Table 6.8: The individual peak flow increase (cfs) for the three most influential ponds on peak discharge for the one-pond-out analysis.

Rank	One Pond Out					
	RI 2	RI 5	RI 10	RI 25	RI 50	RI 100
	Pond-Peak Discharge Increase (cfs)	Pond-Peak Discharge Increase (cfs)	Pond-Peak Discharge Increase (cfs)	Pond-Peak Discharge Increase (cfs)	Pond-Peak Discharge Increase (cfs)	Pond-Peak Discharge Increase (cfs)
1.	1P1 - 1.83	5P11 - 1.57	5P12 - 9.93	5P12 - 18.53	5P12 - 18.58	5P12 - 15.03
2.	1P3 - .5	2P1 - 1.39	4P2 - 4.75	4P2 - 8.31	4P2 - 9.73	4P2 - 13.57
3.	1P2 - .49	3P5 - 1.37	2P1 - 3.27	2P1 - 5.57	6P4 - 9.41	4P1 - 11.09
Sum of Peak Discharge Increases (cfs)	2.82	4.33	17.95	32.41	37.72	39.69

Table 6.9: The peak flow increase (cfs) caused by the removal of the three most influential ponds at the same time for various return intervals.

	Three Ponds Out					
	RI 2	RI 5	RI 10	RI 25	RI 50	RI 100
Ponds Removed	1P1, 1P3, 1P2	5P11, 2P1, 3P5	5P12, 4P2, 2P1	5P12, 4P2, 2P1	5P12, 4P2, 6P4	5P12, 4P2, 4P1
Peak Discharge Increase (cfs)	2.75	4.19	17.16	30.86	34.17	39.08

Pond removal decisions will ultimately be left to land managers who must balance wildlife needs with stream restoration goals and other land owner considerations. This report hesitates to strongly advocate any specific ponds for removal because of considerations beyond the scope of this project.

SUMMARY AND CONCLUSIONS

The hydrology of Box Elder Creek was modeled to explore the effects of 28 stock ponds currently on the watershed. Stock ponds have received little attention in regards to their influence on flow regimes, and this research helped to quantify their impact for water management decisions on the American Prairie Reserve. Limited research on farm dams had previously been completed for watersheds in Austrailia [e.g. Callow and Smetten 2009; Schreider et al 2002; Verstraeten and Prosser, 2008], but no work was found on stock ponds and their watershed-scale effects in the Northern Great Plains. This work is meant to help guide efforts in restoring prairie streams.

Modeling Box Elder Watershed involved a combination of field and computer work. The ponds were identified from aerial photos and verified during field investigations. Each pond's volume was described through a stage-area function fitted to field measurements and then entered into the HEC-HMS model to account for the model's stage and storage requirements. Additional field measurements included those to describe the shapes and roughness parameters of the channel reaches. Physical parameters not measured in the field were abstracted through ArcGIS using HEC-GeoHMS. HEC-GeoHMS was also used to set up the HEC-HMS model and transform the precipitation point data into an appropriate form.

After the model was constructed, the model was refined by the calibration of specific parameters using measured flow data. Because only water height had been recorded, calibration was preceded by the development of a rating curve for the outlet's culverts to convert stage data to flow rates. A HEC-RAS model was built to describe the

hydraulics at the outlet. Once the model was calibrated, the watershed was simulated with all of the ponds left in and all of the ponds taken out for synthesized frequency storms. This served to quantify the cumulative effect of the ponds.

Results showed that the ponds have a noticeable effect on the flow regimes of Box Elder Watershed and indicate that some pond removal will be necessary to mitigate peak flow and volume reductions caused by the inclusion of the ponds. Model simulations with only one pond out at a time showed that most ponds have a negligible individual effect. This means multiple ponds will have to be removed to achieve significant changes. Unfortunately, no simple relationships between a pond's parameters and its influence on flows could be discerned from the data, making pond removal predictions without the aid of a model more difficult for areas outside of Box Elder Watershed. The following list summarizes key findings from the analysis of the hydrologic model for Box Elder Watershed:

- A simulated Box Elder Watershed with no stock ponds demonstrated that the stock ponds are reducing peak flow rates by 12.7% to 24.1% and reducing runoff volumes by 10.1% to 16.8% depending on the return interval of the design storm modeled.

- An analysis of pond parameters and the ponds' corresponding influence on peak flow rate and runoff volume was unsuccessful in finding a simple relationship that could predict a pond's impact and be used for other watersheds.

- A ranking system that combined all the results from runoff volume and peak discharge provided an ordered list of the relative influence of the ponds on Box Elder Watershed.

- The results showed that making watershed management decisions based on runoff volume may be acceptable when there are limited resources. The curve number equation can be applied inexpensively to other watersheds to determine which ponds should take priority for removal.

This project highlights the need for further investigations into stock ponds and their influence on the hydrology of prairie systems. Pond removal is a likely outcome in efforts to restore portions of the Northern Great Plains to a more unaltered condition, and careful planning will be required to maintain suitability for animals living on limited ranges.

REFERENCES CITED

Ahmad, M.M., A.R. Ghumman, and S. Ahmad (2009), Estimation of Clark's instantaneous unit hydrograph parameters and development of direct surface runoff hydrograph, *Water Resources Management*, 23(12), 2417-2435.

Akan, A.O. (2006), *Open Channel Hydraulics*, Butterworth-Heinemann, Burlington, MA.

Anderson, M.L., Z.Q. Chen, M.L. Kayvas, and A. Feldman (2002), Coupling HEC-HMS with atmospheric models for prediction of watershed runoff, *Journal of Hydrologic Engineering,* 7(4), 312-318.

Anselmetti, F.S., R. Buhler, D. Finger, S. Giradclos, A. Lancini, C. Rellstab, and M. Sturm (2007), Effects of Alpine hydropower dams on particle transport and lacustrine sedimentation , *Aquatic Sciences*, 69(2), 179-198.

Aristeidis G.K., and I. K. Tsanis (2010), A method for estimating flash flood peak discharge in a poorly gauged basin: case study for the 13-14 January 1994 flood, Giofiros basin, Crete, Greece, *Journal of Hydrology*, 385(1-4), 150-164.

Baker, V.R. (1977), Stream-channel response to floods, with examples from central Texas, *Geological Society of America Bulletin*, 88(8), 1057-1071.

Barry, D.A., and K. Bajracharya (1995), On the Muskingum-Cunge flood routing method, *Environment International*, 21(5), 485-490.

Beighley, R.E., J.M. Melack, and T. Dunne (2003), Impacts of California's climatic regimes and coastal land use change on streamflow characteristics, *Journal of the American Water Resources Association,* 39(6), 1419-1433.

Beven, K. (1993), Prophesy, reality and uncertainty in distributed hydrological modeling, *Advances in Water Resources,* 16(1), 41-51.

Beven, K.J., and M.J. Kirkby (1979), A physically based, variable contributing area model of basin hydrology, *Hydrological Sciences Bulletin*, 24(1), 43-69.

Bhaduri, B., J. Harbor, B. Engel, and M. Grove (2000), Assessing watershed-scale, long-term hydrologic impacts of land-use change using a GIS-NPS model, *Environmental Management,* 26(6), 643–658.

Bockelmann, B.N., E.K. Fenrich, and R.A. Falconer (2004), Development of an ecohydraulics modelfor stream and river restoration, *Ecological Engineering*, 22(4-5), 227-235.

Bodhaine, G.L. (1968), Measurement of peak discharges at culverts by indirect methods, *U.S. Geological Survey Techniques of Water-Resources Investigations*. 3(A2), 1-60.

Borga, M. (2002), Accuracy of radar rainfall estimates for streamflow simulation, *Journal of Hydrology*, 267(1-2), 26–39.

Bosznay, M. (1989), Generalization of SCS Curve Number Method, *Journal of Irrigation and Drainage Engineering,* 115(1), 139-145.

Boughton, W.C. (1989), A review of the USDA SCS curve number method, *Australian Journal of Soil Research*, 27(3), 511-523.

Callow, J.N., and K.R.J. Smetten (2009), The effect of farm dams and constructed banks on hydrologic connectivity and runoff estimation in agricultural landscapes. *Environmental Modeling Software*, 24(8), 959-968.

Callow, J.N., K.P. Van Niel, and G.S. Boggs (2007), How does modifying a DEM to reflect known hydrology affect subsequent terrain analysis, *Journal of Hydrology*, 332(1-2), 30-39.

Chin, A., L.R. Laurencio, and A.E. Martinez (2008), The hydrologic importance of small- and medium-sized dams: examples from Texas, *The Professional Geographer*, 60(2), 238-251.

Chow, V.T., D.R. Maidment, and L.W. Mays (1988), *Applied Hydrology*, McGraw-Hill, New York, NY.

Ciach, G. J. (2003), Local random errors in tipping-bucket rain gauge measurements, *Journal of Atmospheric and Oceanic Technology*, 20(5), 752-759.

Clark, C.O. (1945), Storage and the unit hydrograph, *Transactions of the American Society of Civil Engineering*, 110, 1419-1446.

Cunderlik, J.M., and S.P. Simonovic (2007), Inverse flood risk modeling under changing climatic conditions, *Hydrological Processes*, 21(5), 563-577.

Cunge, J.A. (1969), On the subject of a flood propagation computation method (Muskingum method), *Journal of Hydraulic Research,* 7(2), 205-230.

DNRC (1968), *Water Resources Survey, Phillips County, Montana*, Montana Water Resources Board, Helena, MT.

Eeles, C.W.O, and J.R. Blackie (1993), Land-use changes in the Balquhidder catchments simulated by a daily streamflow model, *Journal of Hydrology* 145(3-4), 315-336.

Fleming, M., and V. Neary (2004), Continuous hydrologic modeling study with the hydrologic modeling system, *Journal of Hydrologic Engineering*, 9(3), 175-183.

Friedman, J.M., and V.J. Lee (2001), Extreme floods, channel change, and riparian forests along ephemeral streams, *Ecological Monographs*, 72(3), 409-425.

Garbrecht, J. and L.W. Martz (1997), The assignment of drainage direction over flat surfaces in raster digital elevation models, *Journal of Hydrology*, 193(1-4), 204-213.

Garen, D.C., and D.S. Moore (2007), Curve number hydrology in water quality modeling: uses, abuses, and future directions, *Journal of the American Water Resources Association*, 41(2), 377-388.

Graf, W.L. (2006), Downstream hydrologic and geomorphic effects of large dams on American rivers, Geomorphology, 79(3-4), 336-360.

Harris, A., and F. Hossain (2008), Investigating the optimal configuration of conceptual hydrologic models for satellite-rainfall-based flood prediction, *IEEE Geoscience and Remote Sensing Letters*, 5(3), 532-536.

Hill, A.J., and V.S. Neary (2005), Factors affecting estimates of average watershed slope, *Journal of Hydrologic Engineering,* 10(2), 133-141.

Hjelmfelt, A.T. (1980), Curve number procedure as infiltration method, *Journal of the Hydraulics Division*, 106(6), 1107-1110.

Horritt, M.S., and P.D. Bates (2002), Evaluation of 1D and 2D numerical models for predicting river flood inundation, *Journal of Hydrology*, 268(1-4), 87-99.

Ibanez, C., N. Prat, and A. Canicio (1996), Changes in the hydrology and sediment transport produced by large dams on the lower Ebro river and its estuary, *Regulated Rivers: Research and Management,* 12(1), 51-62.

Kang, B., and J.A. Ramirez (2007), Response of streamflow to weather variability under climate change in the Colorado Rockies, *Journal of Hydrologic Engineering*, 12(1), 63-73.

Kenny, F., B. Matthews, and K. Todd (2008), Routing overland flow through sinks and flats in interpolated raster terrain surfaces, *Computers and Geosciences*, 34(11), 1417-1430.

Kingsford, R.T. (2000), Ecological impacts of dams, water diversions and river management on floodplain wetlands in Australia. *Austral Ecology,* 25(2), 109-127.

Knebl, M.R., Z.L. Yang, K. Hutchison, and D.R. Maidment (2005), Regional scale flood modeling using NEXRAD rainfall, GIS, and HEC-HMS/RAS: a case study for the San

Antonio River Basin Summer 2002 storm event, *Journal of Environmental Management*, 75(4), 325-336.

Kondolf, M. G. (1997), Hungry Water: Effects of Dams and Gravel Mining on River *Channels, Environmental Management, 21(4), 533-551.*

Kull, D.W., and A.D. Feldman (1998), Evolution of Clark's unit graph method to spatially distributed runoff, *Journal of Hydrologic Engineering*, 3(1), 9-19.

Lee, K.T., Y.H. Ho, and Y.J. Chyan (2006), Bridge blockage and overbank flow simulations using HEC-RAS in the Keelung River during the 2001Nari Typhoon, *Journal of Hydraulic Engineering,* 132(3), 319-324.

Legesse, D., C. Vallet-Coulomb, and F. Gasse (2003), Hydrological response of a catchment to climate and land use changes in Tropical Africa: case study South Central Ethiopia, *Journal of Hydrology*, 247(3-4), 200-214.

Leopold, L.B. (1994), *A View of the River,* Cambridge, Mass, Harvard University Press.

Li, J. and D.W.S. Wong (2010), Effects of DEM sources on hydrologic applications, *Computers, Environment and Urban Systems,* 34(3), 251-261.

Li, K.Y., M.T. Coe, N. Ramankutty, and R. De Jong (2007), Modeling the hydrological impact of land-use change in West Africa, *Journal of Hydrology*, 337(3-4), 258-268.

Liu, X., J. Peterson, and Z. Zhang (2005), High-resolution DEM generated from LiDAR data for water resource management, *Proceeding of International Congress on Modeling and Simulation 'MODSIM05',* Melbourne, Australia, 1402-1408.

Lu, G.Y., and D.W. Wong (2008), An adaptive inverse-distance weighting spatial interpolation technique, *Computers and Geosciences,* 34(9), 1044-1055.

Maidment, D.R., and D. Djokic (2000), Hydrologic and hydraulic modeling support: with geographic information systems, Environmental Systems Research Institute, Inc., Redlands, CA.

Maingi, J.K., and S.E. Marsh (2002), Quantifying hydrologic impacts following dam construction along the Tana River, Kenya, *Journal of Arid Environments*, 50(1), 53-79.

MathWorks (2010), MATLAB R2010a, Natick, MA.

McLin, S.G., E.P. Springer, and L.J. Land (2001), Predicting floodplain boundary changes following the Cerro Grande wildfire, *Hydrological Processes*, 15(15), 2967-2980.

Middelkoop, H., G. Erkens, and M. Perk (2010), The Rhine delta- a record of sediment trapping over time scales from millennia to decades, *Journal of Soils and Sediments,* 10(4), 628-640.

Miller, J.F., R.H. Frederick, and R.J. Tracey (1973), Precipitation-frequency atlas of the western United States, NOAA Atlas2, National Weather Service, Silver Spring, MD.

Montgomery, D.R., and Dietrich, W.E. (1989), Source areas, drainage density, and channel initiation, *Water Resources Research*, 25(8), 1907-1918.

Nathan, R.J., P. Jordan, and R. Morden (2005), Assessing the Impact of Farm Dams on Streamflows, Part I: Development of Simulation Tools, *Australian Journal of Water Resources,* 9(1), 1-12.

Neal, B.P., Nathan, R.J., Schreider, S.Y., and A.J. Jakeman (2001), Identifying the separate impact of farm dams and land use changes on catchment yield, *Australian Journal of Water Resources*, 5(2) , 165-176.

Ouyang, W., H. Fanghua, K. Song, and X. Zhang (2011), Cascade dam-induced hydrological disturbance and environmental impact in the upper stream of the Yellow River, *Water Resource Management,* 25(3), 913-927.

Paudel, M., E.J. Nelson, and W. Scharffenberg (2009), Comparison of lumped and quasi-distributed Clark runoff models using the SCS curve number equation, *Journal of Hydrologic Engineering*, 14(10), 1098-1107.

Poff, N.L., and D.D. Hart (2002), Why dams vary and why it matters for the emerging science of dam removal, *BioScience*, 52(8), 659-668.

Ponce, V.M., R.H. Hawkins (1996), Runoff Curve Number: Has it reached maturity?, *Journal of Hyrologic Engineering*, 1(1), 9-20.

Ponce, V.M., A.K. Lohani, and C. Scheyhing (1996), Analytical verification Muskingum-Cunge routing, *Journal of Hydrology,* 174(1196) 235-241.

Ponce, V.M. (1991), The kinematic wave controversy, *Journal of Hydraulic Engineering,* 117(4), 511-525.

Powell, G.E., D. Mecklenburg, and A. Ward, (2006), Evaluating channel-forming discharges: a study of large rivers in Ohio, *Transactions of the American Society of Agricultural and Biological Engineers*, 49(1), 35-46.

Ramesh, R., and V. Subramanian (1988), Temporal, spatial and size variation in the sediment transport in the Krishna River basin, India, *Journal of Hydrology*, 98(1-2), 53-65.

Refsgaard, J.C. (1987), A methodology for distinguishing between the effects of human influence and climate variability on the hydrologic cycle, *The Influence of Climate Change Variability on the Hydrologic Regime and Water Resources*, *IAHS*, 168, 557–570.

Sabol, G.V. (1988), Clark Unit Hydrograph and R-parameter estimation, *Journal of Hydraulic Engineering*, 114(1), 103-111.

Schreider, S. Y., A.J. Jakeman, R.A. Letcher, R.J. Nathan, B.P. Neal, and S.G. Beavis (2002), Detecting changes in streamflow response to changes in non-climatic catchment conditions: farm dam development in the Murray–Darling basin, Australia, *Journal of Hydrology,* 262(1-4), 84-98.

Schulze, R. E. (2000), Modeling hydrological responses to land use and climate change: a Southern African perspective, *AMBIO: A Journal of the Human Environment*, 29(1), 12-22.

Simanton, J.R., K.G. Renard, and N.G. Sutter (1973), Procedures for identifying parameters affecting storm runoff volumes in a semiarid environment, *USDA-ARS Agricultural Reviews and Manuals ARM-W-1,* Washington, D.C.

Soil Conservation Service (1985), Hydrology, *National Engineering Handbook*, Washington, D.C.

Sprenger, M. D., L.M. Smith, and J.P. Taylor (2002) Restoration of riparian habitat using experimental flooding, *Wetlands*, 22(1), 49-57.

Srikanthan, R., and D.T. Neil (1989), Simulation of the effect of farm dams on sediment yield from two small rural catchments, *Australian Journal of Soil and Water Conservation,* 2(1), 40-45.

Straub, T.D., C.S. Melching, K.E. Kocher (2000), Equations for estimating Clark Unit-Hydrograph parameters for small rural watersheds in Illinois, *Water Resources Investigations Report 00-4184,* USGS.

Takeuchi, K., T.Q. Ao, and H. Ishidaira (1999), Introduction of block-wise use of TOPMODEL and Muskingum-Cunge method for the hydro-environmental simulation of a large ungauged basin. *Hydrological Sciences Journal,* 44(4), 633–646.

Tarboton, D.G., R.L. Bras, and I. Rodriguez-Iturbe (1991), On the extraction of channel networks from digital elevation data, *Hydrological Processes,* 5(1), 81-100.

Tewolde, M.H., and J.C. Smithers (2006), Flood routing in ungauged catchments using Muskingum methods, *Water SA*, 32(3), 379-388.

USACE (2009), HEC-GeoHMS Geospatial Hydrologic Modeling Extension User's Manual, Hydrologic Engineering Center, Davis, CA.

USACE (2008), River Analysis System HEC-RAS User's Manual, Hydrologic Engineering Center, Davis,CA.

USACE (2008), River Analysis System HEC-RAS Technical Reference Manual, Hydrologic Engineering Center, Davis,CA.

USACE (2000), Hydrologic Modeling System HEC-HMS Technical Reference Manual, Hydrologic Engineering Center, Davis, CA.

Verstraeten, G., and I.P. Prosser (2008), Modeling the impact of land-use change and farm dam construction on hillslope sediment delivery to rivers at the regional scale, *Geomorphology*, 98(3-4), 199-212.

Viessman, W., and G. L. Lewis (2003), *Introduction to Hydrology*, Prentice Hall. Upper Saddle River, NJ.

Wang, L. and H. Liu (2006), An efficient method for identifying and filling surface depressions in digital elevation models for hydrologic analysis and modelling, *International Journal of Geographical Information Science*, 20(2), 193-213.

Whiting, P. J., J.F. Stamm, D.B. Moog, and R. L. Orndorff (1999), Sediment-transporting flows in headwater stream, *GSA Bulletin*, 111(3), 450-466.

Wilkerson, J. and V. Merwade (2010), Incorporating surface storage and slope to estimate Clark unit hydrographs for ungauged Indiana Watersheds, *Journal of Hydrologic Engineering*, 15(11), 918-931.

Williams, G.P., and M.G. Wolman (1984), Downstream effects of dams on alluvial rivers, *U.S. Geological Survey Professional Paper,* 1286.

Wolman, M. G., and J. P. Miller, (1960), Magnitude and frequency of forces in geomorphic processes, *Journal of Geology,* 68(1), 54-74.

Wooldridge, S., J. Kalma, and G. Kuczera (2001), Parameterisation of a simple semi-distributed model for assessing the impact of land-use on hydrologic response, *Journal of Hydrology,* 254(1-4), 16-32.

Wu, S., J. Li, and G.H. Huang (2008), A study on DEM-derived primary topographic attributes for hydrologic applications: Sensitivity to elevation data resolution, *Applied Geography,* 28(3), 210-223.

Xu, K., J.D. Milliman, Z. Yang, and H. Wang (2006), Yangtze sediment decline, partly from Three Gorges Dam, *Eos, Transactions, American Geophysical Union,* 87(19) , 185-196.

Yang, S.L., J.D. Milliman, P. Li, and K. Xu (2011), 50,000 dams later: Erosion of the Yangtze River and its delta, *Global and Planetary Change,* 75(1-2), 14-21.

Yang, J., R.D. Townsend, and B. Daneshfar (2006), Applying the HEC-RAS model and GIS techniques in river network floodplain delineation, *Canadian Journal of Civil Engineering,* 33(1), 19-28.

Yang, S.L., J. Zhang, J. Zhu, J.P. Smith, S.B. Dai, A. Gao, and P. Li (2005), Impact of dams on Yangtze River sediment supply to the sea and delta intertidal wetland response, *Journal of Geophysical Research*, 110.

Yawson, D. K., V.M. Kongo, and R.K. Kachroo (2005), Application of linear and nonlinear techniques in river flow forecasting in the Kilombero River basin, Tanzania, *Hydrological Sciences,* 50(5), 783-796.

Yusop, Z., C.H. Chan, and A. Katimon (2007), Runoff characteristics and application of HEC-HMS for modeling stormflow hydrograph in an oil palm catchment, *Water Science and Technology*, 55(8), 41-48.

Zhang, W., and D.R. Montgomery (1994), Digital elevation model grid size, landscape representation, and hydrologic simulations, *Water Resources Research*, 30(4), 1019-1028.

APPENDICES

APPENDIX A

DATA DICTIONARY

Dataset; digital elevation model
Source; National Elevation Dataset; http://ned.usgs.gov/
Description; Raster data set of elevation, 1/3 arc resolution (approximately 10 meter cell size), North American 1983, Montana State Plane FIPS 2500, Published 2009
Used in parameter abstraction and HEC-HMS model setup

Values represent elevation in meters, ranging from 680 to 1038

Dataset; 6^{th} Code Watershed
Source; Montana State University Natural Resource Information System; http://nris.mt.gov/
Description; Polygon dataset of 6^{th} code watersheds, 1:24,000 scale, published 2006, created by Montana Natural Resources Conservation Service State Office, GCS North American 1983, Montana State Plane, Lambert Conformal Conic projection
Used to help delineate the Box Elder watershed

Attributes of Watershed table

Field	**Type**	**Description**
NAME	TEXT	identifies specific watersheds

Dataset; aerial photos
Source; Montana State Library Natural Resource Information System; http://nris.mt.gov/
Description; Raster data set of orthorectified aerial photos from the 2009 National Agricultural Imagery Program, 1 meter resolution, 5 meter accuracy, published in 2009, North American 1983, Montana State Plane, Lambert Conformal Conic projection
Used in deriving flow paths and delineating subbasins.

Shows landcover and relief of the Box Elder Creek watershed

Dataset; soils
Source; Montana State University Natural Resource Information System; http://nris.mt.gov/
Description; Polygon dataset of soil type, 1:24,000 scale, published in 2007, North American 1983, developed through the National Cooperative Soil Survey of the Natural Resources Conservation Service of the U.S. Department of Agriculture, Montana State Plane
Used in curve number determinations

MUSYM	Hydrologic Soil Group (from muaggatt table)
1022F	C
1090B	C
1251E	D
1332C	C
1400F	D
1441D	C

1523C	D
1920F	C
1970F	D
211B	D
212B	D
250E	D
302B	D
331B	C
402B	D
41A	D
521B	D
604A	C
903A	C
90A	C
923F	C
924E	C
97D	D

Dataset; land cover
Source; Montana State University Natural Resource Information System; http://nris.mt.gov/
Description; Raster dataset of land cover, , Gap Analysis, 90 meter cell size, published in 1998, developed by the Wildlife Spatial Analysis Lab of the University of Montana, North American 1983, Montana State Plane
Used in curve number determination

Value field	Description (from metadata)
3110	Altered Herbaceous
3130	Very Low Cover Grasslands
3150	Low/Moderate Cover Grasslands
3170	Moderate/High Cover Grasslands
3200	Mixed Mesic Shrubs
3300	Mixed Xeric Shrubs
3309	Silver Sage
3310	Salt-Desert Shrub/Dry Salt Flats
3350	Sagebrush
3510	Mesic Shrub-Grassland Associations
3520	Xeric Shrub-Grassland Associations
4000	Low Density Xeric Forest
4280	Mixed Mesic Forest
4290	Mixed Xeric Forest
5000	Water
6300	Shrub Riparian
6400	Mixed Riparian
7600	Badlands
7604	Missouri Breaks
7800	Mixed Barren Sites

APPENDIX B

GRID CELL PARAMETER FILE

Parameter Order: Xcoord Ycoord TravelLength Area
End:

Subbasin: W3P6
GridCell: -8811 28004 0.3214 0.0008
GridCell: -8810 28004 0.3461 0.0024
GridCell: -8811 28005 0.2481 0.0049
GridCell: -8810 28005 0.2994 0.0067
GridCell: -8812 28006 0.0736 0.0009
GridCell: -8811 28006 0.1277 0.0092
GridCell: -8810 28006 0.2049 0.0071
GridCell: -8810 28007 0.1504 0.001
GridCell: -8812 28007 0.0239 0.0008
GridCell: -8811 28007 0.0655 0.0063
End:

Subbasin: W3P5
GridCell: -8827 28012 0.6018 0.0024
GridCell: -8826 28012 0.6541 0.0014
GridCell: -8827 28013 0.5523 0.0076
GridCell: -8826 28013 0.5376 0.0066
GridCell: -8828 28014 0.3961 0.0003
GridCell: -8827 28014 0.4444 0.0086
GridCell: -8826 28014 0.4149 0.008
GridCell: -8828 28015 0.3314 0.003
GridCell: -8827 28015 0.3106 0.01
GridCell: -8826 28015 0.3088 0.007
GridCell: -8828 28016 0.2375 0.0026
GridCell: -8827 28016 0.1963 0.01
GridCell: -8826 28016 0.2091 0.0037
GridCell: -8828 28017 0.1807 0.0001
GridCell: -8827 28017 0.0916 0.0087
GridCell: -8826 28017 0.0887 0.002
GridCell: -8827 28018 0.0239 0.0005
End:
(many lines omitted)

APPENDIX C

CURVE NUMBER TABLE

Land cover	Hydro. Soil Group	CN	Estimated land cover equivalency from McCuen Table 3.18
Badlands	C	85	Western Desert natural (pervious)
Badlands	D	88	Western Desert natural (pervious)
Grassland/Herbacious	C	81	Forest-range herbacious (Fair)
Grassland/Herbacious	D	89	Forest-range herbacious (Fair)
Low/Moderate Cover Grasslands	C	79	Non-Cultivated Range No Mech (Fair)
Low/Moderate Cover Grasslands	D	84	Non-Cultivated Range No Mech (Fair)
Missouri Breaks	C	85	Western Desert natural (pervious)
Missouri Breaks	D	88	Western Desert natural (pervious)
Mixed Barren Sites	C	85	Western Desert natural (pervious)
Mixed Barren Sites	D	88	Western Desert natural (pervious)
Mixed Mesic Shrubs	C	70	Brush (Fair)
Mixed Mesic Shrubs	D	77	Brush (Fair)
Mixed Xeric Shrubs	C	77	Brush (Poor)
Mixed Xeric Shrubs	D	83	Brush (Poor)
Moderate/High Cover Grasslands	C	74	Non-Cultivated Range No Mech (Good)
Moderate/High Cover Grasslands	D	80	Non-Cultivated Range No Mech (Good)
Ponderosa Pine	C	61	Juniper (Good)
Ponderosa Pine	D	71	Juniper (Good)
Sagebrush	C	63	Sage-grass (fair)
Sagebrush	D	70	Sage-grass (fair)
Salt-Desert Shrub/Dry Salt Flats	C	85	Western Desert natural (pervious)
Salt-Desert Shrub/Dry Salt Flats	D	88	Western Desert natural (pervious)
Shrubland	C	77	Brush (Poor)
Shrubland	D	83	Brush (Poor)
Shrub Riparian	C	65	Brush (Good)
Shrub Riparian	D	73	Brush (Good)
Silver Sage	C	63	Sage-grass (fair)
Silver Sage	D	70	Sage-grass (fair)
Small Grain	C	84	Straight Row (poor)
Small Grain	D	88	Straight Row (poor)
Very Low Cover Grasslands	C	86	Non-Cultivated Range No Mech (Poor)
Very Low Cover Grasslands	D	89	Non-Cultivated Range No Mech (Poor)
Xeric Shrub-Grassland Associations	C	81	Forest-range herbacious (Fair)
Xeric Shrub-Grassland Associations	D	89	Forest-range herbacious (Fair)
Altered Herbacious	C	87	Herbaceous-mixture, brush minor element (Poor)
Altered Herbacious	D	93	Herbaceous-mixture, brush minor element (Poor)
Graminoid and Forb Riparian	C	74	Pasture, grassland, forage for grazing (Good)
Graminoid and Forb Riparian	D	80	Pasture, grassland, forage for grazing (Good)

APPENDIX D

TIME TO CONCENTRATION CALCULATION

Watershed Name	**WOutlet**	Notes
Watershed ID	**378**	
Sheet Flow Characteristics		
Manning's Roughness Coefficient, n	0.15	
Flow Length, L (ft)	100	
Two-Year 24-hour Rainfall, P (in)	1.5	
Land Slope, s (ft/ft)	0.0519	
Sheet Flow Tt (hr)	**0.16**	$=.007*(n*L)^{.8}/(P^{.5}s^{.4})$
Shallow Concentrated Flow Characteristics		
Surface Description (1 - unpaved, 2 - paved)	1	
Flow Length, L (ft)	2154	
Watercourse Slope, s (ft/ft)	0.039	
Average Velocity - computed, v (ft/s)	3.19	$=IF(B62=1, 16.1345*s^{0.5}, 20.3282*s^{0.5})$
Shallow Concentrated Flow Tt (hr)	**0.19**	=L/(3600*v)
Channel Flow Characteristics		
Cross-sectional Flow Area, A (ft2)	8	
Wetted Perimeter, P (ft)	20	
Hydraulic Radius - computed, R (ft)	0.40	=A/P
Channel Slope, s (ft/ft)	0.0029	
Manning's Roughness Coefficient, n	0.05	
Average Velocity - computed, v (ft/s)	0.87	$=1.49*(R^{2/3})*(s^{0.5})/n$
Flow Length, L (ft)	6867	
Channel Flow Tt (hr)	**2.19**	=L*/(3600*v)
Watershed Time of travel (hr)	**2.54**	=(Sheet Flow Tt) + (Shallow Concentrated Flow Tt) + (Channel Flow Tt)

(many columns omitted)

APPENDIX E

ONE-POND-IN RESULTS

2 YR RI Storm	29.78 Peak w/o ponds (cfs)			0.067 Volume w/o ponds (in)
Pond Left in	Q Peak cfs	Q % Change	Volume in	V % Change
1P1	29.06	2.418	0.064	4.036
1P2	29.47	1.041	0.066	1.010
1P3	29.45	1.108	0.066	0.439
1P4	29.52	0.873	0.066	0.485
1P6	29.43	1.175	0.066	0.425
2P1	29.51	0.907	0.066	0.506
3P2	29.63	0.504	0.067	0.239
3P3	29.35	1.444	0.066	0.747
3P4	29.20	1.948	0.067	0.153
3P5	29.51	0.907	0.066	0.564
3P6	29.20	1.948	0.066	0.403
4P1	29.06	2.418	0.066	0.593
4P2	29.06	2.418	0.066	0.739
4P3	29.78	0.000	0.067	0.020
4P4	29.20	1.948	0.067	0.198
5P1	29.51	0.907	0.067	0.210
5P3	29.78	0.000	0.067	0.033
5P4	29.78	0.000	0.067	0.226
5P5	29.78	0.000	0.067	0.016
5P6	29.51	0.907	0.067	0.029
5P9	29.77	0.034	0.067	0.166
5P10	29.78	0.000	0.067	0.034
5P11	29.59	0.638	0.066	1.056
5P12	29.70	0.269	0.065	2.152
5P15	29.75	0.101	0.066	0.581
6P1	29.78	0.000	0.067	0.134
6P2	29.78	0.000	0.067	0.014
6P4	29.51	0.907	0.064	3.718

5 YR RI Storm	102.69 Peak w/o ponds (cfs)			0.227 Volume w/o ponds (in)
Pond Left in	Q Peak cfs	Q % Change	Volume in	V % Change
1P1	102.90	-0.204	0.223	1.771
1P2	102.03	0.643	0.226	0.770
1P3	101.95	0.721	0.226	0.479

1P4	102.20	0.477	0.226	0.434
1P6	101.78	0.886	0.226	0.476
2P1	101.11	1.539	0.226	0.757
3P2	102.22	0.458	0.227	0.192
3P3	101.73	0.935	0.226	0.446
3P4	102.41	0.273	0.227	0.089
3P5	101.94	0.730	0.227	0.313
3P6	102.36	0.321	0.227	0.166
4P1	101.15	1.500	0.225	0.893
4P2	100.25	2.376	0.226	0.743
4P3	102.40	0.282	0.227	0.102
4P4	102.08	0.594	0.227	0.221
5P1	102.04	0.633	0.227	0.327
5P3	102.24	0.438	0.227	0.201
5P4	102.21	0.467	0.227	0.372
5P5	102.60	0.088	0.227	0.054
5P6	102.50	0.185	0.227	0.079
5P9	102.14	0.536	0.227	0.155
5P10	102.56	0.127	0.227	0.095
5P11	100.85	1.792	0.227	0.288
5P12	98.19	4.382	0.221	2.924
5P15	101.99	0.682	0.227	0.356
6P1	102.65	0.039	0.227	0.336
6P2	102.69	0.000	0.227	0.039
6P4	102.43	0.253	0.219	3.669

10 YR RI Storm	186.66 Peak w/o ponds (cfs)			0.401 Volume w/o ponds (in)
Pond Left in	Q Peak cfs	Q % Change	Volume in	V % Change
1P1	186.9600	-0.161	0.397	1.005
1P2	185.2600	0.750	0.399	0.678
1P3	185.2600	0.750	0.399	0.489
1P4	185.7200	0.504	0.400	0.419
1P6	185.0000	0.889	0.399	0.490
2P1	183.4300	1.730	0.397	0.951
3P2	185.8000	0.461	0.400	0.214
3P3	185.1100	0.830	0.400	0.435
3P4	186.1700	0.263	0.401	0.100
3P5	185.6300	0.552	0.400	0.279

3P6	186.2400	0.225	0.401	0.140
4P1	183.5100	1.688	0.397	0.986
4P2	181.9700	2.513	0.398	0.856
4P3	183.7500	1.559	0.401	0.151
4P4	185.3200	0.718	0.400	0.285
5P1	185.1600	0.804	0.400	0.418
5P3	185.4800	0.632	0.400	0.287
5P4	184.9500	0.916	0.400	0.221
5P5	186.2900	0.198	0.401	0.088
5P6	186.0200	0.343	0.401	0.129
5P9	185.5600	0.589	0.401	0.195
5P10	185.9500	0.380	0.401	0.137
5P11	186.0800	0.311	0.401	0.172
5P12	175.3700	6.048	0.394	1.869
5P15	184.3500	1.238	0.400	0.411
6P1	186.5400	0.064	0.400	0.443
6P2	186.6300	0.016	0.401	0.066
6P4	185.7800	0.471	0.393	2.185

25 YR RI Storm	314.03 Peak w/o ponds (cfs)			0.663 Volume w/o ponds (in)
Pond Left in	Q Peak cfs	Q % Change	Volume in	V % Change
1P1	314.34	-0.099	0.659	0.607
1P2	314.09	-0.019	0.661	0.410
1P3	311.87	0.688	0.660	0.496
1P4	312.74	0.411	0.661	0.404
1P6	311.26	0.882	0.660	0.500
2P1	307.97	1.930	0.658	0.749
3P2	312.58	0.462	0.662	0.231
3P3	311.55	0.790	0.661	0.426
3P4	313.18	0.271	0.663	0.108
3P5	312.47	0.497	0.662	0.249
3P6	313.41	0.197	0.663	0.125
4P1	308.32	1.818	0.656	1.051
4P2	305.57	2.694	0.657	0.941
4P3	312.38	0.525	0.662	0.189
4P4	311.39	0.841	0.661	0.332
5P1	311.13	0.923	0.660	0.488
5P3	311.60	0.774	0.661	0.348

5P4	310.97	0.974	0.663	0.131
5P5	313.17	0.274	0.663	0.110
5P6	312.60	0.455	0.662	0.161
5P9	311.96	0.659	0.662	0.217
5P10	312.42	0.513	0.662	0.161
5P11	313.46	0.182	0.663	0.105
5P12	293.99	6.382	0.656	1.135
5P15	309.18	1.544	0.661	0.428
6P1	313.15	0.280	0.660	0.509
6P2	310.90	0.997	0.663	0.078
6P4	311.92	0.672	0.655	1.309

50 YR RI Storm	431.00 Peak w/o ponds (cfs)			0.890 Volume w/o ponds (in)
Pond Left in	Q Peak cfs	Q % Change	Volume in	V % Change
1P1	431.24	-0.056	0.886	0.450
1P2	431.06	-0.014	0.887	0.306
1P3	428.07	0.680	0.886	0.465
1P4	429.27	0.401	0.886	0.399
1P6	427.07	0.912	0.885	0.501
2P1	422.08	2.070	0.885	0.564
3P2	429.02	0.459	0.888	0.193
3P3	427.74	0.756	0.886	0.419
3P4	429.84	0.269	0.889	0.110
3P5	429.07	0.448	0.888	0.230
3P6	430.28	0.167	0.889	0.114
4P1	422.99	1.858	0.880	1.083
4P2	419.29	2.717	0.881	0.981
4P3	428.66	0.543	0.888	0.207
4P4	427.22	0.877	0.887	0.354
5P1	426.91	0.949	0.885	0.522
5P3	427.44	0.826	0.886	0.393
5P4	428.59	0.559	0.889	0.095
5P5	429.70	0.302	0.889	0.123
5P6	428.96	0.473	0.888	0.177
5P9	428.19	0.652	0.888	0.161
5P10	428.54	0.571	0.888	0.170
5P11	430.60	0.093	0.889	0.077
5P12	408.53	5.213	0.882	0.851

5P15	424.10	1.601	0.886	0.428
6P1	430.20	0.186	0.887	0.367
6P2	430.57	0.100	0.889	0.087
6P4	427.95	0.708	0.881	0.960

100 YR RI Storm	548.40 Peak w/o ponds (cfs)		1.103 Volume w/o ponds (in)	
Pond Left in	Q Peak cfs	Q % Change	Volume in	V % Change
1P1	548.69	-0.053	1.099	0.359
1P2	548.49	-0.016	1.100	0.249
1P3	545.68	0.496	1.099	0.373
1P4	546.46	0.354	1.099	0.391
1P6	543.19	0.950	1.097	0.504
2P1	538.31	1.840	1.098	0.455
3P2	547.41	0.181	1.101	0.162
3P3	543.92	0.817	1.098	0.416
3P4	546.77	0.297	1.102	0.087
3P5	545.80	0.474	1.100	0.220
3P6	547.46	0.171	1.102	0.113
4P1	537.18	2.046	1.091	1.104
4P2	531.68	3.049	1.092	1.011
4P3	544.87	0.644	1.100	0.222
4P4	542.82	1.018	1.099	0.370
5P1	542.44	1.087	1.097	0.544
5P3	542.95	0.994	1.098	0.421
5P4	546.39	0.367	1.102	0.079
5P5	546.43	0.359	1.101	0.134
5P6	545.29	0.567	1.101	0.189
5P9	545.71	0.491	1.101	0.130
5P10	544.73	0.669	1.101	0.178
5P11	548.07	0.060	1.102	0.060
5P12	526.66	3.964	1.095	0.695
5P15	538.55	1.796	1.098	0.435
6P1	546.81	0.290	1.100	0.295
6P2	547.54	0.157	1.102	0.092
6P4	544.26	0.755	1.094	0.769

APPENDIX F

ONE-POND-OUT RESULTS

2 YR RI Storm	29.78 Peak w/o ponds (cfs)			0.067 Volume w/o ponds (in)	
Pond Taken Out	Q Peak cfs	Q % Change	Volume in	V % Change	Ownership
1P1	27.84	6.50	0.059	11.04	CMR
1P2	26.50	11.01	0.057	14.07	APF Leased
1P3	26.51	10.97	0.057	14.64	APF Leased
1P4	26.48	11.09	0.057	14.60	APF Leased
1P6	26.42	11.30	0.057	14.66	Private
2P1	26.02	12.62	0.057	14.82	APF Leased
3P2	26.06	12.49	0.057	14.94	APF Leased
3P3	26.07	12.45	0.057	14.61	APF Leased
3P4	26.01	12.66	0.057	15.02	CMR
3P5	26.32	11.61	0.057	14.60	CMR
3P6	26.02	12.64	0.057	14.81	MT State Trust Lands
4P1	26.02	12.63	0.057	14.49	APF Leased
4P2	26.02	12.64	0.057	14.68	APF
4P3	26.01	12.66	0.057	15.06	BLM
4P4	26.01	12.66	0.057	15.01	APF
5P1	26.01	12.65	0.057	14.97	APF
5P3	26.01	12.66	0.057	15.06	APF*
5P4	26.01	12.66	0.057	14.99	APF
5P5	26.01	12.66	0.057	15.07	BLM
5P6	26.01	12.66	0.057	15.06	APF
5P9	26.01	12.65	0.057	15.01	CMR
5P10	26.01	12.66	0.057	15.05	MT State Trust Lands
5P11	26.01	12.65	0.057	14.72	MT State Trust Lands
5P12	26.01	12.66	0.057	15.07	Private
5P15	26.01	12.65	0.057	14.84	BLM
6P1	26.01	12.66	0.057	15.07	BLM
6P2	26.01	12.66	0.057	15.07	BLM
6P4	26.01	12.66	0.059	11.85	Private

5 YR RI Storm	102.69 Peak w/o ponds (cfs)			0.227 Volume w/o ponds (in)	
Pond Taken Out	Q Peak cfs	Q % Change	Volume in	V % Change	Ownership
1P1	83.48	18.71	0.193	15.07	CMR

1P2	84.52	17.70	0.191	16.07	APF Leased
1P3	84.51	17.70	0.190	16.37	APF Leased
1P4	84.17	18.04	0.190	16.41	APF Leased
1P6	84.67	17.55	0.190	16.37	Private
2P1	84.98	17.25	0.191	16.09	APF Leased
3P2	84.14	18.06	0.190	16.65	APF Leased
3P3	84.51	17.71	0.190	16.40	APF Leased
3P4	83.85	18.34	0.189	16.76	CMR
3P5	84.96	17.27	0.190	16.53	CMR
3P6	84.37	17.84	0.189	16.68	MT State Trust Lands
4P1	84.53	17.69	0.191	15.95	APF Leased
4P2	84.87	17.36	0.191	16.11	APF
4P3	83.60	18.59	0.189	16.74	BLM
4P4	83.64	18.55	0.190	16.63	APF
5P1	84.07	18.13	0.190	16.52	APF
5P3	83.69	18.50	0.190	16.61	APF*
5P4	83.66	18.54	0.190	16.46	APF
5P5	83.60	18.59	0.189	16.79	BLM
5P6	83.60	18.59	0.189	16.77	APF
5P9	83.60	18.59	0.189	16.77	CMR
5P10	83.60	18.59	0.189	16.74	MT State Trust Lands
5P11	85.16	17.07	0.190	16.60	MT State Trust Lands
5P12	83.59	18.60	0.189	16.85	Private
5P15	83.63	18.56	0.190	16.46	BLM
6P1	83.59	18.60	0.189	16.80	BLM
6P2	83.59	18.60	0.189	16.80	BLM
6P4	83.70	18.50	0.198	13.12	Private

10 YR RI Storm		186.66 Peak w/o ponds (cfs)		0.401 Volume w/o ponds (in)	
Pond Taken Out	Q Peak cfs	Q % Change	Volume in	V % Change	Ownership
1P1	143.61	23.06	0.349	13.08	CMR
1P2	145.32	22.15	0.347	13.41	APF Leased
1P3	145.32	22.15	0.347	13.60	APF Leased
1P4	144.83	22.41	0.346	13.67	APF Leased
1P6	145.59	22.00	0.347	13.60	Private
2P1	147.17	21.16	0.349	13.13	APF Leased

3P2	144.81	22.42	0.346	13.86	APF Leased
3P3	145.50	22.05	0.347	13.65	APF Leased
3P4	144.42	22.63	0.345	13.98	CMR
3P5	145.10	22.27	0.346	13.81	CMR
3P6	144.41	22.63	0.345	13.94	MT State Trust Lands
4P1	146.95	21.27	0.349	13.10	APF Leased
4P2	148.65	20.36	0.348	13.23	APF
4P3	144.67	22.50	0.345	13.93	BLM
4P4	145.09	22.27	0.346	13.80	APF
5P1	145.37	22.12	0.346	13.67	APF
5P3	145.41	22.10	0.346	13.72	APF*
5P4	145.00	22.32	0.346	13.90	APF
5P5	144.06	22.82	0.345	14.02	BLM
5P6	144.18	22.76	0.345	13.99	APF
5P9	145.16	22.23	0.346	13.89	CMR
5P10	144.22	22.74	0.345	13.98	MT State Trust Lands
5P11	145.50	22.05	0.345	13.92	MT State Trust Lands
5P12	153.83	17.59	0.352	12.22	Private
5P15	145.24	22.19	0.346	13.70	BLM
6P1	143.93	22.89	0.347	13.65	BLM
6P2	143.89	22.91	0.345	14.02	BLM
6P4	144.80	22.43	0.354	11.89	Private

25 YR RI Storm	314.03 Peak w/o ponds (cfs)		0.663 Volume w/o ponds (in)		
Pond Taken Out	Q Peak cfs	Q % Change	Volume in	V % Change	Ownership
1P1	241.58	23.07	0.588	11.38	CMR
1P2	241.80	23.00	0.587	11.57	APF Leased
1P3	243.87	22.34	0.587	11.49	APF Leased
1P4	243.11	22.58	0.587	11.58	APF Leased
1P6	244.41	22.17	0.587	11.49	Private
2P1	247.42	21.21	0.589	11.24	APF Leased
3P2	243.24	22.54	0.585	11.75	APF Leased
3P3	244.25	22.22	0.587	11.56	APF Leased
3P4	242.70	22.71	0.585	11.87	CMR
3P5	243.42	22.49	0.586	11.73	CMR
3P6	242.44	22.80	0.585	11.85	MT State

					Trust Lands
4P1	246.95	21.36	0.591	10.93	APF Leased
4P2	250.16	20.34	0.590	11.04	APF
4P3	243.66	22.41	0.585	11.79	BLM
4P4	244.57	22.12	0.586	11.65	APF
5P1	244.77	22.06	0.587	11.50	APF
5P3	244.15	22.25	0.586	11.63	APF*
5P4	244.82	22.04	0.585	11.87	APF
5P5	242.73	22.70	0.585	11.86	BLM
5P6	243.18	22.56	0.585	11.82	APF
5P9	244.03	22.29	0.585	11.77	CMR
5P10	243.25	22.54	0.585	11.83	MT State Trust Lands
5P11	242.45	22.79	0.585	11.88	MT State Trust Lands
5P12	260.38	17.08	0.591	10.84	Private
5P15	245.74	21.75	0.587	11.57	BLM
6P1	242.08	22.91	0.587	11.46	BLM
6P2	241.86	22.98	0.584	11.90	BLM
6P4	242.34	22.83	0.593	10.67	Private

50 YR RI Storm	431.00 Peak w/o ponds (cfs)		0.890 Volume w/o ponds (in)		
Pond Taken Out	Q Peak cfs	Q % Change	Volume in	V % Change	Ownership
1P1	326.87	24.16	0.798	10.37	CMR
1P2	327.06	24.12	0.796	10.51	APF Leased
1P3	329.47	23.56	0.798	10.35	APF Leased
1P4	328.47	23.79	0.797	10.42	APF Leased
1P6	330.34	23.35	0.798	10.31	Private
2P1	332.93	22.75	0.799	10.25	APF Leased
3P2	328.23	23.84	0.795	10.62	APF Leased
3P3	330.25	23.38	0.797	10.39	APF Leased
3P4	328.10	23.87	0.795	10.70	CMR
3P5	328.47	23.79	0.796	10.59	CMR
3P6	327.74	23.96	0.795	10.70	MT State Trust Lands
4P1	335.46	22.17	0.803	9.73	APF Leased
4P2	336.93	21.83	0.802	9.84	APF
4P3	329.29	23.60	0.796	10.60	BLM
4P4	330.82	23.24	0.797	10.46	APF

5P1	331.31	23.13	0.798	10.30	APF
5P3	330.73	23.26	0.797	10.44	APF*
5P4	327.76	23.95	0.794	10.72	APF
5P5	328.53	23.77	0.795	10.69	BLM
5P6	329.14	23.63	0.795	10.64	APF
5P9	328.94	23.68	0.795	10.65	CMR
5P10	329.26	23.61	0.795	10.64	MT State Trust Lands
5P11	327.18	24.09	0.794	10.74	MT State Trust Lands
5P12	345.78	19.77	0.801	9.97	Private
5P15	333.17	22.70	0.798	10.37	BLM
6P1	327.33	24.05	0.797	10.43	BLM
6P2	327.25	24.07	0.795	10.72	BLM
6P4	336.61	21.90	0.802	9.84	Private

100 YR RI Storm	548.40 Peak w/o ponds (cfs)		1.103 Volume w/o ponds (in)		
Pond Taken Out	Q Peak cfs	Q % Change	Volume in	V % Change	Ownership
1P1	437.23	20.27	0.996	9.72	CMR
1P2	437.57	20.21	0.994	9.83	APF Leased
1P3	437.70	20.19	0.996	9.70	APF Leased
1P4	439.30	19.89	0.996	9.69	APF Leased
1P6	441.89	19.42	0.997	9.57	Private
2P1	439.29	19.90	0.997	9.62	APF Leased
3P2	437.73	20.18	0.993	9.92	APF Leased
3P3	441.71	19.45	0.996	9.66	APF Leased
3P4	438.97	19.95	0.993	9.99	CMR
3P5	439.42	19.87	0.994	9.86	CMR
3P6	438.36	20.07	0.993	9.97	MT State Trust Lands
4P1	448.78	18.17	1.004	8.97	APF Leased
4P2	451.26	17.71	1.003	9.07	APF
4P3	440.82	19.62	0.994	9.86	BLM
4P4	443.08	19.20	0.996	9.71	APF
5P1	443.36	19.15	0.998	9.53	APF
5P3	442.76	19.26	0.996	9.68	APF*
5P4	438.42	20.05	0.993	10.01	APF
5P5	439.63	19.83	0.993	9.94	BLM
5P6	440.58	19.66	0.994	9.89	APF

5P9	438.49	20.04	0.993	9.95	CMR
5P10	440.78	19.62	0.994	9.90	MT State Trust Lands
5P11	437.67	20.19	0.992	10.01	MT State Trust Lands
5P12	452.72	17.45	0.999	9.40	Private
5P15	446.43	18.59	0.997	9.63	BLM
6P1	437.69	20.19	0.995	9.77	BLM
6P2	437.69	20.19	0.993	9.98	BLM
6P4	446.54	18.57	1.000	9.29	Private

*Ownership was questionable since the pond appeared to lie on the boundary line between APF deeded land and CMR.